Class VI Injection Well Application

Contains proprietary business information.

Attachment 01: Narrative

40 CFR §146.82(A)

Stonewell Project
Marion County, Ohio

16 January 2026

Table of Contents

List of Figures

Figures are located following the References at the end of this document (Section 15 *Figures.)*.

List of Tables

List of Acronyms and Abbreviations

1D MEM	one-dimensional mechanical earth model
2D	two-dimensional
3D	three-dimensional
25Cr	25-Chrome
25Cr80	25 Chrome, minimum yield strength of 80,000 pounds per square inch
ACZ	above confining zone
AMPP	Association for Materials Protection and Performance
AoR	Area of Review
API	American Petroleum Institute
CAA	Clean Air Act
CCS	carbon capture and sequestration
CCS1	Illinois Basin–Decatur Project Injection Well
CO_2	carbon dioxide
CRA	corrosion resistant alloys
CWA	Clean Water Act
DOE	Department of Energy
ECRS	Eastern Continental Rift Basin
EGRP	Eastern Granite-Rhyolite Province
EPA	Environmental Protection Agency
EPSG	European Petroleum Survey Group
ERRP	Emergency and Remedial Response Plan
fbgl	feet below ground level
fbsl	feet below sea level
FWR	Fort Wayne Rift
FEMA	Federal Emergency Management Agency
GSDT	Geologic Sequestration Data Tool
h	Thickness
HDT	high-resolution dip meter tool
IBDP	Illinois Basin–Decatur Project
IEc	Industrial Economics
IPaC	Information for Planning and Consultation
k	permeability
ktpa	kilotonnes per annum
LAS	log ascii standard
mD	millidarcy
mg/L	milligrams per liter
MSF	Marion South Fault
Mt	million tonnes
Mtpa	million tonnes per annum
N/A	not applicable
NGT	natural gamma spectroscopy tool
NOV	National Oilwell Varco
NPDES	National Pollution Discharge Elimination System

NRI	Nationwide Rivers Inventory
O&G	oil and gas
ODNR	Ohio Department of Natural Resources
PBI	proprietary business information
pH	acidity or alkalinity measurement
PISC	post-injection site care
SRT	step rate test
STO ACZ1	Stonewell Above Confining Zone Monitor Well 1
STO INJ1	Stonewell Injection Well 1
STO OBS1	Stonewell Deep Observation Well 1
STO USDW1	Stonewell USDW Monitoring Well 1
SU	standard units
TBD	to be determined
TCS	total closure stress
TD	total depth
TDS	total dissolved solids
TWT	two-way-time
UIC	Underground Injection Control
US	United States
USDW	underground source of drinking water
USFWS	United States Fish and Wildlife Service
USGS	United States Geological Survey
UWI	unique well identifier
XRD	x-ray diffraction

1. Project Contact Information and Background [40 CFR §146.82(a)(1)]

1.1 Project Contact Information

Project Name: Stonewell

Project Operator: Vault GSL CCS LP

Project Contact: Scott Jordan, Project Manager
Vault GSL CCS LP
1125-17th Street, Suite 1275
Denver, Colorado 80202
Email: stonewell@vault4401.com
Phone: 713-930-4401

Stonewell Injection Well 1 (STO INJ1) Location:

Marion County, Ohio
Latitude: 40.64989° N
Longitude: 83.23105° W

1.2 Project Background

The objective of the Stonewell Project is to effectively capture CO_2 produced at a nearby ethanol facility (Standard Industrial Classification [SIC] code 2869-08), and safely and permanently sequester approximately 5.1 million tonnes (Mt) of CO_2 over 12 years in the Mt. Simon Sandstone. One well is expected to be sufficient for injection of the project's intended mass flow rate of 425 kilotonnes per annum (ktpa) of CO_2 into the Mt. Simon Sandstone. This Underground Injection Control (UIC) Class VI application describes and supports this effort in accordance with the US Environmental Protection Agency's (EPA's) Class VI regulations in Title 40 of the Code of Federal Regulations (40 CFR §146.81).

Vault GSL CCS LP, a private company, will be the owner, operator, and permit holder for the injection well STO INJ1 and the transport pipeline. A stratigraphic well (Stonewell / INJ1, API #: 34-101-2-0223-00-00) will be drilled under an Ohio Department of Natural Resources (ODNR) Division of Oil and Gas Resources Management Permit to Drill a Stratigraphic Well. This stratigraphic well is intended to be used as the Stonewell Injection Well 1 (STO INJ1) upon issuance of the final Class VI authorization to inject. Neither an injection depth waiver nor an aquifer exemption expansion is being requested for this project.

The target injection formation, the Mt. Simon Sandstone, is of sufficient depth and temperature at the site to maintain the injected CO_2 in a supercritical state. The Mt. Simon Sandstone has served as a suitable injection interval for Class I, II and VI wells in the region for multiple decades. The Rome Formation is the primary confining zone. There are significant thicknesses of

other strata at the project site that will additionally prevent upward movement of fluids including the Glenwood Shale, the Utica Shale, and the Queenston Formation/Maquoketa Group.

There are four primary wells associated with the project: Figure 1 shows the location of STO INJ1 and the Stonewell Deep Observation Well 1 (STO OBS1), and Figure 2 shows the proposed locations of STO INJ1, the Stonewell Deep Observation Well 1 (STO OBS1), the Stonewell Above Confining Zone Monitor Well 1 (STO ACZ1), and the Stonewell USDW Monitoring Well 1 (STO USDW1). Table 1 shows the coordinates, depth, and intended use for each well.

Within the Area of Review (AoR), there are currently no deep stratigraphic boreholes, State or Federal EPA approved subsurface clean-up sites, springs, surface or subsurface mines, quarries, State, Tribal, or Territory boundaries. Surface bodies of water within the AoR include Little Sandusky River, Tymochtee Creek, Prairie Run, Maple Run, Morral Run, Bell Harraman Ditch, Thompson Ditch, Carrol Ditch, several unnamed intermittent streams, and several unnamed wetlands. A discussion of area infrastructure within the AoR is included in Attachment 09: Emergency and Remedial Response Plan, 2025) and Figure 1 shows the required information per 40 CFR §146.82(a)(2). The state-permitted stratigraphic well (Stonewell / INJ1), which the project intends to use as STO INJ1 upon issuance of the final Class VI authorization to inject, will be drilled prior to issuance of the draft Class VI permit. Information on oil and gas wells (O&G) and water wells within the AoR can be found in Section 4.1 *Tabulation of Wells Within the AoR* of Attachment 02: AoR and Corrective Action Plan, (2025).

The state-permitted stratigraphic well (Stonewell / INJ1) will be the first project-related well drilled and will be used to collect site-specific data consistent with the specifications of 40 CFR §146.86 and §146.87 (Attachment 05: Pre-operational Testing Program, 2025). Subsequent project wells, including STO OBS1, STO ACZ1, and STO USDW1, will collect additional site-specific data for the project (Attachment 05: Pre-operational Testing Program, 2025). The data gathered will be processed and analyzed to confirm or re-assess the project modeling efforts and current understanding.


Claimed as PBI

1.3 Local, State, and Federal Emergency Contacts [40 CFR §146.82(a)(20)]

Table 2 provides emergency contact information in the event of an emergency at the project site.

Table 2: Local, state, and federal emergency contacts

Agency	Phone Number
Emergency Dispatch – Police, Fire, or Medical Emergency	911
Marion Township Fire Department	740-387-5404
Morral-Salt Rock Township Fire Department	740-465-2005
Marion County Sheriff's Department	740-382-8244
Ohio State Police Marion Post	740-383-2181
Environmental services contractor to be determined (TBD)	TBD
US EPA Region 5 UIC Program Director	312-353-7648 (UIC Region 5 Director)
US EPA Region 5 UIC Class VI Wells/Carbon Sequestration	312-353-3944 (Class VI UIC Wells/Carbon Sequestration)
EPA National Response Center (24 hours)	800-424-8802
Ohio Environmental Protection Agency	800-282-9378 (Emergency Spill Hotline)
Ohio Department of Natural Resources (ODNR) Division of O&G Resources	844-642-2551 (Emergency Response)

1.4 Summary of Other Permits Required

Stonewell Project activities associated with development of the Class VI injection well include construction of well pads, access roads, and site infrastructure. Table 3 provides a summary of federal permits, under programs listed in 40 CFR 144.31(e)(6), and their applicability for the Stonewell Project. Except for this Class VI application, no other permits or construction approvals have been applied for or received.

Table 3: Federal permit applicability under 40 CFR 144.31(e)(6) listed programs for the Stonewell Project.

Program	Activity	Permit(s) Required
Hazardous Waste Management program under Resource Conservation and Recovery Act (RCRA)	CO_2 injection	Not applicable (N/A), injected CO_2 is a non-hazardous waste under 40 CFR 261.4(h).
UIC program under Safe Drinking Water Act (SDWA)	CO_2 injection	Class VI UIC permit.
National Pollutant Discharge Elimination System (NPDES) program under Clean Water Act (CWA)	Well pad construction Access road construction	Coverage under Construction Site Stormwater - General Permit NPDES program administered by the state of Ohio.
Prevention of Significant Deterioration (PSD) program under Clean Air Act (CAA)	CO_2 injection	N/A, CO_2 injection facility is not a major source, as defined in the CAA. CCS is considered a best available control technology for major sources.
Nonattainment program under CAA	CO_2 injection	N/A, Marion County is currently in attainment for all criteria pollutants.
National Emission Standards for Hazardous Air Pollutants (NESHAP) pre-construction approval under the CAA	CO_2 injection	N/A, CO_2 injection is not considered a NESHAP source of hazardous air pollutants.
Ocean dumping permits under Marine Protection Research and Sanctuaries Act	Well pad construction Access road construction	N/A, onshore project with no proposed ocean dumping.
Section 404 of CWA	Well pad construction Access road construction	N/A, construction activities are planned outside of waters of the U.S. No dredge or fill material into waters of the U.S. is anticipated.
State or Other relevant environmental permits, including state permits 40 CFR 144.31 (e)(6)(ix)		
Ohio Environmental Protection Agency Stormwater Program	Well pad construction Access road construction	Coverage under Construction Site Stormwater - General Permit, administered by Ohio EPA.
Ohio Department of Natural Resources Division of Oil and Gas Resources Management	Drilling of stratigraphic well (Stonewell / INJ1)	Permit to Drill a Stratigraphic Well (API #: 34-101-2-0223-00-00)

1.5 Landowners Within the AoR

A list of names and addresses of all owners of record of land within the AoR of the Stonewell Project can be found in PBI Appendix 1A-*List of Landowners Within the AoR*.

2. Site Characterization [49 CFR 126.82(a)(2), (3), (5) and (6)]

Unless otherwise stated, all depths are in reference to feet below ground level (fbgl).

2.1. Regional Geology, Hydrogeology, and Local Structural Geology [40 CFR §146.82(a)(3)(vi)]

The Stonewell Project site is in northern Marion County, Ohio, U.S.A and is located within the geologic region known as the Arches Province (Figure 3). This region has a basement primarily composed of crystalline Precambrian rocks that are unconformably overlain by Paleozoic sedimentary rocks (Figure 4). These Paleozoic strata overlay three broad Precambrian arches, which are the Findlay, Kankakee, and Cincinnati, which divide the Michigan, Appalachian, and Illinois Paleozoic Basins (Figure 3 and Figure 4). The project site is on the east limb of the Findlay Arch and has approximately 3,000 feet of Cambrian through Silurian strata (Figure 4).

The Cambrian Mt. Simon Sandstone and the Arches Province has been the focus of research into geological carbon sequestration due to the intersection of reservoir thickness, permeability, and depth. Previously conducted computational modeling of the Mt. Simon Sandstone in the Arches Province concluded that large-scale injection into the Mt. Simon Sandstone reservoir may be achieved in the region (Sminchak, 2012). The Mt. Simon Sandstone has served as a suitable injection interval in the province for Class I wells in the region for decades (INEOS Nitriles, 2016; Vickery Environmental Inc., 2020). In the adjacent Illinois Basin, the Mt. Simon Sandstone has been investigated for carbon sequestration potential for over two decades through the Midwest Regional Carbon Sequestration Partnership's Illinois Basin–Decatur Project (IBDP) (Wickstrom et al., 2005; Greenberg, 2021), CarbonSAFE programs (Leetaru et al., 2019; Korose, 2022; Whittaker, 2022; Whittaker and Carman, 2022), and the commercial Illinois Industrial Carbon Capture and Storage Project at Decatur Illinois (Gollakota and McDonald, 2014).

In northwestern Ohio, the Precambrian basement is composed of crystalline rocks of varying origins and ages. Eustatic sea level fluctuations coupled with tectonics allowed for the accumulation of both marine and terrestrial sediments in the Arches Province and surrounding basins. In the Ohio portion of the Arches Province, the Paleozoic strata are relatively shallow and thin (less than 4,000 feet) compared to strata in surrounding sedimentary basins (Baranoski, 2002). For example, up to 18,000 feet of Paleozoic strata accumulated in the Reelfoot Rift and Rough Creek Graben, which are significant features within the southern portion of the Illinois Basin related to processes linked to subsidence (Kolata and Nimz, 2010). In portions of western Ohio, clastics of the Neoproterozoic Middle Run Formation were deposited on the crystalline basement and are unconformably overlain by the Cambrian Mt. Simon Sandstone (Drahovzal et al., 1992). However, the Middle Run Formation is not expected to be present at the project site.

The Cambrian Mt. Simon Sandstone and Rome Formation are among the oldest and deepest Paleozoic strata in Ohio (Figure 5). The Mt. Simon Sandstone will serve as the injection zone, and the Rome Formation will be the primary confining zone for the Stonewell Project. These sediments were deposited in a near shore environment fed by drainage systems that transgressed

to a shallow shelf/pro-delta depositional environment (Freeman, 1953; Janssens, 1973; Green, 2018).

By late Cambrian, much of Ohio was covered by a shallow sea. This sea regressed in the Ordovician due to both eustatic and tectonic forces, which resulted in the Knox Unconformity (Figure 5, Janssens, 1973). The Arches Province was near the wave-base in the Middle Silurian and much of the sediment deposition during this time was diverted to the surrounding basins. During the Devonian, the sea regressed, and uplift occurred due to the Acadian Orogeny, which allowed for non-deposition and erosion along the arches. Following this, sea level transgressed into parts of Ohio during the Devonian-Mississippian, depositing marine sediments. Ohio was a low-relief coastal plain swamp in the Pennsylvanian and was filled with deltaic sediments related to the Alleghenian Orogeny during the Permian. This uplift during the late Paleozoic to early Mesozoic further separated the surrounding sedimentary basins from the Arches Province and eroded previously deposited sediment (Ohio Division of Geological Survey, 2014).

Erosion and/or nondeposition prevailed along the arches throughout the Mesozoic and Cenozoic. During the Pleistocene Epoch, the region was covered by continental ice sheets that deposited hundreds of feet of glacial sediment in the region, some of which now serve as shallow groundwater aquifers (Ohio Division of Geological Survey, 2014).

2.2. Regional Stratigraphy

Figure 5 is a site-specific stratigraphic column for the Stonewell Project and will be referred to throughout this narrative.

Geophysical logs from regional wells were used to construct the static model (Figure 6, Figure 7, and Figure 8). The regional continuity of the Paleozoic strata in the vicinity of the project site [40 CFR §146.82(a)(3)(i)] is demonstrated through cross-sections of the site model (Figure 6 and Figure 8). Quaternary glacial sediments overlie the bedrock (Figure 5) and are discussed further in Section 2.9 *Hydrologic and Hydrogeologic Information.*

To develop a comprehensive understanding of the site-specific geology for this project, a database of publicly available geophysical well logs from Ohio and Indiana was compiled. The well logs were interpreted and used to develop a static model for the project site. The wells that were used to construct the static model are presented in Appendix 1B-*Wells used for Geologic Evaluation* and shown in Figure 7.

Within 50 miles of the Stonewell Project, 95 wells penetrate the Precambrian Basement, and 134 wells penetrate the Mt. Simon Sandstone, all of which were used to assess the site-specific geology (Figure 7). The Ohio Liquids Disposal well (UWI 34143202370000) is located approximately 50 miles north of the project site and is part of a field that contains nine Mt. Simon Sandstone Class I injection wells, some of which have been plugged and abandoned (Figure 7). These wells penetrate the Precambrian Basement and use the Mt. Simon Sandstone as an injection zone. In this field, The Rome Formation and the Conasauga Formation are the primary confining zone, and the Kerbel Formation is a monitoring zone (Vickery Environmental Inc., 2020). This site will be discussed more in Section 2.6.2 *Mineralogy, Diagenesis, Porosity and Permeability*. Approximately 50 miles west in Lima, Ohio, the BP Chemical 2 Class I

injection well (UWI 34003200670000) is part of a field that also utilizes the Mt. Simon Sandstone for wastewater storage. The wells in this field penetrate through the entire Mt. Simon Sandstone into the Middle Run Formation (Figure 7).

Figure 8 shows a map and cross section of the closest wells to the Stonewell Project that penetrate into the Mt. Simon Sandstone, with focus on the Mt. Simon Sandstone injection zone and the Rome Formation primary confining zone. The Forry Evelyn well (UWI 34101202070000) is the nearest well to penetrate the entire thickness of the Mt. Simon Sandstone, which is approximately 3.5 miles northeast of the project site. The Gracely Farms 1 and 2 wells (UWIs 34101201680000 and 34101201760000) are approximately five miles south of the Stonewell Project site and also penetrate the entire Mt. Simon Sandstone thickness (Figure 8).

2.2.1. Precambrian Basement Complex

In western Ohio, the Precambrian Basement is divided into three provinces: 1) the Eastern Granite-Rhyolite Province (EGRP), 2) the East Continent Rift System (ECRS), and 3) the Grenville Province (Figure 9). The Stonewell Project site is located on the Grenville Province, although the precise boundary among these provinces is difficult to determine (Baranoski et al., 2009). The Grenville Province in the region is an allochthonous terrain composed of metamorphic rocks intruded by igneous rocks (Figure 9).

The Eastern Granite Rhyolite Province (EGRP) is a large Precambrian autochthonous terrain composed of primarily unmetamorphosed igneous and felsic volcanic rocks (Figure 9; Denison et al., 1984; Wickstrom et al., 1992). It is likely the oldest of the Precambrian provinces in the project region with the ECRS faulting through and the Grenville thrusting over the EGRP rocks.

The ECRS is a mid-Proterozoic rift system that crosscuts and is partially overlying the EGRP, and the Fort Wayne Rift (FWR) is a part of this rift system. A boundary between the EGRP and the ECRS exists west of the project site (Figure 9, Baranoski et al., 2002). In the Arches Province, the ECRS contains intrabasinal volcanic rocks and sandstones of the Neoproterozoic Middle Run Formation.

The Middle Run Formation was first recognized in the Ohio Department of Natural Resources (ODNR) Division of Geological Survey #2627 core located in Warren County approximately 88 miles south-southwest of the project (Figure 10). Sediments of the Middle Run Formation were deposited in the ECRS and surrounding area, and seismic, magnetic, and gravity data suggest a genetic relationship between the ECRS, the FWR, and flanking clastic rift basins that contain the Middle Run Formation (Figure 9, Dickas et al., 1992, Drahovzal et al., 1992, Baranoski et al., 2009). This formation has been identified in portions of Ohio, Kentucky, and Indiana, and it may be at the project site (Drahovzal et al., 1992). Specific to the Stonewell Project, the FWR is located to the west of the Stonewell Project site (Figure 9), though the exact boundary is unknown, and is discussed in more detail in Section 2.3 *Regional Structure*.

As previously stated, the allochthonous terrain of the Grenville Province is composed of metamorphic rocks intruded by igneous rocks (Figure 9). These rocks have been thrust over the existing terrains to the (present-day) west during the Proterozoic Grenville Orogeny when Laurentia collided with other continents and created the supercontinent Rodinia (Baranoski et al.,

2009). The Grenville Province extends across eastern Canada, the eastern United States and into Central America and contributed to the source of Early Cambrian siliciclastic strata in the Arches Province and Appalachian Basin (Bickford et al., 1986).

The Grenville Front is a geomagnetic anomaly west of the project site and is used as the boundary between the Grenville Province and the Precambrian provinces to the west (Figure 9). The anomaly is correlated to the erosional edge of the Grenville Province rocks that were thrust over older Precambrian rocks during the Grenville Orogeny (Bickford et al., 1986; Drahovzal et al., 1992; Atekwana, 1996; Lidiak, 1996; Baranoski et al., 2009; Green, 2018). The Grenville Front will be discussed in more detail in Section 2.3 *Regional Structure*.

The Stonewell Project site is located on the Grenville Province approximately 15 miles east of the Grenville Front.

Figure 11 shows that the Precambrian Basement deepens from approximately [redacted] feet below sea level (fbsl) in the center and southwest portion of the mapped area to more than [redacted] fbsl in the east toward the Appalachian Basin.

2.2.2. Mt. Simon Sandstone/Injection Zone (Cambrian)

The Potsdam Supergroup of the Cambro-Ordovician Sauk sequence unconformably overlies Precambrian rock in the Arches Province and includes the Mt. Simon Sandstone, the Rome Formation, the Conasauga Formation, and the Kerbel Formation (Figure 5, Figure 6, and Figure 8). Specific to this project, the Mt. Simon Sandstone is the injection zone, and the Rome Formation is the primary confining zone (Figure 5).

The Mt. Simon Sandstone is interpreted to primarily be a transgressive terrestrial to shallow marine sequence that is a laterally extensive deposit throughout the Arches Province, the Illinois Basin, and the Michigan Basin (Janssens, 1973; Kolata and Nelson, 1990). It is thickest in northeastern and east-central Illinois (Janssens, 1973; Leetaru and McBride, 2009). Throughout the Midwest, the Mt. Simon Sandstone sedimentology was impacted by a wide range of depositional environments including shallow marine, deltaic, fluvial, eolian, and coastal (Janssens, 1973; Bowen et al., 2011; Saeed and Evans, 2012; Baranoski, 2013; Freiburg et al., 2016).

In western Ohio, the Mt. Simon Sandstone is composed of friable, fine-grained to conglomeratic quartz and arkosic sandstone that generally fine upwards (Janssens, 1973). Most of the Mt. Simon Sandstone is poorly consolidated, though some intervals have siliceous cement. The Mt. Simon Sandstone grades into the overlying Rome Formation, and portions of the Mt. Simon Sandstone may be dolomitic and oolitic. The clastic grains are generally frosted, mostly rounded, and poorly sorted, though individual beds may be well sorted. Glauconite and fossils are not present in the Ohio portion of the Mt. Simon Sandstone (Janssens, 1973), though trace fossils have been identified (Saeed and Evans, 2012).

As previously mentioned, the Mt. Simon Sandstone has been the focus of numerous studies and has served as the injection interval in the Arches Province for Class I UIC wells for multiple decades, which will be discussed more in Section 2.6.2 *Mineralogy, Diagenesis, Porosity and*

Permeability (Vickery Environmental, Inc., 1989; INEOS Nitriles, 2016; Vickery Environmental Inc., 2020). The Mt. Simon Sandstone is also the injection interval in the adjacent Illinois Basin through a number of US Department of Energy (DOE) funded projects including the Regional Carbon Sequestration Partnerships' IBDP's CCS1 injection well (Greenberg, 2021) and the CarbonSAFE program (Leetaru et al., 2019; Korose, 2022; Whittaker and Carman, 2022). In the Illinois Basin, the Mt. Simon Sandstone is relatively thick and subdivided into Lower, Middle, and Upper intervals. Due to the relatively thin nature of the Mt. Simon Sandstone at the project site, it has not been subdivided into smaller units (Figure 5).

The elevation map of the Mt. Simon Sandstone, which represents the top of the planned injection zone, shows the continuity of the unit across a wide region and that it deepens from Claimed as PBI feet in the southwest and center portion of the mapped area to more than Claimed as PBI feet in the east (Figure 12). Figure 13 shows the thickness of the Mt. Simon Sandstone to be slightly more than Claimed as P feet thick around the project site, and it regionally thins eastward toward the Appalachian Basin. Within the AoR, the Mt. Simon Sandstone thickness ranges between Claimed as PBI feet (Section 2.6.1 *Injection Zone and Confining Zone Extent and Thickness*).

2.2.3. Rome Formation (Primary Confining Zone) (Cambrian)

The Rome Formation conformably overlies the Mt. Simon Sandstone. Throughout portions of the Arches Province and Appalachian Basin, the Rome Formation is a complex sequence of carbonates, shales, siltstones, and sandstones (Janssens, 1973; Harris and Baranoski, 1997). These strata formed as a result of the transgression that deposited the Mt. Simon Sandstone continued throughout the Cambrian period (Saeed and Evans, 2012).

Specific to western Ohio, the Rome Formation is primarily microcrystalline dolomite with interbedded fine-grained clastics. Ooids, peloids, and pyrite are found throughout the formation (Calvert, 1962). It thickens eastward across Ohio and develops a sandy interval in west-central Ohio that is sandwiched between upper and lower dolomitic intervals (Janssens, 1973). Thin intervals of bioturbated shale and siltstone are also found within the Rome Formation (Saeed and Evans, 2012). The horizontal transition from the fine-grained clastics of the Eau Claire Shale to the dolomitic clastics of the Rome Formation and overlying Conasauga Formation occurs west of the Stonewell Project site (Figure 14; Janssens, 1973; Hansen, 1998b).

In portions of western Ohio, the Rome Silt forms the base of the Rome Formation, but this siltstone is not expected at the project site. The Rome Formation (above the siltstone where it exists) is a low porosity, tight microcrystalline dolostone. This lithofacies serves as a confining zone at the Ohio Liquids Disposal well (Vickery Environmental, Inc., 1989; Vickery Environmental Inc., 2020) and will be primary confining zone at the Stonewell Project site (Figure 5, Figure 6, and Figure 8).

Figure 15 shows that the Rome Formation deepens from Claimed as PBI feet in the southwest map area to over Claimed as PBI feet in the east. Figure 16 is a regional thickness map of the Rome Formation and shows that the rock is between Claimed as PBI feet thick in the mapped area. At the Stonewell Project site, the Rome Formation is expected to be more than Claimed as feet thick and will be described in more detail in Section 2.6.2 *Mineralogy, Diagenesis, Porosity and Permeability*.

2.2.4. Conasauga Formation (Cambrian)

The Conasauga Formation conformably overlies the Rome Formation. In west-central Ohio the contact between the formations (Figure 14) is observed where microcrystalline dolomite of the Rome Formation transition into interbedded, fine-grained glauconitic clastics of the Conasauga Formation (Janssens, 1973). In north-central Ohio the Conasagua Formation was deposited in a more proximal environment, and Banjade (2011) describes its lithology as mixed siliclastic and carbonate sediments based on core from the Ohio Liquids Disposal Well (approximately 50 miles north of the Stonewell Project site; Figure 8). In this well, the formation generally has an upward coarsening and thickening sequence of clastic beds with planar laminations, cross beds, flaser beds, massive beds, hummocky cross stratification, and ripple marks (Banjade, 2011). Banjade (2011) interprets shallow marine sedimentary structures and trace fossils of the lower Conasauga Formation to be consistent of an offshore, shallow shelf and pro-delta depositional environment. The sediment was sourced from the northwest and the lack of marine fossils in the upper section of the formation suggest the depositional environment shallowed to a marginal marine setting (Janssens, 1973; Michael C. Hansen, 1998; Saeed and Evans, 2012).

The transition of the Eau Claire Shale to the Conasauga and Rome Formations occurs west and south of the Stonewell Project site (Figure 14; Janssens, 1973; Hansen, 1998b). Section 2.6 *Injection and Confining Zone Details* describes the gradational sequence of the Conasauga Formation/Rome Formation/Eau Claire Shale primary confining zone at the BP Chemical 2 well in Richland Country, Ohio (approximately 50 miles west of the project site; Figure 7). This well is situated where the Eau Claire Shale of the Illinois Basin grades into the Rome and Conasauga formations, with the top of the Conasauga Formation being equivalent to the top of the Eau Claire Shale (Figure 14). The gamma-ray signature of the Conasauga Formation increases from the northeast (Ohio Liquids Disposal well) to the southwest (BP Chemical 2), and the bulk density logs decrease from northeast to southwest (Figure 8). The well log character in the Forry Evelyn and Gracely Farms 1 wells indicates that the Conasauga Formation at the Stonewell Project site is similar to that of the Ohio Liquids Disposal well. However, Forry Evelyn and Gracely Farms 1 wells have more dolomite in the Conasauga Formation compared to the Ohio Liquids Disposal well and more mixed siliciclastics and carbonates compared to the BP Chemical 2 well (Figure 8).

2.2.5. Kerbel Formation (ACZ Monitoring) (Cambrian)

The Kerbel Formation is an upward coarsening deltaic sandstone that conformably overlies the Conasauga Formation and will serve as the above confining zone (ACZ) monitoring interval for the Stonewell Project (Figure 5). This rock was sourced from the north and forms a north-south oriented deltaic lobe (Kerbel Delta) throughout central Ohio that reaches a maximum thickness of [redacted] feet in north-central Ohio (Janssens, 1973). The Kerbel Formation is absent in southern, extreme western, and eastern Ohio and dolomite content increases upward (Hansen, 1998). Gupta et al. (2017) determined that the Kerbel Formation has reservoir potential in northcentral Ohio where it is primarily a clean sandstone and correlates to the Gatesville Formation in western Pennsylvania (Janssens, 1973). The Kerbel Formation is prognosed to be [redacted] feet thick at the Stonewell Project site.

2.2.6. Knox Supergroup (Trempealeau Formation/Copper Ridge Dolomite/Knox Dolomite (Cambro-Ordovician)

Sediment deposition by the Kerbel Delta had stopped by the late Cambrian, which allowed for the deposition of carbonates of the Trempealeau Formation; this formation is also called the Copper Ridge Dolomite in portions of Ohio (Figure 5; Conner et al., 2016). The Trempealeau Formation/Copper Ridge Dolomite represents the beginning of an extensive interval of carbonate deposition across the Arches Province and adjacent areas (Wickstrom et al., 2005). These rocks are interpreted to have been deposited in a shallow marine carbonate shelf environment and are the basal strata of the Knox Supergroup (Figure 5; Komara, 2017). Carbonates and siliciclastics of the Knox Dolomite overly the Trempealeau Formation in western Ohio (Riley et al., 2002; Wickstrom et al., 2005).

The transition from passive margin deposition to the Taconic Orogeny convergent boundary created the Knox Unconformity and associated karst topography in the Early Ordovician (Figure 5). At the Stonewell Project site, the Knox Unconformity separates the passive margin carbonates from the overlying interbedded clastics and carbonates of the Wells Creek/Glenwood Shale/Gull River strata (Droste and Patton, 1985).

East of the project site in Morrow County in central Ohio, the Trempealeau/Copper Ridge Dolomite play is one of the most prolific hydrocarbon plays in the state's history. This play produces oil out of vugular, fractured dolomite that was created during the formation of the Knox Unconformity (Figure 5), with peak production occurring between 1963 and 1964 (Sutton, 1965). This play does not extend to Marion County, Ohio.

Wells Creek Formation/Glenwood Shale (Confining) (Ordovician)
The Middle Ordovician Wells Creek Formation directly overlies the Knox Unconformity at the project site and consists of a mixture of siliciclastics and carbonates, with dolomitic shale being the primary facies (Figure 5; Droste and Patton, 1985; Wickstrom et al., 2005). This rock was deposited in a shallow sea that transgressed following the uplift associated with the Knox Unconformity and can be differentiated into several members throughout the Midwest. At the Stonewell Project site, the Glenwood Shale is the basal unit of the Wells Creek Formation and will serve as an additional confining zone for the Stonewell Project (Droste and Patton, 1985; Wickstrom et al., 2005).

2.2.7. Black River Group/Gull River Formation (Ordovician)

The micritic to finely crystalline limestone of the Black River Group was deposited in subtidal to intertidal conditions (Figure 5; Wickstrom et al., 2005). This formation consists of lithographic limestone with sandstone, chert, and brown shales. The Gull River Formation is the basal interval of the Black River Group and is described as a relatively pure limestone with lenses of brown dolomite. Thin interbedded limestone is present in the upper section of the Black River Group, and bentonites at the top of the group are evidence that the Taconic Orogeny was increasing in intensity to the east (Drahovzal et al., 1992; Wickstrom et al., 2005). These rocks may be dolomitized near faults (Wickstrom et al., 2005).

2.2.8. Galena Group/Trenton Limestone (Ordovician)

Deepening of the sea resulted in the deposition of the marginal-platform to open-shelf facies of the Ordovician Trenton Limestone of the Galena Group (Figure 5). As a result of subsidence of the proto-Appalachian Basin and the early stages of the Taconic Orogeny, the end of deposition of the basal Trenton Limestone facies is marked by a change in depositional strike. This caused shallowing of the sea to the northwest and the deposition of thick carbonate platform facies of the Trenton Limestone over the Arches Province. These carbonates are further subdivided into the Curdsville, Logana, and Lexington Members in southwestern Ohio (Wickstrom et al., 2005).

The Trenton Limestone is a common hydrocarbon-bearing unit in the Midwest. In areas of western Ohio and eastern Indiana, the Trenton Limestone has produced hydrocarbons where it is dolomitized and has fracture/vuggy porosity (Wickstrom et al., 2005; Hickman et al., 2015). The Lima-Indiana Trend was first discovered in 1884 and led to Ohio being the leading oil-producing state at the turn of the twentieth century. This trend produces out of fractured, dolomitized Trenton Limestone/Black River Group strata, and much of the oil was produced in reservoirs associated with the Bowling Green Fault System (22 miles northwest of the project site), which will be further discussed in Section 2.3 *Regional Structure* (Division of Geologic Survey, 2004). No recoverable hydrocarbons have been observed in the Trenton Limestone strata in the area of the Stonewell Project site.

2.2.9. Utica Shale (Confining) (Ordovician)

The Utica Shale conformably overlies the Trenton Limestone at the project site and grades eastward into the limestone of the Point Pleasant Formation (Hickman et al., 2015). These rocks represent a regional sea level transgression that occurred across the eastern United States that resulted in a deeper, anoxic, interplatform depositional environment (Wickstrom et al., 2005; Hickman et al., 2015). The dark, organic-rich Utica Shale was deposited in a marine basin with low-energy and restricted circulation (Bergstrom and Mitchell, 1992). In the Appalachian Basin portion of eastern Ohio (Figure 3), the Utica Shale/Point Pleasant Formation are an unconventional play that produces oil and gas. This play is not found at the Stonewell Project site (Hickman et al., 2015).

2.2.10. Queenston Formation/Maquoketa Group (Confining) (Ordovician)

The red shale of the Queenston Formation is part of the Queenston Delta Complex, which is a regional clastic wedge that was deposited westward from the Taconic Orogeny and extends from Ontario to Alabama (Figure 5; Fisher and Nightengale, 2006; Hickman et al., 2015). This formation is the time equivalent of the Maquoketa Group in the Illinois Basin. In Ohio, it conformably overlies the Utica Shale and grades to the coarser clastics of the Juniata Formation eastward in the Appalachian Basin. It is interpreted to have been deposited in a mudflat environment that was periodically flooded during a eustatic regression (Wickstrom et al., 2005). The Queenston Formation will serve as an additional confining zone at the Stonewell Project site (Figure 5).

2.2.11. Clinton Formation and Cabot Head Shale (Silurian)

The Clinton Formation of the Medina Group (Figure 5) is composed of interbedded clastics that were deposited in the fluvial-deltaic environment that persisted to flow westward from the Taconic Highlands (Haneberg-Diggs, 2015). The Clinton Formation interfingers with and eventually transitions to the finer-grained marine clastics of the Cabot Head Shale in western Ohio (Knight, 1969). In eastern Ohio, the underlying organic-rich Utica Shale sourced hydrocarbons that migrated into the interbedded sand layers of the Clinton Formation. More than 80,000 wells have been drilled in this play, and the Clinton Formation is also used for natural gas storage or wastewater injection in these depleted reservoirs in eastern Ohio (M.C. Hansen, 1998). The Clinton Formation is not a significant reservoir in western Ohio and is often called the "Clinton Sand" by oil and gas drillers. This terminology also includes the overlying Dayton Formation/Packer Shell and Rochester Shale (M.C. Hansen, 1998; Haneberg-Diggs, 2015).

2.2.12. Dayton Formation/Packer Shell and Rochester Shale (Silurian)

A shallow sea transgressed over the study area during the Silurian, as recorded by the depositional transition of fluvio-deltaic sands to marine carbonates of the Dayton Formation (Clinton Group; Figure 5). This strata is primarily limestone, thickens eastward across Ohio, and is also called the "Packer Shell" in eastern Ohio (Haneberg-Diggs, 2015). As previously stated, oil and gas operators often integrate the Dayton Formation with the underlying Clinton Formation and the overlying Rochester Shale "Clinton Sand" clastics (Hansen, 1998). The Rochester Shale is a thin, dark gray, fossiliferous shale with interbedded carbonates and serves as seal to the Clinton Sand play in eastern Ohio (M.C. Hansen, 1998; Haneberg-Diggs, 2015). Together, the Dayton Formation, Packer Shell, and Rochester Shale are part of the Clinton Group (which does not include the underlying Clinton Formation; Figure 5).

2.2.13. Lockport Dolomite (Lowermost USDW) (Silurian)

The Lockport Dolomite represents a time of extensive shallow carbonate platform reef building that extended across northern and eastern Ohio (Figure 5, Hansen, 1998a). This dolomite is fossiliferous, slightly argillaceous, and develops porosity associated with patch reefs in the basal section. At the project site, the Lockport Dolomite is the lowermost underground source of drinking water (USDW) (Riley et al., 2012), and will be further discussed in 2.9.3 *Determination of Lowermost USDW*.

2.2.14. Tymochtee Dolomite/Greenfield Dolomite (Silurian)

The Tymochtee Dolomite of the Salina Group is the bedrock at the project site (Figure 5), which will be discussed further in Section 2.9 *Hydrologic and Hydrogeologic Information*. The Tymochtee Dolomite, in turn, is underlain by the Greenfield Dolomite. These strata are composed of dolomite with some shale interbeds and evaporite zones. The Salina Group is subdivided into seven units based on lithology in portions of eastern Ohio. It has also been used for underground mining, salt-solution mining, and propane storage within the salt-solution mines in eastern Ohio (Janssens, 1973; Wickstrom et al., 2005).

2.2.15. Undifferentiated Salina Group (Silurian)

The upper undifferentiated strata of the Salina Group occur just east of the project site (Figure 5). These strata are composed of interbedded dolomite, shale, and evaporites and subdivided into seven units based on lithology in portions of eastern Ohio. It has also been used for underground mining, salt-solution mining, and propane storage within the salt-solution mines in eastern Ohio (Janssens, 1973; Wickstrom et al., 2005). Generally, in the area of the project site the Salina Group is mapped as undifferentiated, so while there are seven distinct units recognized in eastern Ohio, in the northwestern part of the state the Salina Group is primarily microcrystalline dolomite (Janssens, 1973). The undifferentiated Salina Group will be discussed further in Section 2.9 *Hydrologic and Hydrogeologic Information*.

2.2.16. Quaternary Sediments

Ohio experienced numerous glacial intervals during the Quaternary Period, and glacial processes and post-glacial streams deposited up to 700 feet of sediment throughout northern and western Ohio with greatest thicknesses occurring in bedrock valleys (Figure 5, Division of Geologic Survey, 2017). Specifically, the Stonewell Project site is located on Wisconsinan Woodfordian glacial deposits composed of various moraine and outwash deposits. These deposits will be discussed in detail in Section 2.9 *Hydrologic and Hydrogeologic Information*.

2.3. Regional Structure

The structural geology of the Stonewell Project region has been influenced by changes in tectonic regimes from the Precambrian to present times. The Stonewell Project site is within the Arches Province, a tectonically stable region, which is defined by three radiating Precambrian arches (Kankakee, Findlay, and Cincinnati) that divide the Michigan, Illinois, and Appalachian Basins (Figure 3). The project site is on the eastern flank of the Findlay Arch (Figure 3 and Figure 4). The Precambrian rocks forming the arches are separated from the overlying Paleozoic strata by an extensive unconformity.

The Precambrian Basement in western Ohio is a stable, largely crystalline, tectonic assemblage associated with the amalgamation of the proto–North American continent. In this region, the basement can be divided into three domains of differing origins: 1) the EGRP, 2) the ECRS and the FWR, and 3) the Grenville Province. See Section 2.2.1 *Precambrian Basement Complex* for a description of the Precambrian Basement in western Ohio. The Precambrian Basement underlying the Stonewell Project site is the Grenville Province.

The Grenville Front is approximately 19 miles west of the Stonewell Project site and represents a regional, north-south oriented tectonic zone associated with the Mesoproterozoic Grenville Orogeny (Baranoski et al., 2009; Figure 10 and Figure 17). This front marks an approximate boundary of the EGRP/ECRS to the west and the Grenville Province to the east. At this boundary, the Grenville Province rocks were thrust over the EGRP and ECRS terrains in a present-day west-northwestward direction, causing the Grenville Province Basement to be found in areas west of the actual structural front (Figure 17; Wickstrom et al., 2005).

In western Ohio and southern Michigan, the Grenville Front thrust is hypothesized to be expressed at the surface by the Bowling Green Fault System. The fault system is also 19 miles west of the project site and has been mapped from surface exposures and subsurface data (Figure 10 and Figure 17; Onasch, 2007). The system is interpreted to be a series of faults that extend to the Precambrian Basement with both strike-slip and dip-slip motion (Wickstrom et al., 1992). Vertical offset varies from 400 feet in the northern extent to less than 100 feet in southern (Onasch, 2007). The Maumee Fault is a northeast-southwest trending fault that is approximately 60 miles northwest of the project site (Figure 17). This fault obliquely intersects the Bowling Green Fault System and is interpreted to be a left-lateral strike-slip fault associated with the Grenville Front and Bowling Green Fault System (Wickstrom et al., 1992).

The Bowling Green Fault System has likely influenced the stratigraphic evolution of western Ohio, as well as fluid flow through the strata of the region (Onasch, 2007). Solution collapse, dolomitization, and mineralization within and around the fault system suggest that it locally focused the flow of subsurface fluids (Onasch, 2007). Much of the oil produced from the Lima-Indiana Trenton Limestone play was produced from reservoirs associated with the dolomitization of the Trenton Limestone around the Bowling Green Fault System (Section 2.2.8 *Galena Group/Trenton Limestone*). Along with providing a pathway for the localized dolomitization of the Trenton Limestone reservoir, the Bowling Green Fault System created both stratigraphic and structural trapping mechanisms (Wickstrom et al., 1992).

The Marion Fault is a northwest-southeast trending fault approximately one mile southwest of the project AoR and is also interpreted to be part of the Bowling Green Fault System (Figure 17; Onasch, 2007; Section 2.4 *Maps and Cross Sections of the AoR*). The Marion Fault will be described in detail in Section 2.5 *Faults and Fractures.* The Outlet, Tiffin, Crawford, and Harlem faults also all have a similar northwest-southeast trend as the Marion Fault, and several other unnamed faults with similar orientations have been mapped in the area. Relatively little Precambrian offset is observed at the Crawford and Harlem faults, although the basement structure becomes complex at the intersection of the Tiffin Fault and an unnamed west-east trending fault (Figure 17).

The Outlet Fault is a synthetic shear zone within the Bowling Green Fault System (Figure 17, Wickstrom et al., 1992). Well core collected near the Outlet Fault shows that the Trenton Limestone is extensively fractured, although the core was fractured to a lesser extent than at the main branch of the Bowling Green Fault System to the west. In addition, vertical offset along the Outlet Fault is minimal and hydrocarbon trapping mechanisms along the fault are equivalent to that along the Bowling Green fault system (Wickstrom et al., 1992).

The northeast-southwest trending Auglaize Fault is approximately 25 miles west of the project site. It is associated with the ECRS and is not exposed at the surface (Figure 17). The Auglaize Fault is interpreted to crosscut the Fort Wayne Rift of the ECRS (Wickstrom et al., 1992; Baranoski et al., 2009), although the offset and western extent of this feature is questionable.

The Anna-Champaign, Logan, and Bellefontaine Outlier faults, as well as numerous unnamed faults of northwest-southeast orientation, are mapped just south of the Auglaize Fault (Figure

17), though none of the faults have a clear surface expression. These faults were identified in a regional east-west Consortium for Continental Reflection Profiling (COCORP) seismic reflection profile that was collected in 1987 (Baranoski et al., 2009). This profile and additional data demonstrate that there is up to 100 feet of vertical displacement along the faults and the Mt. Simon Sandstone is absent on individual fault blocks. These faults are interpreted to be associated with the Anna Seismic Zone, which will be discussed in Section 2.8 *Seismic History* (Ruff et al., 1994).

High density, two-dimensional (2D) seismic data acquired specifically for the Stonewell Project indicates there are no significant structural features identified within the project's AoR that would impact CO_2 sequestration and containment. The 2D seismic data is discussed in detail in Section 2.5 *Faults and Fractures*. The structural features listed above are significantly removed from the project area and are not considered impactful to carbon sequestration operations.

2.4. Maps and Cross Sections of the AoR[40 CFR §146.82(a)(2), §146.82(a)(3)(i)]

Figure 18 shows the AoR for the Stonewell Project which is defined by the maximum extent of the critical delta pressure front. The AoR also encompasses the maximum extent of the CO_2 plume over 62 years (Attachment 02: AoR and Corrective Action Plan, 2025). Figure 18 includes all existing wells within the area. The input data and physical processes incorporated into Stonewell Project static and computational models, as well as methodology used to delineate the AoR, are described in the AoR and Corrective Action Plan (Attachment 02: AoR and Corrective Action Plan, 2025).

The Mt. Simon Sandstone is the injection zone, and the Rome Formation is the primary confining zone. Both formations extend laterally beyond the AoR limits. This is demonstrated by the regional thickness maps (Figure 13 and Figure 16), the cross sections shown in Figure 6 and Figure 8, and 2D seismic data discussed below (Figure 19, Figure 20, Figure 21, Figure 22, Figure 23, Figure 24, Figure 25, Figure 26, Figure 27, Figure 28, Figure 29, Figure 30, Figure 31, Figure 32, Figure 33, Figure 34, Figure 35, Figure 36, and Figure 37).

The strata of the Mt. Simon Sandstone and the Rome Formation are thick with no evidence of stratigraphic pinch-out within the AoR. Claimed as PBI [redacted] Additionally, there is no indication that structural trapping by faults or domes could occur within the AoR.

2D seismic data (Figure 19, Figure 20, Figure 21, Figure 22, Figure 23, Figure 24, Figure 25, Figure 26, Figure 27, Figure 28, Figure 29, Figure 30, Figure 31, Figure 32, Figure 33, Figure 34, Figure 35, Figure 36, and Figure 37) that was acquired specifically for the Stonewell Project indicate the Mt. Simon Sandstone and Rome Formation strata are laterally continuous, and there are no faults are observed to transect the primary confining zone or the top of the Mt. Simon

Sandstone injection zone in the Stonewell AoR (Section 2.5 *Faults and Fractures*). Faults are not expected to impact injection or containment (Section 2.5 *Faults and Fractures*).

The Silurian Lockport Dolomite is the lowermost USDW within the AoR. The top of the USDW is prognosed at [redacted] feet depth, and its base is approximately [redacted] feet above the top of the Rome Formation confining zone at the Stonewell Project site (Section 2.9.3 *Determination of Lowermost USDW*). There are no structural features or faults observed to intersect the Lockport Dolomite in the AoR. As described in Section 2 *Site Characterization*, there are several additional confining zones between the Rome Formation and the Lockport Dolomite in the AoR.

Within the AoR, there are no active oil and gas wells. A permit was filed in 1984 to drill the James E. Needs #1 well (UWI 34101201700000) in Sec 9 of Big Island Township in Marion County. The permit expired and the well was never drilled according to the Ohio Department of Natural Resources Division of Oil and Gas public database (Ohio Division of Geologic Survey, 2004). The latest water well data search indicates that 167 groundwater wells are located within the Stonewell AoR; well depths range from 55 fbgl to 255 fbgl with an average depth of 102 fbgl (Figure 18).

There are no existing wells that penetrate the primary confining zone in the AoR at the Stonewell Project site.

2.5. Faults and Fractures [40 CFR §146.82(A)(3)(ii)]

Figure 19 shows the location of ten 2D seismic lines and [redacted] miles of data that were acquired to characterize the subsurface within the Stonewell Project AoR and to provide information regarding surface structure and stratigraphy. Four of the seismic lines fully traverse the AoR (Lines 63, 83, 27, and 309) and three of these lines (1, 2, and 26) are partially located within the AoR. Lines 3, 231N, and 231S are located to the east of the AoR (Figure 19). The synthetic seismogram and the seismic lines used for interpretation are shown in Figure 20, Figure 21, Figure 22, Figure 23, Figure 24, Figure 25, Figure 26, Figure 27, Figure 28, Figure 29, Figure 30, Figure 31, Figure 32, Figure 33, Figure 34, Figure 35, Figure 36, and Figure 37. The vertical seismic sections are shown in two-way-time (TWT).

A high density 2D seismic program was acquired with a vibrator truck on roadways in March 2024 and March 2025 (Figure 19). The vibrator truck used a 4-120Hz broad band sweep of 20 second duration as the seismic source for these data. A source and receiver spacing of 40 feet was used to enable high density processing to identify both shallow and deep subsurface features. Long offsets were obtained to enable additional inversion work to identify any lithological changes at target.

The west-east oriented seismic lines that fall within the AoR, Line 26 (Figure 21), Line 27 (Figures 22 and 23), Line 1 (Figure 24), and Line 309 (Figure 25), all indicate that the Paleozoic stratigraphy is laterally continuous, gently dipping to the northwest, and generally undeformed within the AOR. These seismic lines show localized minor dip changes in the Mount Simon Sandstone interval where the stratigraphy thickens as it infills the pre-existing Precambrian paleo-topography. The Mt Simon Sandstone seismic stratigraphy also shows onlap onto the Precambrian unconformity at the edges of the thickness changes indicating these are

sedimentological and not structural in origin. The overlying Rome, Conasauga and Kerbel formations are mainly horizontal with a gentle, regional northwest dip. In these strata, minor thickness changes occur above the areas where Mt Simon Sandstone infills Precambrian topography Claimed as PBI

The remaining west-east oriented 2D lines fall outside the AOR and show similar regional stratigraphic continuity and structure with faulting encountered in Line 231 N (Figure 31), and one fault in Line 3 oriented NW-SE (Figure 33). Each of the interpretated faults will be described in detail in Sections 2.5.1 *Faults* and Section 2.5.2 *Fault Orientation*.

Paleozoic strata for the north-south oriented seismic lines 63 (Figure 27), 83 (Figure 28), 2 (Figure 29), and 231S (Figure 32) show a gentle northwest dip as well as localized thickening and thinning of the Mt Simon Sandstone due to infilling of the pre-existing Precambrian topography. Claimed as PBI

This is demonstrated by the onlapping of Mt. Simon Sandstone reflectors to the Precambrian surface. All of the seismic lines also show that seismic reflectors above the Mt. Simon Sandstone are relatively parallel and continuous until ~75 ms (TWT) where more variability in the strata is observed. Lateral discontinuities are not observed in the Paleozoic reflectors, which indicates that the Paleozoic strata have not been faulted.

2.5.1. Faults

There are no faults that transect the injection zone mapped within the Stonewell Project AoR.

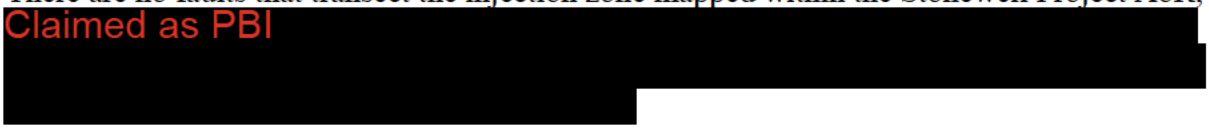

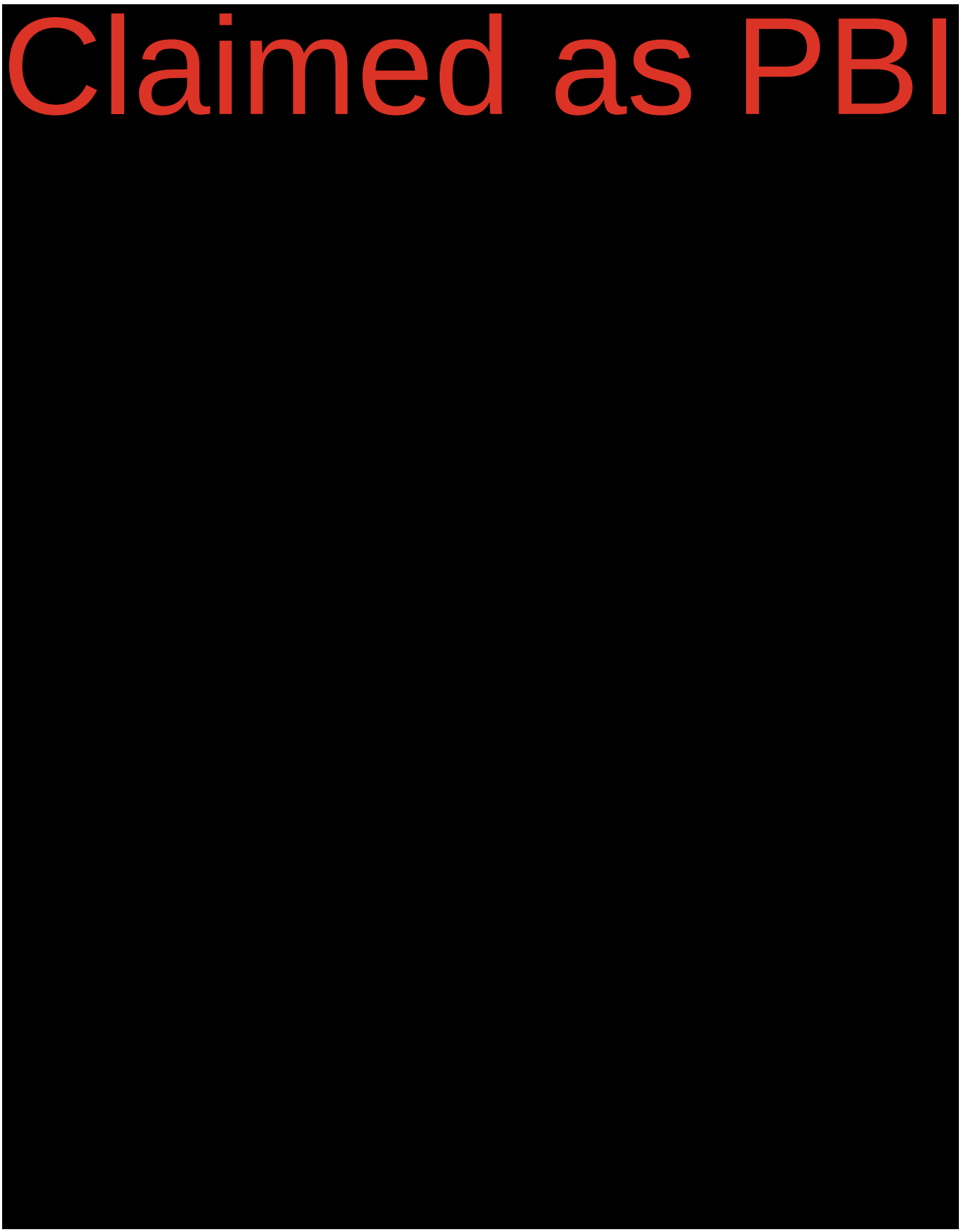
Claimed as PBI

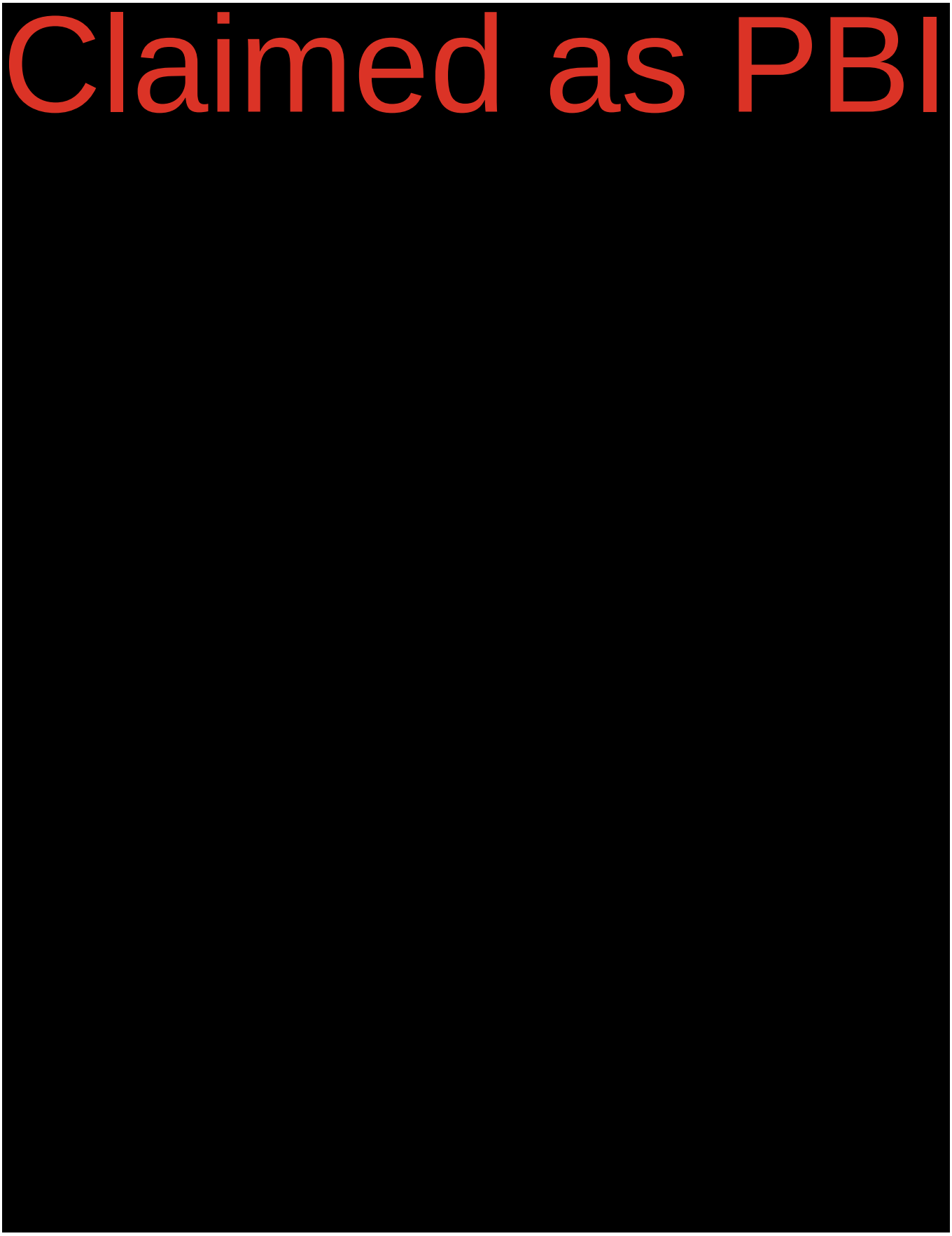
Claimed as PBI

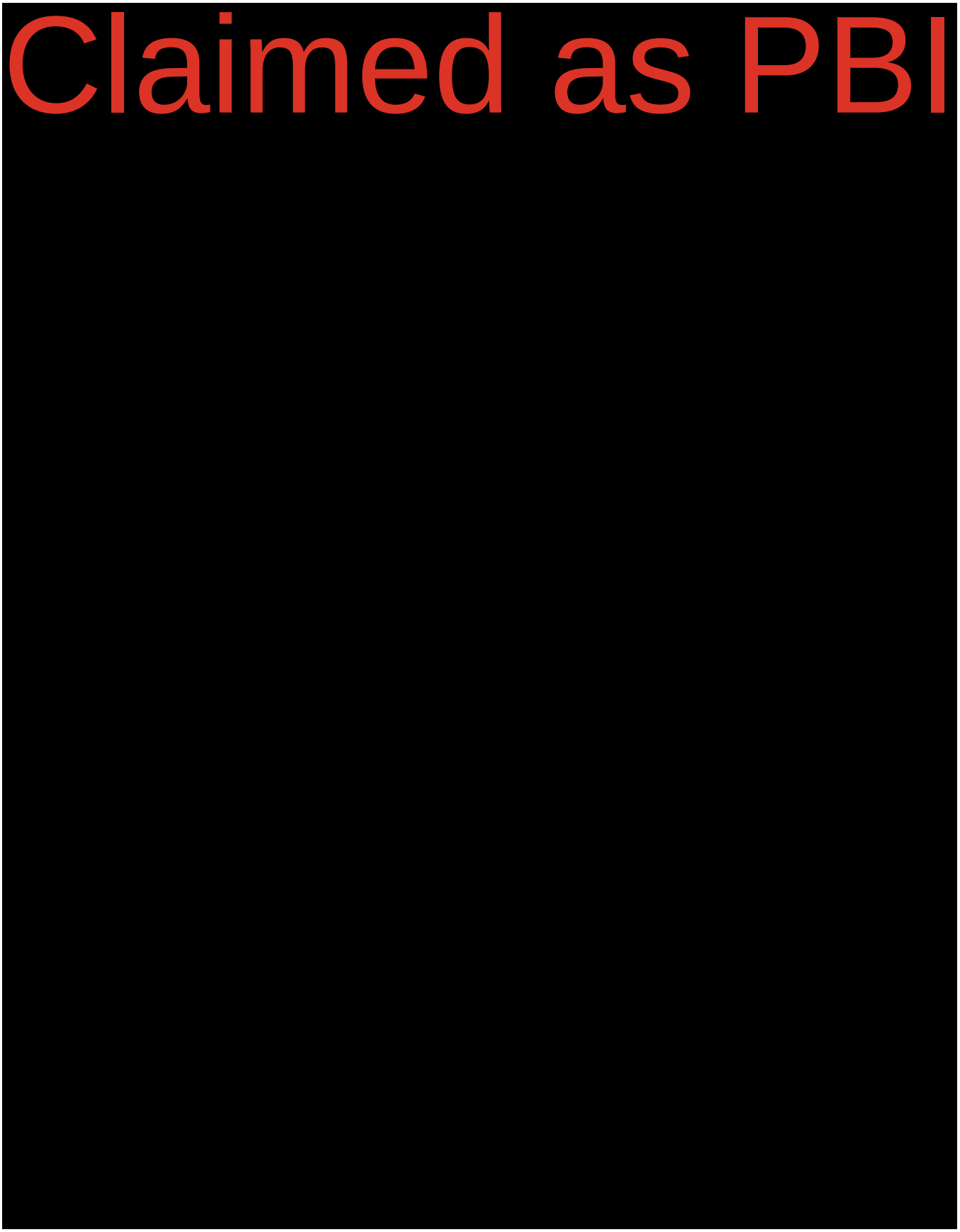
Claimed as PBI

2.5.2. Fault Orientation

At the project site, the Precambrian Basement is separated from the overlying Cambrian Mt. Simon Sandstone by an unconformity that spans hundreds of millions of years. The 2D seismic survey described in Section 2.5 *Faults and Fractures* was used to identify faults and interpret fault orientation. In addition, publications on regional faults in western Ohio were used to interpret fault orientations in the 2D seismic (Drahovzal et al., 1992; Baranoski et al., 2009; Baranoski, 2013). This methodology provides fault orientation, as well as a range of likely orientations for faults identified in the seismic data.

2.5.2.1. Seismic Interpretations

2.5.2.2. Regional Fault Interpretations

Several published papers note faults in the region, including a Precambrian Basement structure map published by Baranoski (2013; Figure 40). Most of the faults in the region are inferred by magnetic, gravity, well contour, and contour residual techniques, though several faults were interpreted from 2D surveys (Onasch, 2007; Baranoski et al., 2009; Fakhari, 2016; Bloxson and Valdez, 2024). Most of the interpreted faults have strikes that range between 116° and 182° degrees with a peak frequency of approximately 145° (Figure 41).

Regionally, the orientation of basement structures interpreted from magnetic and gravimetric surveys also support the orientation of faults interpreted near the project area where is composed of Grenville-aged rock. The Eastern Granite Rhyolite Province (EGRP) is to the west of the project site (Figure 9) and is dominated by older Keweenawan Basement features. Basement rocks to the east of the project site in the Appalachian Basin primarily have Iapetan-aged basement features (Figure 42). Grenville-aged basement features interpreted at this larger scale (which includes the regional faults in Figure 41) have an equivalent orientation range to those faults interpreted in the 2D seismic survey.

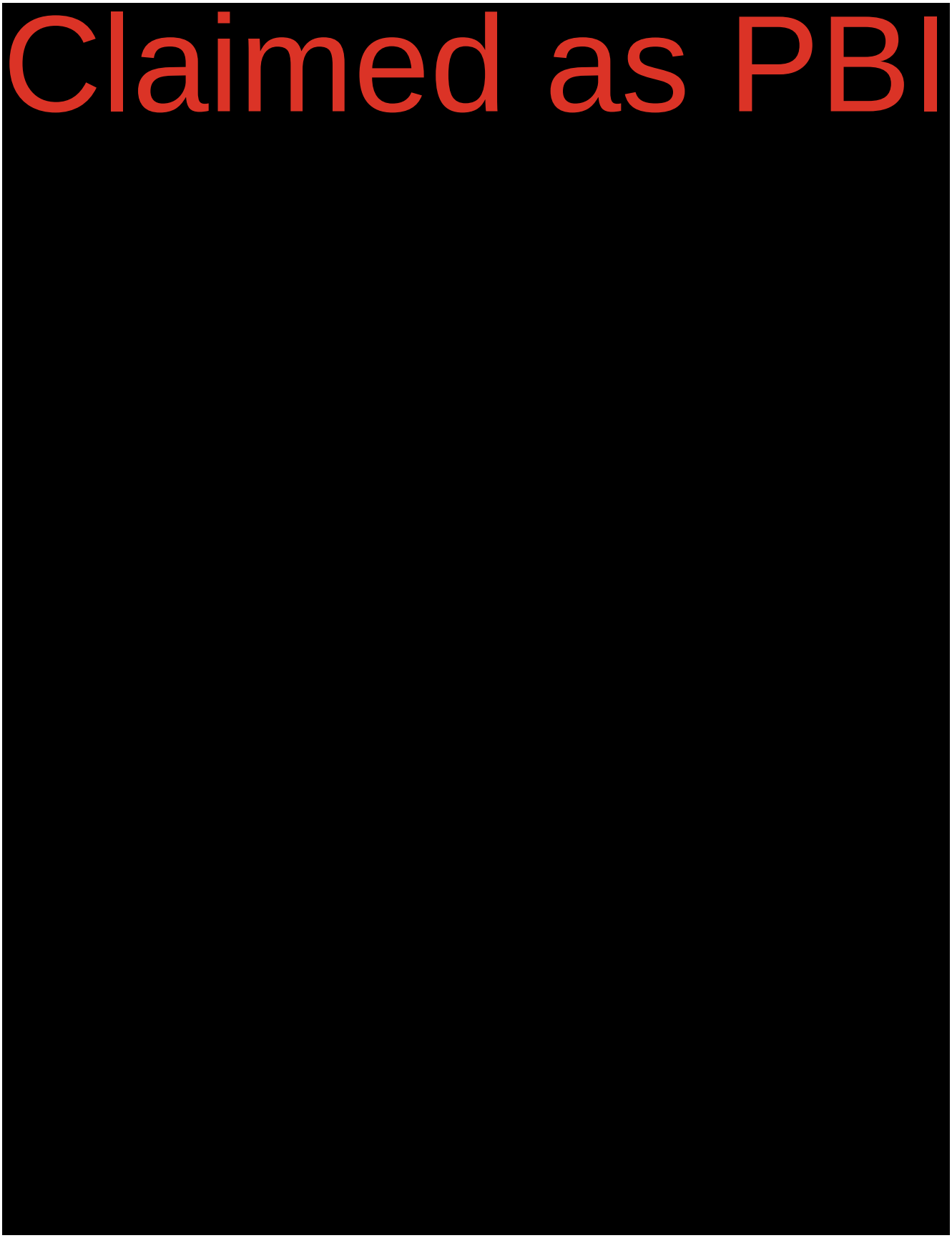
Claimed as PBI

Claimed as PBI

2.5.4. Fault Slip Analysis

Claimed as PBI

2.5.4.1. Delta Pressure

Table 5 shows the list of values from the 1D MEM used in this analysis. Based on Byerlee's law, the friction angle used was $\mu = 0.6$ ($0.6 \leq \mu \leq 1.0$; Byerlee, 1978) to introduce slip at the lowest increase in pore pressure. Cohesion has a value of zero, which is a conservative approach that does not allow for any increase in fault strength due to alteration of the fault plane. Fault orientations were taken from the 2D seismic interpretations (Table 4 and Figure 45) and regional data (Figure 41) and given a range in the sensitivity analysis to account for interpretation uncertainties. Pore pressure was determined in the 1D MEM and is within the range or values expected for normally to slightly under-pressured reservoirs (0.415 psi/ft +/- .025). Thermal variations were not considered in this iteration.

The 1D MEM construction (Section 2.5.5 *Mechanical Earth Model*) outlines the data and assumptions used in the construction of the 1D MEM, as well as the resulting stress tensor used

in the analysis. Table 5 shows the list of values from the 1D MEM used in this analysis. Regional maximum stress orientation is 065° / 245° and was derived from the World Stress Map (Heidbach et al., 2016) and additional information from Hurd and Zoback 2012). The regional fault type is strike- slip ($S_{Hmin} < S_v < S_{Hmax}$). The friction angle used was $\mu = 0.6$ and was based on Byerlee's Law ($0.6 \leq \mu \leq 1.0$) to introduce slip at the lowest increase in pore pressure. Cohesion was assigned a value of zero, which is a conservative approach and does not allow for any increase in failure stress due to fault morphology or lithology.

FSP 2.0 is fault slip potential modeling software and was used to transform the three-dimensional (3D) stress tensor field defined by the 1D MEM to shear and normal stress on individual fault plane orientations. It was also used to calculate the increase in pore pressure required to critically stress a fault plane. This software uses Monte Carlo analysis of the parameters and range of values for the parameters to determine probability cases for the slip potential and the sensitivity of pore pressure to changes in the individual parameters. Figure 46 shows the input variables and ranges, as well as a graphical representation of the delta pressure required for a fault to slip at a given pressure (fault slip potential). Table 6 lists fault orientations used and the probability (P1, P50, and P90) and the probability if a given delta pressure to cause fault slip. The P50 values are the deterministic values for fault slip potential using the interpreted fault orientations and inputs (Table 5, Table 6, Figure 41, and Figure 45), and the P1 and P99 representing the minimum and maximum delta pressure required to slip the faults (Figure 46).

2.5.4.2. Delta Pressure Potential at Faults

Reservoir simulations were performed using the planned injection parameters to obtain a 3D pressure profile during and after CO_2 injection (Attachment 02: AoR and Corrective Action Plan, 2025). The resultant model was used to derive a change in pressure (delta pressure) at the top and base of the Mt. Simon Sandstone versus distance from the injector (Figure 47). Three radial profiles were used for this exercise (Figure 48).

2.5.4.3. Delta Pressure at the top of the Mt. Simon Sandstone

2.5.4.4. Delta Pressure at the base of the Mt. Simon Sandstone

Claimed as PBI

2.5.4.5. Fault Seals

Claimed as PBI

2.5.4.6. Fractures Associated with Faults

Claimed as PBI

2.5.5. One Dimensional Mechanical Earth Model

A one-dimensional mechanical earth model (1D MEM) is a collection of measurements, calculations, and models used to characterize the mechanical properties of rocks and rock disparities (fractures and faults), as well as the pressures and stresses acting on them at depth. For the purposes of this investigation, the relevant data and thus the extent of the 1D MEM encompasses principal stress orientations, principal stress magnitudes, and affecting conditions.

2.5.5.1. Principle Stress Orientations

Current stress indicators (focal mechanisms, stress inversions, and borehole studies presented by Hurd and Zoback (2012) identify the region at and around the Marion Project site as a strike-slip domain. Specifically,

$$SHmax > Sv > Shmin \quad (1)$$

$SHmax$ is the maximum horizontal stress, Sv is the vertical stress, and $Shmin$ is the minimum horizontal stress. These three stresses are mutually perpendicular to each other, and the stresses are aligned with the three principal stress axes (s_1, s_2, s_3) in the earth ($SHmax = s_1$, $Sv = s_2$ and $Shmin = s_3$). Claimed as PBI

2.5.5.2. Principle Stress Magnitudes

Vertical stress (Sv), minimum horizontal stress ($Shmin$), and maximum horizontal stress ($Shmax$) were calculated using the methodologies described below.

2.5.5.3. Vertical Stress (Sv)

Claimed as PBI

2.5.5.4. Minimum Horizontal Stress (Shmin)

Minimum horizontal stress for the model utilized petrophysical calculations of closure stress for three wells in the region (Forry Evelyn, Gracely Farms 1, Gracely Farms 2) and normalizing the stress values to a gradient at the Mt. Simon Sandstone level (Section 2.7 *Geomechanical and Petrophysical Information*). This methodology uses Lacy's equation (Lacy, 1997) to convert a dynamic Young's modulus to a static modulus and a modified uniaxial strain equation (Barree et al., 2009) to determine closure stress. From these results, a minimum stress gradient and deviation was calculated at the Mt. Simon Sandstone interval for each well (Figure 50) providing an average and range for the minimum horizontal stress gradient in the region (Table 7).

2.5.5.5. Maximum Horizontal Stress (Shmax)

There is insufficient data to directly calculate a maximum horizontal stress. Instead, the Mohr Coulomb theory is used to determine an upper limit for the maximum horizontal stress assuming a critically stressed crust. This uses the methodology outlined in Zoback (2010), which in turn builds on Jaeger and Cook (1971), and demonstrates that where a critically stressed fault is at the frictional limit:

$$\frac{\sigma_1}{o_3} = \frac{S1-P_P}{s_3-P_p} = \left[(\mu^2+1)^{\frac{1}{2}} + \mu\right]^2 \quad (3)$$

where σ_1 is the maximum effective stress, σ_3 is the minimum effective stress, S_1 is the maximum stress, S_3 is the minimum stress, Pp is the pore pressure, and μ is the coefficient of friction. From Heidbach et al. (2016) and Hurd and Zoback (2012), the region is a strike-slip fault regime (Anderson's faulting theory) so that $S_1 = S_{Hmax}$, $S_2 = S_v$, and $S_3 = S_{hmin}$. Equation 3 can then be written as a limit for SHmax where:

$$\frac{SHmax-Pp}{Shmin-Pp} \leq \left[(\mu^2+1)^{\frac{1}{2}} + \mu\right]^2 \quad (4)$$

If a conservative value for the coefficient of friction is assumed (m = 0.6) and the calculated valued for Shmin in the region (2.5.5.2 *Principle Stress Magnitudes*), the equation can be simplified as a maximum value for SHmax:

$$SHmax = 3.1(Shmin - Pp) + Pp \quad (5)$$

Using this equation, the upper limit of *SHmax* was calculated, as well as the maximum stress gradient and deviation at the Mt. Simon Sandstone interval for each well. This provides an average and range for the minimum horizontal stress gradient in the region (Table 7).

2.5.5.6. Pore Pressure

Pore pressure was determined using an average of calculated pore pressure gradients from wells with geomechanical analysis in the region (Figure 43) and weighted by both the distance from the project site and structural similarity. Claimed as PBI [redacted]

2.5.5.7. Model Outputs

Table 7 is the numeric outputs of the 1D MEM expressed as gradients, which were used as inputs for the fault slip potential modeling described in Section 2.5.4 *Fault Slip Analysis*. Conservative calculations were used to define upper boundaries rather than to calculate exact values. These results increase confidence that calculated failure pressure limits used in the fault slip analysis are minimum limits and likely underestimate the increase in pore pressure required to critically stress a fault.

2.5.6. Data Gaps

As the current seismic data is comprised of 2D seismic surveys, uncertainty remains regarding fault orientation (dip and azimuth) and whether areas without 2D coverage contain uninterpreted faults. A 3D seismic survey would provide better characterization of fault orientation and possibly identify any faults in areas not covered by the existing 2D survey. Additionally, the 3D survey will provide a data source for various inversion techniques that may assist analyzing for fractures within the AoR. Additional fracture data may also be derived from micro-resistivity imaging logs, which will help better constrain the stress values used in the 1D MEM. In addition to image logs, extended leak off tests performed on the injection zone will provide additional data for constraining stress (specifically *Shmin*) and pore pressure values in the mechanical earth model.

2.5.7. Impact on Containment

Based on the analysis and interpretation of the seismic data, faults are not observed to transect the injection and primary confining zones in the Stonewell AoR. This is supported by the nearly flat geometry of the stratigraphy and the continuity of individual seismic reflector within the injection and primary confining zones as described in detail in at the start of Section 2.5 *Faults and Fractures*. The lack of formation top offset within the Stonewell Project AoR supports the interpretation that faults do not transect the primary confining zone within the AoR.

Structures are also interpreted in the Precambrian Basement within the AoR (Figure 48). These structures are not expected to impact containment upward. Downward migration along the faults would be under the same conditions outlined in the geomechanical analysis (Section 2.7.1 *Geomechanics*) and as such would not be under consideration to re-activate. In addition to the calculated pressures needed to reactivate a fault, the increased pressure with depth would also have to be overcome to transmit fluids downward. Minor faults identified in seismic data collected for other CO_2 sequestration projects in the Midwest suggest that minor faults in the Precambrian and Mt. Simon Sandstone strata are not expected to act as conduits through the confining zone (Greenberg, 2021) and present no endangerment to USDWs.

A baseline 3D surface seismic survey will be conducted at the Stonewell Project site as part of the Pre-operational testing program (Attachment 05: Pre-operational Testing Program, 2025). The baseline data will be used to augment the existing 2D seismic surveys to confirm structural orientations, interpretations around fault-slip behavior, and evaluation of storage and containment. The data gathered during the pre-operational phase of the project will be used for further geomechanical modeling to evaluate fault and fracture stability during the injection phase of the project

2.5.8. Tectonic Stability

The Stonewell Project site is central within the North American craton, where a relatively thin sedimentary layer overlying a thick crystalline basement makes up the continental lithosphere. This intraplate setting is thousands of miles from the nearest active plate margin, is considered very tectonically stable, has a very low probability of natural seismic activity above M2.5, and has a very low relative frequency of discrete, natural tectonic events. Section 2.8 *Seismic History* includes a detailed discussion about earthquakes near the Stonewell Project site.

The 2D seismic data acquired for the project demonstrate that there are no interpreted faults that transect the Rome Formation within the Stonewell Project AoR. The eight faults interpreted around the AoR, as well as structures confined to the Precambrian Basement within the AoR, will not experience critically stressed conditions due to injection operations at STO INJ1, as indicated by the fault slip analysis (Section 2.5.4.2 *Delta Pressure Potential at Faults*) The orientation of the mapped faults relative to the current day principal stress do not allow for activity under any conditions foreseen during the life of the project and demonstrate that under static conditions, the faults are currently very stable.

Given these conditions, the Stonewell Project site is currently tectonically stable and will remain so under the dynamic conditions introduced through injection operations.

2.5.9. Addressing Uncertainty

A 3D surface seismic survey will be acquired for the project prior to submitting the Pre-Operational Narrative to evaluate injection and primary confining zone properties, map Precambrian Basement topography, and characterize any identifiable basin fill or faults. Detailed mapping and attribute analysis with this dataset will be used to confirm the lack of large-scale faulting within the AoR. The 3D surface seismic survey will be designed to obtain full fold data over the predicted extent of the CO_2 plume after 12 years of injection and proposed 50-year Post-injection Site Care and Site Closure (PISC) period to provide an indirect measurement of CO_2 plume migration over time (Attachment 06: Testing and Monitoring, 2025; Attachment 08: Post-injection Site Care and Site Closure, 2025).

As detailed in (Attachment 05: Pre-operational Testing Program, 2025), 4-inch core and geophysical logs, which include sonic and image logs, will be acquired while drilling the STO INJ1 well. These will be used to assess the nature of identifiable fractures and their impact on long-term integrity of the primary confining and injection zones.

The static model will be updated with the 3D seismic data and well analyses, and a Pre-operational Narrative will be submitted to the EPA that will provide the new data and updated static and computational models. Narrative text, maps, and cross sections related to faults and fractures will be updated with the new data.

2.6. Injection and Confining Zone Details [40 CFR §146.82 (a)(3)(iii)]

2.6.1. Injection Zone and Confining Zone Extent and Thickness

The Mt. Simon Sandstone is the injection zone for the Stonewell Project. Computational modeling indicates that the injected CO_2 will remain in the Mt. Simon Sandstone (Attachment 02: AoR and Corrective Action Plan, 2025). The Rome Formation will be the primary confining zone for the Stonewell Project (Figure 5). Regional characteristics of the injection and confining zones are also described in Section 2.2 *Regional Stratigraphy*.

Available public data were collected and integrated to develop site-specific subsurface maps, petrophysical relationships, and a static model of the Stonewell Project site. Within the Stonewell Project AoR, the injection zone thickens to the east (Figure 38) and there are minor elevation variations at the top Mt. Simon Sandstone (Figure 12). The Rome Formation primary confining zone does not exhibit significant elevation and thickness variations (Figure 15, Figure 16, and Figure 39).

Claimed as PBI [redacted] herefore, CO_2 plume development is expected to be controlled dominantly by sedimentological heterogeneities within the injection zone resulting from lithological variations and diagenetic processes.

Analysis of geophysical log response, core descriptions, and mineralogy of Ohio Liquid Disposal and BP Chemical 2 wells (Section 2.6.2 *Mineralogy, Diagenesis, Porosity, and Permeability*) confirmed that the most significant controls on lithofacies variation and heterogeneity for the Mt. Simon Sandstone and Rome Formation were compaction, dolomitization, feldspar dissolution and consequent creation of secondary porosity. These processes are discussed in detail in Section 2.6.2 *Mineralogy, Diagenesis, Porosity, and Permeability*. Density logs and the resulting effective porosity logs (Section 2.7.2 *Petrophysics*) best capture lithofacies variations in the injection and primary confining zones. Six clastic to dolomitic facies (dolomite, tight dolomitic clastics, shale, tight siltstone/sandstone, quartz sandstone, and arkosic sandstone) were defined for the key petrophysical wells. Effective porosity logs of nearby wells were the input for the geostatistical property modeling described in Attachment 02: AoR and Corrective Action Plan (2025), which adequately captures depositional and diagenetic facies variations (Section 2.6.2 *Mineralogy, Diagenesis, Porosity, and Permeability*). The primary confining zone will provide a laterally extensive barrier to prevent upward migration of injection zone fluids over time.

2.6.2. Mineralogy, Diagenesis, Porosity, and Permeability

Public log and core information from four key wells in Ohio provide significant data that has been used to characterize the injection and primary confining zones at the Stonewell Project site. Available wells that penetrate the Mt. Simon Sandstone or deeper are from UIC Class I sites and O&G wells that have well logs, core, and fluid injection data from the Mt. Simon Sandstone and Rome Formation (Figure 51). The Forry Evelyn well (UWI 34101202070000) is approximately 3.5 miles northeast of the Stonewell Project site and represents the closest complete analog for the injection and confining zones. The Gracely Farms 1 well (UWI 34101201680000) is approximately 5 miles south of the site and also serves as a geologic analog for the storage system, though it does not penetrate the entire thickness of the Mt. Simon Sandstone (Figure 51). These nearby wells are discussed in more detail in Section 2.7.2 *Petrophysics*.

Additional wells used for characterization are the Ohio Liquids Disposal well (UWI 34143202370000) and the BP Chemical 2 well (UWI 34003200670000); both are UIC Class I wells that use the injection zone for disposal (Figure 51). The Ohio Liquids Disposal well is in Sandusky County, Ohio approximately 50 miles north of the project site, and the confining zone strata for that well are the Rome and Conasauga formations, as well as beds within the Knox Group. The BP Chemical 2 well is in Richland Country, Ohio, approximately 50 miles west of the project site. This well is situated where the Eau Claire Shale of the Illinois Basin begins grading into the Rome and Conasauga formations, and this gradational sequence is the primary confining zone at the BP Chemical 2 site. For the purposes of this project, the top of the Conasauga Formation is equivalent to the top of the Eau Claire Shale at the BP Chemical 2 well.

The Ohio Liquids Disposal well is one of nine storage wells within a field that has been injecting fluid into the Mt. Simon Sandstone since the 1970s. Vickery Environmental Inc. performed an extensive study that examined mineralogy, porosity, permeability, and diagenesis in the disposal wells (Vickery Environmental, Inc., 1989; Vickery Environmental Inc., 2020) and provides thin section descriptions of the Mt. Simon Sandstone, Rome, and Conasauga Formations from numerous wells located within the disposal field. The results from this study are consistent with the petrophysical results, including porosity and permeability distribution, observed in the geophysical logs from the Forry Evelyn and Gracely Farms 1 wells that are adjacent to the Stonewell Project site. As such, the Ohio Liquids Disposal well also serves as an analog for the Stonewell Project site due to extensive data and analysis (Section 2.6.2.1 *Analog Well: Ohio Liquids Disposal*). These petrophysical trends are further discussed in Section 2.7.2 *Petrophysics*.

2.6.2.1. Analog Well: Ohio Liquids Disposal (UWI 34143202370000)

The Ohio Liquids Disposal well (UWI 34143202370000; Figure 52) in Sandusky County, OH, was drilled in an equivalent geologic setting, and has correlative stratigraphy, to that expected at the Stonewell Project site. As such it is considered an analog well for the project site. Vickery Environmental, Inc. (1989; 2020) provides a detailed mineralogic and petrographic analysis of the injection and confining strata found in wells at the Sandusky County disposal site (Figure 52). The mineralogy determined by X-ray diffraction (XRD) (quartz, potassium (K-) feldspar, dolomite, clay) for Mt. Simon Sandstone from all wells at the Ohio Liquids Disposal site is

presented below in Table 8. The described mineralogy is also used as input for geochemical modeling (Section 2.10 *Geochemistry*).

Table 8: Mt. Simon Sandstone XRD mineralogy ranges reported from the Ohio Liquids Disposal site (Vickery Environmental, Inc., 1989; Vickery Environmental Inc., 2020).

Mineral	Formation	Composition Range
Quartz	Mt. Simon Sandstone	24% to 92%
K-feldspar	Mt. Simon Sandstone	6% to 55%
Dolomite	Mt. Simon Sandstone	2% to 36%
Clay	Mt. Simon Sandstone	< 3%

At the Ohio Liquids Disposal site, the moderately well-sorted, very fine to coarse, subangular to rounded sandstone of the Mt. Simon Sandstone is primarily composed of quartz, K-feldspar, and dolomite, with pinkish beds containing more feldspar. In general, quartz grains are larger and rounder than the feldspar grains, which show significant dissolution features and are associated with zones of slightly higher gamma American Petroleum Institute (API) values and increased porosity (Section 2.7.2 *Petrophysics*). Clays are concentrated along laminations and are both detrital and autochthonous (Figure 52; Vickery Environmental, Inc., 1989). Quartz (including overgrowth) is the dominant cement throughout the Mt. Simon Sandstone. Dolomite cement occurs within the top half of the sandstone, is variable, and is both grain-replacing and pore-filling near the top of the formation (Vickery Environmental, Inc., 1989). The average effective porosity and permeability for the Mt. Simon Sandstone in the Ohio Liquids Disposal well are 15% and 47 mD, respectively (Figure 52).

The Rome Formation is described as a dolomitic packstone/wackestone with argillaceous laminations throughout the formation in the Ohio Liquids Disposal site. In this well, the Rome Formation has average porosity and permeability values of 5% and 0.4 mD (Figure 52). Sandy beds are more common in the middle of the formation. Thin section analysis of the Rome Formation shows that the upper and lower intervals are composed of packstones, wackestones, and grainstones that have been pervasively dolomitized resulting in complete replacement of original carbonate grains which has significantly reduced porosity and permeability. Sandier layers in the middle of the Rome Formation also have been extensively dolomitized. Pores in the carbonate lithologies are primarily intragranular, moldic, and described as ‘very poorly connected’ with permeability values less than 1 mD (Figure 52; Vickery Environmental, Inc., 1989).

The mineralogic/petrographic data and cementation patterns reported by Vickery Environmental, Inc., (1989 and 2020) suggest that four distinct stages of diagenesis (following burial compaction) affected the Mt. Simon Sandstone and the Rome Formation though the extent to which the rocks were affected by diagenesis varies based on primary mineralogy:

- Grain-coating chlorite,
- Quartz/feldspar overgrowth cementation,
- Extensive dolomitization and replacement of primary carbonate grains, and
- Feldspar dissolution.

The order of diagenetic events is supported by the observation that dolomite cement envelopes the quartz/feldspar overgrowth cement, which in turn covers grains coated in chlorite (Vickery Environmental, Inc., 1989). However, the dolomitic cement is not found in beds with secondary pores created by feldspar dissolution in the Mt. Simon Sandstone. This suggests that beds of the Mt. Simon Sandstone were dolomitized after continued burial and compaction, but before feldspar dissolution. The Mt. Simon Sandstone has the highest porosity in intervals that have experienced significant feldspar dissolution, as suggested by the increased gamma values and relatively high porosity and permeability values, and the lowest porosity in thin beds that have been dolomitized near the top of the sandstone (Vickery Environmental, Inc., 1989).

The Rome Formation experienced extensive dolomitization and thus has poorly connected intragranular, moldic, and vuggy pores. The dolomitized grainstones in the upper and lower portions of the Rome Formation have less porosity than the middle, sandier interval of the Rome Formation.

2.6.3. Mt. Simon Sandstone (Injection Zone)

The Mt. Simon Sandstone is present across western Ohio and can be correlated regionally as shown in the cross-sections in Figure 6 and Figure 8. Reservoir characteristics for the Mt. Simon Sandstone in the Forry Evelyn, Gracely Farms 1, BP Chemical 2, and Ohio Liquid Disposal wells are described below and their log-derived effective porosities and permeabilities are reported in Table 9. The Forry Evelyn and Gracely Farms 1 wells are both less than 5.5 miles away from the project site. These wells have equivalent porosity and permeability trends that resemble those described in the Ohio Liquids Disposal well (Section 2.6.2.1 *Analog Well: Ohio Liquids Disposal*).

Claimed as PBI [redacted]

Bowen et al. (2011) concluded that porosity types in the Mt. Simon Sandstone in the Arches Province range from intergranular porosity, elongate and oversized pores, fracture porosity, and dissolution porosity. These authors also note that porosity does not necessarily decrease with depth. Rather it varies laterally and vertically depending on depositional facies, mineralogy, and diagenesis. Quartz and feldspar overgrowth cement, iron-bearing illitic clays, kaolinite, chlorite, iron oxides, and dolomite reduce porosity in the Mt. Simon Sandstone. In addition, Sminchak (2012) examined geophysical well logs, rock samples, drilling logs, and geotechnical tests collected from the Mt. Simon Sandstone in the Arches Province and concluded that the Mt. Simon Sandstone has sufficient porosity and permeability for large-scale injection of CO_2 into the Mt. Simon Sandstone.

Another source of vertical heterogeneity within the Mt. Simon Sandstone is the presence of relatively low porosity/ permeability streaks within the strata that is likely caused by a greater abundance of dolomite cement in these intervals. This effect is more pronounced in the eastern side of the Findlay Arch and is observed in the Ohio Liquid Disposal wells (Figure 51 and 52) and as described by Janssens (1973). The basal half of the Mt. Simon Sandstone in the BP Chemical 2 well also exhibits intervals of relatively low porosity/ permeability which correspond to relatively low gamma ray values in quartz siltstone/sandstone beds. These intervals with poorer reservoir quality are likely attributed to the absence of porosity-creating feldspar dissolution (Figure 55).

Additional site specific information regarding the injection zone will be acquired when the project wells are drilled through the Pre-operational Testing Program and will include, but are not limited to, well logging, fluid sampling, and core acquisition and analysis (Attachment 05: Pre-operational Testing Program, 2025).

The baseline 3D surface seismic data will be calibrated to the well data and will be used to derive 3D seismic inversion datasets. This will allow the project to characterize variations in injection zone porosity and lithology away from the project wells over the imaging area of the 3D surface seismic data volume.


Claimed as PBI

2.6.4. Rome Formation (Primary Confining Zone)

The lithology of the confining strata of the Rome Formation in the Ohio Liquids Disposal well field is a dolomitic packstone/wackestone with argillaceous laminations that act as barriers to vertical movement of fluids in the primary confining zone in this field (Vickery Environmental, Inc., 1989; Vickery Environmental Inc., 2020) (Section 2.6.2.1 *Analog Well: Ohio Liquids Disposal*). Pores are observed to be intragranular, moldic, and described as poorly connected with permeability values less than 1 mD (; Vickery Environmental, Inc., 1989). Equivalent average porosity and permeability values of the confining beds of the Rome Formation are encountered in the Forry Evelyn (Figure 53) and Gracely Farms 1 (Figure 54; Section 2.6.2.1 *Analog Well: Ohio Liquids Disposal*). All wells have average effective porosity of 5 to 8% and permeability values less than 1 mD. Particularly, the dolomitic lower and upper portions of the Rome Formation have lower effective porosity and permeabilities of 3 to 4% and less than 1 mD, respectively. The dolomitic lower and upper portions of the Rome Formation have lower effective porosity and permeability which will be discussed further in Section 2.7.2 *Petrophysics*. The Ohio Liquids Disposal well has the lowest Rome Formation porosity and permeability values of 6% and 0.6 mD (Table 10).

The well logs and petrophysical results of the Rome Formation from the Forry Evelyn and Gracely Farms 1 wells suggest that the Rome Formation experienced extensive dolomitization as at the Ohio Liquids Disposal field (Figure 52, Section 2.6.2.1 *Analog Well: Ohio Liquids Disposal;* Section 2.7.2 *Petrophysics*). Dolomitization greatly reduced porosity in the Rome Formation and occurred prior to widespread porosity enhancing feldspar dissolution primarily within the Mt. Simon Sandstone. Figure 52 shows core photographs of the Rome Formation depicting the sporadic, isolated (unconnected) moldic pores that result in low average permeability values of less than 1 mD. Similar lithologic and petrophysical characteristics are expected to be encountered in the Rome Formation at the project site.

2.6.5. Addressing Uncertainty

Vault GSL CCS LP will collect a 3D seismic survey and conduct a comprehensive core and logging program at the STO INJ1 well prior to injection to characterize the injection and confining zones (Attachment 05: Pre-operational Testing Program, 2025). The site-specific data collected from the injector will update injection and confining zone depths, thicknesses and petrophysical characteristics including capillary pressure measurements and relative permeability curves for the site. The calibrated logs also will be used to update the seismic well tie for seismic interpretation. These data will be used to calibrate and reduce uncertainty within the static and computational models (Attachment 02: AoR and Corrective Action Plan, 2025).

2.7. Geomechanical and Petrophysical Information [40 CFR §146.82 (a)(3)(iv)]

2.7.1. Geomechanics

A 13-layer geomechanical model was constructed to test the integrity of the primary confining zone at the Stonewell Project site. Average values of Young's Modulus, Poisson's Ratio, and bulk compressibility were calculated for the injection zone and the lower portion of the primary confining zone, the Rome Formation, using data from the Ohio Liquids Disposal well (Figure 7, Figure 51, Figure 52, and Table 11). The Rome Formation at the Stonewell Project site was divided into four separate sub-units (A, B, C, and D) based on the petrophysical analysis (Section 2.7.2 *Petrophysics*). Average values of total closure stress (TCS) and pore pressure are shown in Table 12. The large difference between the TCS and the pore pressure indicates that there is a sufficient buffer that will allow a significant injection rate to occur without opening existing fractures.

Figure 56 shows a log with the calculated geomechanical properties, including bulk compressibility, Poisson's ratio, Young's modulus (dynamic and static), overburden stress, and TCS, calculated on 0.5-foot intervals, based on a log analysis using data from the Ohio Liquids Disposal well. These geomechanical data were then used to model the Rome Formation confining zone integrity with an anticipated injection rate of 425 ktpa into the Mt. Simon Sandstone.

The geomechanical model predicts that fracturing will not occur in the injection zone or the Rome Formation primary confining zone at the planned injection rate of 425 ktpa. The geomechanical model does indicate fracturing will occur in the Mt. Simon Sandstone at 1.93 times the operational injection rate (822 ktpa). To create fractures in the Rome Formation, the injection rate would need to be 3.05 times the operational injection rate (1,296 ktpa).

During the Pre-Operational Testing program, a variety of site-specific data from the injection and primary confining zones will be acquired in the project wells to support further geomechanical modeling as per 40 CFR §146.82(a)(3)(iii) and §146.82(a)(3)(iv). Information on the core testing that will provide ductility information for the injection and confining zones are provided the Pre-Operational Testing Program (Attachment 05: Pre-operational Testing Program, 2025).

These data include:

- Caliper, dipole sonic, and image logs,
- Triaxial testing to establish geomechanical parameters such as rock strength, ductility, Young's Modulus, Poisson's Ratio, and fracture gradient,
- Step-rate tests and pressure transient analyses,
- In situ stress information, including measurements or determinations of vertical stress, maximum horizontal stress, and minimum horizontal stress, and
- Capillary pressure measurements on core samples from both injection zone and confining zone strata.

2.7.2. Petrophysics

Petrophysical analysis of the Mt. Simon Sandstone and the Rome Formation was completed using the four key wells in Figure 51 and Table 13. These petrophysical analyses were used to evaluate the characteristics of the primary confining and injection zones (Figure 57, Figure 58, Figure 59, Figure 60, and Figure 61). For the analyses, log ascii standard (LAS) files and routine core data were acquired from the Ohio State Geological Survey. Geophysical well logs, core plugs, and well test data were used to calibrate the petrophysical calculations to derive effective porosity and permeability (Section 2.6.2 *Mineralogy, Diagenesis, Porosity, and Permeability*). These analyses will be re-visited once the project acquires site-specific well logs and core data in the project wells (Attachment 05: Pre-operational Testing Program, 2025).

Table 13: Well logs used for petrophysical analysis. Log abbreviations can be found at the beginning of this document.

Well Name	UWI	Well Logs
Forry Evelyn	34101202070000	Gamma ray, caliper, photoelectric, density, neutron, sonic, latero-log 8, latero-log deep, latero-log shallow
Gracely Farms 1	34101201680000	Gamma ray, caliper, photoelectric, density, neutron, delta-T, latero-log deep, latero-log shallow
BP Chemical 2	34003200670000	Gamma ray, SP, caliper, deep resistivity, medium resistivity, bulk density, density porosity limestone, density porosity sandstone
Ohio Liquid Disposal	34143202370000	Gamma ray, caliper, deep resistivity, density, spontaneous potential, bulk density, density porosity limestone, density porosity sandstone

Core and log data were calibrated to well test data that was publicly available from the Ohio Liquids Disposal and BP Chemical 2 wells (Figure 52 and Figure 55; INEOS Nitriles, 2016; Vickery Environmental Inc., 2020). Porosity and permeability cross plots and histograms were made using this data which enabled better analysis of wells that did not have core data and improved the static model (Figure 57, Figure 58, Figure 59, and Figure 60). The Forry Evelyn and Gracely Farms 1 are the closest wells to the project site and were the primary focus of this petrophysical analysis.

Pre-processing work on the raw log data, including depth shifting, unit conversion, and synthetic log generation, was performed prior to the petrophysical calculations. Gamma, neutron porosity, sonic, PE, and density logs were used to derive the petrophysical properties for the four key wells, which included:

- Effective porosity,
- Permeability,
- Mineralogy (where data quality was reliable),
  - Volume Shale (VSH_V),
  - Volume Quartz (Quartz_V),
  - Volume Limestone (Limestone_V),
  - Volume Dolomite (Dolomite_V),
  - Volume Sphalerite (Sphalerite_V),
  - Precambrian (Basalt_V),
  - Bound Water (BVW_V),

Table 14 and Table 15 summarize porosity and permeability values, respectively, as determined from nearby geophysical well logs (Figure 51; Section 2.6.2 *Mineralogy, Diagenesis, Porosity and Permeability*) that were calibrated using data from core and testing in the Mt. Simon Sandstone and the Rome Formation. The petrophysical values were incorporated into the static model for the Stonewell Project site (Attachment 02: AoR and Corrective Action Plan, 2025). For the Mt. Simon Sandstone, the 4 key wells all have average porosity and average permeability values that range from 15 to 18% and 41 to 74 mD. The Gracely Farms 1 well has the highest Mt. Simon Sandstone average porosity (18%) and permeability values (74 mD), and the Forry Evelyn and Ohio Liquids Disposal wells have similar, slightly lower values (Table 14 and Table 15).The effective porosity/permeability cross plots (Figure 57), effective porosity histograms (Figure 58), and permeability histograms (Figure 59) indicate that Mt. Simon Sandstone has higher porosity and permeability values compared to the Rome Formation.

The resulting porosity and permeability petrophysical logs for these four key wells show that the Mt. Simon Sandstone is primarily composed of interbedded higher porosity/permeability and average porosity/permeability sandstone intervals. These porosity and permeability contrasts are likely due to the development of secondary porosity and inhibition of cement due to the presence of K-feldspar in the beds that exhibit high gamma ray values (Figure 60 and Figure 61; Section 2.6.2 *Mineralogy, Diagenesis, Porosity, and Permeability*; Janssens, 1973; Vickery Environmental, Inc., 1989; Vickery Environmental Inc., 2020).

The Rome Formation has significantly lower average effective porosity and permeability values compared to the Mt. Simon Sandstone and the well logs show continuous sections of tight dolomitic rocks interbedded by a section of relatively porous but low permeability rock in the middle of the Rome Formation (Figure 53 and Figure 54). To investigate these porosity and permeability variations, the Rome Formation was subdivided into four sub-units based on the Forry Evelyn and Gracely Farms 1 geophysical log analysis: A (base), B, C, and D (top) (Figure 60, Figure 61, and Table 15).

The A and D sub-units are heavily dolomitized and have significantly reduced porosity that is not interconnected as evidence by permeability values of 0.15 mD or less. The Rome A dolomite directly overlies the Mt. Simon Sandstone (Figure 60, Figure 61, and Table 16) and it is 43 feet and 40 feet thick at the Forry Evelyn and Gracely Farms 1 wells respectively. Both wells have average porosity of 3% and average permeability of 0.02 mD and 0.15 mD, respectively.

The Rome B subunit is slightly more porous (7 to 9%; Figure 60, Figure 61; Table 16) than its underlying Rome A subunit. It contains tight and porous clastics interbedded with relatively thin dolomite layers and has average permeability of 0.41 mD and 0.98 mD at the Forry Evelyn and Gracely Farms 1 wells, respectively. The low permeability values suggest that even though this subunit contains slightly more porous space than the Rome A, pores are not connected and the zone will serve as a competent seal.

The clastic content at the top of the Rome B and base of the Rome C increases as the gamma ray values also increase, and the dolomite content decreases, resulting in a Rome C that is relatively porous with an average porosity of 12% in both the Forry Evelyn and Gracely Farms wells (Figure 60 and Figure 61; Table 16). However, its average permeability of less than 2 mD suggests that pores are poorly connected in the Rome C interval (Figure 60 and Figure 61; Table 16).

The Rome D subunit represents the top of the Rome Formation and immediately underlies the Conasauga Formation. The log responses and petrophysical analysis for this unit indicate a tight dolostone with 63 and 65 feet of thickness at the Forry Evely and Gracely Farms 1 wells respectively. Average porosity and permeability are between 3 to 4% and 0.001 to 0.005 mD for both wells (Figure 60 and Figure 61; Table 16).

Figure 62 displays the lateral continuity of the Rome Formation in the four key petrophysical wells. The transition from deeper marine clastics of the Eau Claire Shale in the west (BP Chemical 2) to shallower-water Rome Formation/Conasauga Formation dolostones and tightly cemented dolomitic clastics to the east in wells on the Findlay Arch (Gracely Farms 1, Forry Evelyn, and Ohio Liquids Disposal wells) is also shown in Figure 62. Though shale content decreases from west to east in Figure 62, the integrity of the Rome Formation primary confining zone is maintained by the impermeable dolomites and dolomitic clastic facies at the project site (Figure 60 and Figure 61).

The porosity and permeability values reported for the Forry Evelyn and Gracely Farms 1 wells in (Figure 60 and Figure 61show that the dolostones and dolomitic clastics of the Rome A and Rome D subunits represent a competent seal, with average permeabilities less than or equal to 0.2 mD. The low permeability values of less than 2 mD for the Rome B and Rome C also indicate that porosity in these intervals is not effective (i.e., connected), and the Rome B and C can serve as a confining zone. The Rome Formation has been mapped both regionally throughout western Ohio and locally with 2D seismic profiles acquired specifically for the Stonewell Project. In general, the Rome Formation becomes more permeable east of the Bowling Green Fault in northern Ohio (Figure 17). However, within the project area, the Rome B and C facies are expected to have low permeability and are bound by the impermeable dolostones of the Rome A and Rome D, which are laterally extensive and continuous (Figure 62). At the Stonewell

Project site, the entire thickness of the Rome Formation is prognosed to be 257 feet thick, with 37 and 62 feet of tight dolostone in the Rome A and Rome D subunits, respectively. The Rome A, B, C, and D subunits are continuous, mapped with 2D seismic lines across the project area, and incorporated into the geocellular model. This succession of impermeable Rome Formation dolostones will provide a highly competent confining zone at the Stonewell project site.

The competence of the Rome Formation primary confining zone is additionally demonstrated at the Ohio Liquids Disposal well field (Figure 52) (Vickery Environmental, Inc., 1989; Vickery Environmental Inc., 2020), where fluid is injected and contained within the Mt. Simon Sandstone. In this field, there is no pressure communication between the Mt. Simon Sandstone and the top of the Kerbel Formation, as measured by a monitoring well (Vickery Environmental Inc., 2020). In the Ohio Liquids Disposal well shown in Figure 52, the Rome Formation is approximately 212 feet thick, and there are 62 feet of tight dolostone within the Rome A and Rome B directly overlying the Mt. Simon Sandstone top. The Rome D subunit has also been cored in this field and described in Figure 52, and the impermeable nature of the entire Rome Formation is evident in core descriptions and permeability measurements in the Ohio Liquids Disposal well.

The Precambrian Basement underlying the project site is located in the crystalline Grenville Province, though the Middle Run Formation may exist at the project site. The Middle Run Formation is dominantly arkosic sands and conglomerates related to rift basins. Because of their age and depth of burial, rocks of the Middle Run Formation have low porosity and negligible permeability as reported by Shrake (1991). Neither crystalline nor Middle Run Basement rocks have significant porosity and permeability so that fluid flow within these units is negligible and any pressure communication with the overlying Mt. Simon Sandstone will be limited.

Cumulative shale/siltstone thickness was calculated for the Forry Evelyn well (Figure 53 and Table 17) using a combination of gamma and Vshale geophysical log cutoffs (gamma > 60 API; Vshale > .25) and density derived facies (shale or siltstone). Average porosities were calculated from a combination of neutron porosity, density porosity, and effective porosity logs. This method shows that there are approximately 38 feet of cumulative shale/siltstone within the primary confining zone. Above the primary confining zone, there is a cumulative shale/siltstone thickness of over 1,000 feet (Table 17). A majority (883 feet) of these fine-grained clastics are within the Queenston Formation/Maquoketa Group and the Utica Shale. Interbedded shale/siltstone layers within the Trenton, Gull River/Glenwood Shale, Trempealeau, Kerbel, and Conasauga Formations contribute an additional 131 feet (Table 17).


Claimed as PBI


Claimed as PBI

2.7.3. Addressing Uncertainty

The comprehensive core and logging program for STO INJ1 is designed to provide a robust dataset and reduce uncertainty at the Stonewell Project site (Attachment 05: Pre-operational Testing Program, 2025). Triaxial compression and rock compressibility tests will be performed to characterize Young's modulus, Poisson's ratio, rock strength, compressibility, in-situ fluid pressures, and ductility. These calculations will be incorporated into existing geomechanical analyses and updates will be made as needed.

As previously stated in Section 2.5.3 *Fractures*, imaging logs from STO INJ1 will be used to characterize fractures at the Stonewell Project site. Additionally, SRTs will be performed to determine fracture opening pressure, fracture propagation pressure, and fracture closure pressure in the injection zone. These tests and logs will be used to update primary stress fields and fracture gradient calculations at the Stonewell Project site.

2.8. Seismic History [40 CFR §146.82(a)(3)(v)]

Based on Federal Emergency Management Agency (FEMA) classification the Stonewell Project site has a very small probability of experiencing damaging earthquake effects. The site is more than 375 miles northeast of the Strongest Shaking Zone E associated with the New Madrid Seismic Zone (Figure 63).

The project site is more than 30 miles east of the Anna Seismic Zone, which is a small seismic zone with moderately frequent though episodic earthquakes (Dart and Hansen, 2008). Some earthquakes within the Anna Seismic Zone coincide with known faults (i.e., Anna-Champaign Fault), and there is no paleoseismological evidence for significant post-Paleozoic activity (Dart and Hansen, 2008).

Seismic activity in Ohio is monitored and recorded by both the National Earthquake Hazards Program and the Ohio Seismic Network (OhioSeis). OhioSeis monitors seismic activity from its network of seismograph stations located throughout the state; stations are concentrated in the most seismically active areas or where conditions are best for detection of small earthquakes. The United States Geological Survey (USGS) Earthquake Hazards Program records earthquakes having a magnitude of 2.0 or greater and is augmented with OhioSeis stations.

Figure 64 displays all of the earthquakes recorded by USGS since 1800 with a magnitude of 1.0 or greater and all seismic activity recorded by OhioSeis within a 100-mile radius of the Stonewell Project site; these are also listed in Appendix 1C-*Seismic Events*. The largest earthquake within this 100-mile radius occurred in 1937 approximately 56 miles southwest of the project site with a magnitude of 5.4 Mw (USGS, 2024). The most recent earthquake occurred on 29 December 2024 approximately 90 miles northwest of the project site and had a magnitude of 2.9 moment duration (Md) (OhioSeis, 2025). The nearest earthquake occurred on 11 July 1930 approximately 3.8 miles from the project site and had a magnitude of 3.1. No earthquakes have been recorded that have an epicenter within the project AoR, and earthquakes are not expected to interfere or compromise containment at the Stonewell Project site (Appendix 1C-*Seismic Events*).

2.9. Hydrologic and Hydrogeologic Information [40 CFR §146.82(a)(3)(vi), §146.82(a)(5)]

A USDW is defined by the EPA as an aquifer that (40 CFR §146.3):

- Supplies any public water system
- Contains a sufficient quantity of groundwater to supply a public water system; and
  - Currently supplies drinking water for human consumption, or
  - Contains fewer than 10,000 mg/L (milligrams per liter) total dissolved solids (TDS),which is not an exempted aquifer.

The following sections provide information regarding available USDW resources and delineation of the lowermost USDW, which is the base of the Silurian Lockport Dolomite at the project site. Water well, monitoring well, and dry well records were collected for the project AoR from the ODNR Division of Geological Survey (ODNR).

Numerous wetlands, identified through satellite imagery, are located throughout the AoR but none are located at the project well site. There are no known springs within the AoR. Groundwater wells within the AoR include 167 water wells with total depths ranging from 55 to 255 fbgl with an average depth of 102 fbgl. Of these 167 wells, only one sources water from the unconsolidated sediments overlying Silurian bedrock. However, it remains unclear from publicly available information as to which member these wells draw water from. The AoR and Corrective Action Plan includes a detailed discussion of the number and locations of the shallow groundwater wells within the AoR (Attachment 02: AoR and Corrective Action Plan, 2025).

2.9.1. Local Hydrology

The Stonewell Project site is located within the Lake Erie drainage basin, with STO INJ1 located in the southern Sandusky sub-basin of the Ohio portion of the Lake Erie watershed. This watershed drains rural, agricultural land and communities across northern Ohio (Figure 65). The project site is located near the Little Sandusky River, which is part of the Sandusky sub-basin.

There are two main sources of shallow groundwater in Marion County, Ohio:

1. Quaternary-aged Woodfordian unconsolidated sand and gravel, lacustrine, and ground moraine deposits, and
2. Silurian carbonates of the Salina Group, including the Tymochtee Dolomite/Greenfield Dolomite and the undifferentiated strata of the upper Salina Group, and the Lockport Dolomite, which is the lowermost USDW (Crowell, 1979); Figure 5 and Figure 66).

The area within and surrounding the Stonewell Project site primarily utilizes the aquifers of the Silurian carbonate bedrock, which consist of hydraulically interconnected beds of limestone and dolomite (Norris and Fidler, 1973).

2.9.2. Near Surface Aquifers

During the Pleistocene Epoch, Ohio experienced several glacial intervals, and glacial sediments were deposited on top of the Paleozoic bedrock throughout much of the state except in the southeast portion. These glacial deposits affect surface hydrology and aquifers in the region with 600 to 700 feet of till, drift, lake, and valley fill sediment in northern areas of the state.

The Stonewell Project is situated in a region of Quaternary glacial deposits composed of the Wisconsinan Woodfordian moraine and associated lacustrine clay (Figure 67). The Woodfordian deposits tend to be interbedded outwash sands, gravels and lacustrine clays and are generally less than 100 feet thick within the Stonewell project area (Figure 66, Figure 67, and Figure 68). Domestic wells producing from these Quaternary deposits typically yield less than three to four gallons per minute due to high clay content and thus these units are not commonly used as sources of water and in the vicinity of the Stonewell Project site these deposits do not serve as USDWs.

In western and central Marion County, water wells are typically drilled through the glacial deposits and into the carbonate Salina Group, including the Tymochtee/Greenfield Dolomites which are less than 100 feet thick and comprise the primary near surface aquifer in the region, and the underlying Lockport Dolomite, which is nearly 200 feet and is the lowermost USDW at the project site. The Undifferentiated Salina strata, which overly the Tymochtee/Greenfield Dolomites, are present in the eastern part of the AoR but pinch out westward and are expected to be absent at the location of STO INJ 1 (Figure 5, Figure 66, and Figure 69). Groundwater wells, typically less than 300 feet deep, drilled into these shallow Silurian bedrock units may yield 100 to 500 gallons per minute, although some wells have yielded in excess of 1,000 gallons per minute (Figure 70; Crowell, 1979, Norris and Fidler, 1973; Wilson, 1987). The groundwater is sourced from joints, fractures, bedding planes and solution channels (Casey, 1994; Eberts, S.M. and George, L.L., 2000). Hardness and sulfur content in the Silurian bedrock aquifer however may deter domestic use (Crowell, 1979).

Studies on the regional groundwater flow direction do not differentiate individual units but rather group aquifers based on rock type. The regional groundwater flow direction for carbonate aquifers, which includes the Tymochtee/Greenfield Dolomite and Lockport Dolomite, is generally from drainage divides towards the major streams and Lake Erie, with a major component of horizontal flow across surface water divides (Norris and Fidler, 1973; Bugliosi, 1990). Near the Stonewell Project site area, groundwater generally flows to the north-northwest towards Lake Erie (Norris and Fidler, 1973; Eberts and George, 2000).

2.9.3. Determination of Lowermost USDW

At the Stonewell Project site, the Lockport Dolomite is the lowermost USDW (Figure 71; Riley et al., 2012). Water samples from the bedrock aquifers in Marion County up to 310 feet deep have TDS values ranging from 497 to 604 mg/L with most producing from the Salina Group, including the Lockport Dolomite (Crowell, 1979). The Ohio EPA Division of Drinking and Groundwater maintains the Ambient Ground Water Monitoring Network as part of an effort to characterize general water quality conditions across Ohio (Ohio EPA). A monitoring well approximately 3 miles east of the AoR in the undifferentiated Salina Group has a total depth of 200 feet deep and average TDS concentrations of 689 mg/L. An additional monitoring well approximately 9 miles southwest of the AoR penetrates the limestone bedrock (including the Tymochtee/Greenfield Dolomite and Lockport Dolomite) has a total depth of 205 feet deep, and average TDS concentrations of 773 mg/L.

At the Stonewell Project site, the depths to the top and bottom of the Lockport Dolomite are prognosed to be [redacted] fbgl and [redacted] fbgl, respectively, and the dolomite is expected to be approximately [redacted] feet thick (Figure 6 and Figure 66). There are four water wells within the AoR with total depths greater than 193 feet and inferred to be within the Lockport Dolomite. The base of the Lockport Dolomite USDW is separated from the top of the primary confining zone by 2,252 vertical feet.

Regional groundwater flow direction in the Lockport Dolomite is generally to the north-northwest (Norris and Fidler, 1973; Eberts, S.M. and George, L.L., 2000).

2.9.4. Addressing Uncertainty

To reduce the uncertainty of the depth to the Lockport Dolomite, and its relative thickness within the AoR, the lithology will be logged during the drilling of the STO USDW1, STO ACZ1, STO INJ1, and STO OBS1 wells.

To confirm the lowermost USDW, the project will attempt to collect a formation water sample from strata below the expected lowermost USDW (Lockport Dolomite).

2.9.5. Non-USDWs

Based on regional data and mapping, the injection zone formation water TDS is approximately 205,000 mg/L at the Stonewell Project site (Figure 72). Isotopic data also suggest that the Mt. Simon Sandstone brine originated as connate seawater and was also influenced by evaporite dissolution (Labotka et al., 2015). Therefore, the Mt. Simon Sandstone is not a USDW.

12

2.9.6. Topographic Description

The Stonewell Project is located in Marion County, Ohio:

- Sections 14-15, 20-29, 32-36, Township 4S Range 14E; and
- Section 30-31, Township 4S Range 15E; and
- Sections 1-5, 8-12, 14-15, Township 5S Range 14E; and
- Sections 6-7, Township 5S Range 15E.

The site is in the Till Plains physiographic province with generally flat to rolling topography underlain by glacial till. The ground elevation at the well site is [redacted] feet.

The land within the project AoR is considered an area of minimal flood hazard as established by FEMA. The proposed project site is located outside of flood hazard risk areas. The nearest flood hazard risk is a FEMA Zone A flood hazard risk, 1% chance of annual flooding along the Little Sandusky River, located approximately 1.5 miles north of STO INJ1 (Figure 73, FEMA).

2.10. Geochemistry [40 CFR §146.82(a)(6)]

2.10.1. Baseline Geochemical Characterization

Geochemical modeling was performed to assess the maximum reactivity of CO_2 interactions within the injection zone and at the injection-confining zone interface. Modeling inputs included mineralogy of the injection and confining zones, injection gas composition, and aqueous chemistry. Data collected as part of the Pre-operational Testing Program will be used to update the geochemical modeling (Attachment 05: Pre-operational Testing Program, 2025) and a Pre-operational Narrative including the updated baseline geochemical characterization will be submitted to the EPA.

Geological characterization and mineralogy of the injection and the confining systems are discussed in detail in Sections 2.6 *Injection and Confining Zone Details* and 2.7.2 *Petrophysics*. A mineralogical dataset including XRD and petrographic thin-section point counting data was compiled from samples spanning the entirety of the Mt. Simon Sandstone and Rome Formation from three wells associated with the Vickery Environmental, Inc. Class I UIC permit in Sandusky County, OH (Vickery Environmental, Inc., 1989; Vickery Environmental Inc., 2020) which are considered strong analogs for the Stonewell Project site. Only XRD data were used for model inputs.

2.10.1.1. Mineralogical Model Input

The Mt. Simon Sandstone in west-central Ohio consists primarily of arkose and subarkose sandstones comprised of mostly quartz and feldspar minerals (entirely K-feldspar based on XRD analyses) with some carbonate cement and grains (dolomite and calcite) and a small clay mineral component (primarily chlorite) (Table 18; Vickery Environmental, Inc., 1989). Mt. Simon Sandstone samples have highly variable quartz-feldspar ratios. To address this variability within

the geochemical modelling, the Mt. Simon mineralogy was evaluated in two groups: an arkose-dominated lithology having 40% or more total feldspar, and a quartz-dominated lithology having less than 40% total feldspar.

The part of the primary confining unit at the Stonewell Project site is the low porosity dolomitic strata of the Rome Formation. Two samples collected near the base are representative of the tight dolomite component of the Rome Formation; they contain high dolomite contents (93 and 94 wt.%) measured by XRD, and low total porosities (0.8 and 1.2%) measured by point counting (Vickery Environmental, Inc., 1989). The tight dolostones could potentially interact with CO_2-influenced liquids. The two Rome Formation XRD samples collected from the Vickery UIC investigation were averaged to generate a single representative model input to define the primary confining unit model cases.

Three mineralogical inputs were used in model runs: primary confining unit, injection zone arkose lithology, and injection zone quartz lithology. Mineralogical inputs for each of the three groups were generated by calculating the mean abundances of each mineral from the XRD datasets. XRD samples were analyzed for clay mineralogy, so individual clay mineral abundances were directly averaged in instances where results were provided as weight fractions of the total sample, and individual clay mineral proportions were applied to a total clay component in instances where results were provided as weight fractions of the clay-sized component (Table 18).


Claimed as PBI

2.10.1.2. Aqueous Model Input

Mt. Simon Sandstone formation water data is available from the Vickery UIC permit applications for Disposal Well No 1 and Disposal Well No. 4 (Vickery Environmental, Inc., 1989; Vickery Environmental Inc., 2020). The Mt. Simon Sandstone formation water samples contained measured TDS concentrations ranging from 120,000 to 132,000 milligrams per liter (mg/L), with an average of 126,000 mg/L. A TDS concentration of 205,000 mg/L is expected at the Stonewell Project site, so these water samples are considered representative. Formation water pH values are relatively consistent across the samples with all values ranging from 6.0 to 6.9 standard units (SU). These measurements indicate that injection zone formation water chemistry is neutral to slightly acidic.

Three samples of the formation water were averaged to generate a representative Mt. Simon Sandstone formation water composition (Table 19). This representative sample contained a calculated charge imbalance error of 0.45%. A charge imbalance error of +/- 5% is conventionally considered high quality data for brine solutions.

Formation water data is not available from the primary confining unit due to the low porosity and permeability within the Rome Formation. The aqueous input for the Rome Formation was generated by equilibrating the representative Mt. Simon Sandstone composition with the mineralogical input of the primary confining unit. This technique has been applied to estimate porewater chemistry of low permeability rocks in multiple studies (Gaus et al., 2005). Results of this calculation were used as the aqueous geochemical input for the primary confining unit model runs and are provided in Table 19.

2.10.1.3. Injection Gas Input

The composition of the gas stream for injection is expected to consist of >98% CO_2, with minor impurities including oxygen, hydrogen sulfide, and hydrogen (Table 20). Other constituents such as carbon monoxide, glycol, non-condensable gases, anticipated to be present in minor quantities, are not expected to chemically interact with injection or confining zone minerals and were not included in model inputs. To examine the impact of impurities within the CO_2 stream on mineral reactivity, a high impurity and low impurity case were evaluated in the modeling effort (Table 20). For nearly all model cases, the lower impurity gas composition (i.e., higher CO_2 component) was observed to be more reactive (greater geochemical change), and thus only the results from the low impurity compositions have been presented here to provide the most conservative estimates of the extent of mineral reactions.

Claimed as PBI

2.10.2. Geochemical Modeling

Geochemical modeling was performed to evaluate the reactivity of the solid-liquid-gas system during and following CO_2 injection. Two modeling approaches were used for this evaluation:

1. equilibrium modeling (thermodynamic considerations only), and
2. reaction pathway modeling (thermodynamic and kinetic considerations).

Multiple model cases were generated to assess the maximum reactivity of geochemical interactions within the injection zone and at the injection-confining zone interface. Model case inputs differed to address mineralogical heterogeneity in the injection zone and variability in injection gas impurities. Model runs were conducted at a pressure of 1,925 psi and a temperature of 120 °F that are the expected maximum pressure and temperature values at the end of the gas injection period at the interface between the injection zone and the primary confining unit.

In all models, the formation-injectate-fluid system was modeled as porous material fully saturated with one liter of fluid in the defined effective pore space. Computational modeling predicts a maximum CO_2 saturation of 0.78 at the interface between the injection zone and the primary confining unit. This conservative gas saturation value is assumed for all model runs. The saturation value was incorporated into calculations using the ideal gas law to calculate the number of moles of CO_2 and impurity gases H_2, O_2, and H_2S that are introduced into the modeled systems. These values were supplied as model inputs, and CO_2 solubility within formation water was calculated in the modeling software based on temperature, pressure, and compositional inputs using a Henry's Law approach (Bethke, 1998; Gundogan et al., 2011; Parkhurst and Appelo, 2013).

Following methods proposed in Trémosa et al (2014) for modeling geochemical compatibility of geologic carbon sequestration, geochemical modeling efforts employed a batch reactor modeling approach where the formation-injectate-fluid system was assumed to be a perfectly mixed reactor with homogenous distribution of every chemical compound and reactant.

Equilibrium modeling was conducted using the USGS software package PHREEQC (Parkhurst and Appelo, 2013). Equilibrium modeling was completed for each mineral model case by fixing individual mineral saturation indices to a value of zero in the presence of the formation water and

injectate gas, thereby quantifying mineral and aqueous changes associated with equilibrium with injectate gas.

Reaction pathway modeling was conducted using the React module in Geochemist's Workbench (Bethke, 1998). Reaction pathway modeling was completed for all model cases. Each model was set to run for an initial injection period of 12 years and a subsequent period of 50 years post-injection for a total model runtime of 62 years.

2.10.2.1. Equilibrium Modeling

For the Rome Formation primary confining unit, the mineral reactions predicted to occur include the complete dissolution of chlorite and kaolinite and the partial dissolution of K-feldspar. Dolomite exhibited minor dissolution, which indicated relative geochemical stability. Quartz and dawsonite were predicted to precipitate. Porewater pH decreased by approximately 1.28 standard units (SU) at equilibrium, which was mainly due to the dissolution of CO_2 into formation water (Table 21). Quartz precipitation is the primary driver of net mineral mass increases. However, its slow reaction kinetics suggests limited impact within operational timescales.

In the injection zone where arkose lithologies dominated, the mineral reactions predicted by equilibrium geochemical modeling included the complete dissolution of clay minerals (chlorite, illite, smectite) and partial dissolution of calcite and K-feldspar. Dawsonite, dolomite, quartz, and siderite precipitation were predicted (Table 21). In modeling of the quartz-dominated lithologies, the formation water pH decreased by approximately 1.44 standard units (SU) at equilibrium, which was a slightly greater pH decrease than in the arkose lithology and was attributed to the comparatively lower initial calcite content that resulted in reduced buffering capacity (Table 21). Quartz precipitation dominated net mass increases, as was observed in the arkose lithology. However, the slow kinetics of quartz reactions suggest minimal short-term changes during CO_2 injection operations.

The extent of the mineral mass increase as determined through equilibrium geochemical modeling was variable and depended most strongly on mineralogy inputs. The modeling indicated that variability in gas impurities would have negligible impact on the overall direction or magnitude of mineral reactions (Table 21). The primary confining unit (Rome Formation) was predicted to experience some net mineral mass increase, with models predicting between 1.81 and 1.83% net mass increase. The influence of the gas impurity range was found to be minimal in primary confining unit model scenarios. Net mineral precipitation is also predicted for both of the Mt. Simon Sandstone lithologies. The arkose lithology was predicted to experience between 3.68 and 3.74% net mineral mass increase, and the quartz lithology was predicted to experience between 3.17 and 3.21% increase. The quartz lithology was predicted to be less reactive than the arkose lithology due in large part to the lower degree of reactivity of quartz compared to feldspar minerals.


Claimed as PBI

2.10.2.2. Reactive Pathway Modeling

At the Mt. Simon Sandstone – Rome Formation interface, the kinetic modeling results predict that porewater pH will decline to 4.93 SU over 62 years (Figure 74). An initial pH decrease occurs during CO_2 injection that is followed by gradual stabilization after injection ceases. Clay minerals and feldspar were predicted to dissolve early, and dolomite remains generally stable throughout (Figure 75). Dawsonite forms during injection and remains stable post-injection, contributing to CO_2 trapping. Quartz precipitation is also predicted to begin during injection and proceed slowly.

A minor net mineral mass decrease (-0.008%) is accompanied by a slight porosity increase (+0.016%). Over time, this trend is expected to reverse due to persistent quartz precipitation, which aligns with equilibrium modeling projections that predicted an increase in mineral mass (Figure 75). As with equilibrium modeling, gas composition variations had negligible effects on reaction directions or magnitudes in any of the modeled cases.

In the arkose-dominated part of the injection zone lithology, pH decreased to 4.90–4.91 SU during the 62-year period. The pH decline during gas injection is steady except for a brief, slightly elevated period during injection and stabilization occurs post-injection. Stabilization of pH occurs post-injection. Nearly complete dissolution of clay minerals and partial dissolution of K-feldspar occur (Figure 76). Hematite forms rapidly during early injection and temporarily offsets mass loss from dissolution. Dawsonite and dolomite precipitate during injection and contribute to CO_2 trapping. Quartz precipitation continues slowly post-injection.

Overall, a minor net mineral mass decrease (-0.0375%) corresponds to a small porosity increase (0.0005% of total porosity). As quartz precipitation persists, porosity is expected to decline over geologic timescales.

In the quartz -dominated injection zone lithology, geochemical trends are similar to the arkose lithology. Formation water pH decreases to 4.83–4.84 SU and stabilizes post-injection. This pH range is consistent with other lithologies but reflects the quartz lithology's lower initial calcite content and reduced buffering capacity. Clay minerals nearly dissolve completely, and feldspar dissolves partially (Figure 77). Some calcite dissolution occurs during injection, acting as a pH buffer. Hematite and dawsonite are predicted to precipitate rapidly during injection, contributing to mass stability. Dolomite and quartz precipitation continue post-injection, with quartz dominating long-term mass increases. A small net mineral mass decrease (-0.0302%) is predicted over the modeled time period, corresponding to a porosity increase of 0.0005% of total porosity. Over time, quartz precipitation is expected to reverse these trends.

2.10.3. Geochemical Impacts on Storage and Containment

Equilibrium and kinetic modeling each indicate that geochemical reactions are mainly driven by CO_2 dissolution into formation water. The process generates carbonic acid, which dissociates into bicarbonate and carbonate and lowers the pH while increasing alkalinity. These changes alter mineral solubilities and prompt the dissolution of certain minerals (e.g., calcite, feldspar, and clays) and precipitation of others (e.g., dawsonite, dolomite, siderite, and quartz). These carbonate reactions are part of mineral trapping mechanisms that stabilize CO_2 in solid phases. Quartz precipitation accounts for the largest net mineral mass increase but proceeds at slow kinetic rates, minimizing its immediate impact on porosity.

The Rome Formation primary confining zone demonstrated geochemical stability and compatibility with CO_2 storage. These results align with studies that conclude dolomite formations are compatible with CO_2 injection and storage (Mohamed et al., 2012).

Both feldspar-dominant and quartz-dominant lithologies of the injection zone displayed comparable geochemical responses to CO_2 injection regardless of the dominant mineral type. Minor decreases in porosity associated with mineral precipitation are predicted in both injection zone lithologies at equilibrium conditions.

The geochemical modeling for the Stonewell Project site indicates that CO_2 injection induces a predictable sequence of geochemical reactions with minimal impact on reservoir quality or containment over operational timescales. Carbonate mineral formation is a primary driver of long-term mineral trapping, while pH buffering and mineral dissolution reactions influence short-term geochemical behavior. The summary of kinetic reaction pathway modeling is shown in Table 22.

Claimed as PBI

The CO_2 trapping mechanisms that include dissolution and mineral trapping were also evaluated with the computational modeling presented in Attachment 02: AoR and Corrective Action Plan, (2025). Table 23 indicates the trapping mechanisms and percentage of CO_2 trapped 50-year post-injection at the Stonewell Project site as predicted by the computational modeling that considers the spatial and three-dimensional extent of the storage site. The geochemical and computational modeling results are largely consistent as the computational modeling predicts that about 87.8% of the CO_2 at the end of PISC will be structurally and residually trapped and most of the remainder will be trapped by dissolution (Figure 78). Whereas the computational modeling predicts a slight decrease in mineral mass and geochemical modeling indicates a slight increase, all methods indicate mineralization will play a very small role during the operational period of the project.

Claimed as PBI

2.10.4. Potential Geochemical Impacts to USDWs

The lowermost USDW within the AoR is the Silurian Lockport Dolomite, which is overlain by Tymochtee and Greenfield dolomites and the undifferentiated Salina Group, which primarily consists of microcrystalline dolomite. Upward migration of CO_2 into these USDWs is unlikely, as described in Section 2.6 *Injection and Confining Zone Details*. In the event of a leak allowing CO_2 to migrate vertically into the lowermost USDW, the geochemical impacts of the gas-USDW aquifer interactions are not expected to be significant. Should CO_2 dissolution into the lowermost USDW groundwater occur, pH would decrease slightly, and the concentration of bicarbonate ions would increase due to carbonic acid dissociation reactions. There would be a negligible impact on total alkalinity of the shallow groundwater by adding dissolved CO_2. The slight decrease in pH resulting from carbonic acid formation could result in some dissolution of the dolomitic matrix; however, this carbonate dissolution produces bicarbonate ions that react with the carbonic acid to buffer any pH decrease. A study that modeled the results of CO_2 release into an aquifer (Berger and Roy, 2011) demonstrated that dissolution of dolomite buffered the pH and the main resulting changes to the groundwater chemistry were increases in magnesium, calcium, and bicarbonate ions. Since pH is buffered by carbonate mineral dissolution, the likelihood of increased acidity mobilizing metals is negligible (Berger and Roy, 2011). Groundwater quality monitoring in the lowermost USDW wells will include monitoring of pH, magnesium, and calcium, allowing for the detection of any inadvertent releases of CO_2 into the USDWs.

In addition to the Lockport Dolomite USDW, Tymochtee/Greenfield Dolomite USDW, and Salina Group USDW, in some areas near the project site there are shallow aquifers in sands and gravels of the Woodfordian moraine deposits (Section 2.9.2 *Near Surface Aquifers*; Crowell, 1979) The glacial tills and moraines contain a high proportion of fragments of the underlying limestone bedrock and thus have a variable content of carbonate minerals (Shrake et al., 2009). Migration of CO_2 into these shallow aquifers is highly unlikely; however, if such a release occurred, decreases to groundwater pH within the sand and gravel aquifer would also be buffered in part by dissolution of carbonate minerals present in the till. In addition, there may be additional capacity for pH buffering from protonation and metal complexation reactions within clay minerals present in till aquifers. The potential to mobilize additional constituents into the groundwater, including metals, is influenced by the mineralogy of the aquifer, although increased groundwater concentrations of any mobilized metals would be negligible (Berger and Roy, 2011) and likely mitigated by sorption to aquifer sediments. A review of field studies of the impact of CO_2 releases on groundwater quality concluded that trace metal releases are generally small and do not pose a significant risk to groundwater quality (Qafoku et al., 2015).

The lithology of USDWs will be logged during the drilling of project wells.

2.11. Other Information (Including Surface Air and/or Soil Gas Data, if Applicable)

(Attachment 05: Pre-operational Testing Program, 2025) presents the data that will be collected in order to determine and verify the depth, thickness, mineralogy, lithology, porosity, permeability, and geomechanical information of the injection zone, confining zone, and other relevant geologic formations via petrophysical logging and analysis, and core acquisition and testing. In addition, baseline 3D surface seismic data will be acquired during the pre-injection phase of the project to assist in characterizing injection zone and confining zone rock properties away from the project wells.

At this time, the project does not plan to acquire baseline atmospheric or soil gas data nor are there plans to pursue atmospheric or soil gas monitoring during the injection phase of the project.

2.12. Site Suitability *[40 CFR §146.83]*

2.12.1. Summary

The Mt. Simon Sandstone at the Stonewell Project site meets all requirements necessary to serve as a competent injection zone and can sequester an estimated 5.1 Mt of CO_2 over 12 years as evidenced through geologic evaluation, static modeling, and computational modeling results, and AoR delineation reported in Attachment 02: AoR and Corrective Action Plan, (2025). The Rome Formation will be an effective primary confining zone based on their thickness, continuity, and low porosity and permeability at the project site.

Table 24 summarizes the properties of the Mt. Simon Sandstone that contribute to its suitability as an injection zone.

CO_2 plume development will likely be controlled by heterogeneities within the Mt. Simon Sandstone, and these heterogeneities will be characterized using a combination of well log, core, and 3D surface seismic data (Attachment 05: Pre-operational Testing Program, 2025).

No wells penetrate the confining zone within the AoR. The closest well penetration of the confining zone is the Forry Evelyn well, which is located approximately 3.5 miles northeast of the injection well (ODNR; S&P Global).

FEMA classifies the project site to have a very low risk of experiencing damaging earthquake effects, the project site is located in seismic category A with no potential shaking effects (Figure 63). A small area in the north part of the AoR (Figure 73) has a minimal flood hazard risk of a 1% chance of experiencing annual flooding ((FEMA).

2.12.2. Primary Confining Zone

The Rome Formation is the primary confining zone at the project site where it is estimated to be [redacted] feet thick and is laterally continuous across the AoR and broad surrounding area (Attachment 02: AoR and Corrective Action Plan, 2025). The internal stratigraphy of the Rome Formation contains several mappable sub-units that are extensively dolomitized with greatly reduced connected porosity and low permeability values averaging 0.1 mD that will serve as effective confining units. Data gathered during the pre-operational phase of the project will be used to verify that the Rome Formation is a highly competent confining zone (Section 6 *Pre-operational Logging and Testing*).

2.12.3. Lowermost USDW

The Silurian Lockport Dolomite is the lowermost USDW at the project site with a depth to the base of the formation of [redacted] fbgl. The base of the Lockport Dolomite is expected to be about [redacted] feet above the top of the primary confining zone.

2.12.4. Additional Confinement Strata

The Glenwood Shale, the Utica Shale, and the Queenston Formation/Maquoketa Group are all additional confining beds between the primary confining zone and the lowermost USDW (Lockport Dolomite) and will prevent injection zone fluids from reaching the lowermost USDW should they migrate past the primary confining zone.

2.12.5. Structural Integrity

The 2D seismic data acquired for the project indicates there are no faults or fractures, or other natural conduits, which can be identified to transect the injection zone within the AoR that would allow injection zone fluid migration beyond the primary confining zone. All faults in the project area identified through the 2D seismic surveys are outside of the AoR. Fault slip analyses of these faults outside of the AoR conclude that there is a very low probability of fault slippage occurring due to the planned injection operations. A future baseline 3D surface seismic survey at the Stonewell Project site will further reduce uncertainty associated with formation thickness/depth and potential structural features.

2.12.6. Capacity and Storage

The AoR and Corrective Action Plan show that the Mt. Simon Sandstone at the Stonewell Project Site storage location has more than sufficient capacity and the hydrogeologic characteristics necessary to store an estimated 5.1 Mt over the life of the project.

Computational modeling was used to simulate multiphase (brine and CO_2) flow in the subsurface and considered the injection zone and primary confining zone geologic and hydrogeologic characteristics. The computational modeling included one injection well within the sequestration site and resulting AoR. Major CO_2 trapping mechanisms modeled include structural/stratigraphic trapping, residual phase trapping, solubility trapping, and mineral trapping. The computational model demonstrates that the pressure front will dissipate rapidly in the PISC phase of the project, and the CO_2 plume movement stabilizes and will be confined to the injection zone (Attachment 02: AoR and Corrective Action Plan, 2025).

2.12.7. Injection Zone and Compatibility with the Injectate

The well casing, tubing, and cement used through the primary confining zone and injection zone will be CO_2 resistant (Attachment 04: Injection Well Construction Plan, 2025).

2.12.8. Addressing Uncertainty

Vault GSL CCS LP has proposed a comprehensive core and logging program at the Stonewell Project site in (Attachment 05: Pre-operational Testing Program, 2025) as well as a 3D seismic survey to address uncertainties prior to injection operations. The purpose of acquiring these data is to validate current understanding of subsurface conditions and site suitability and provide site specific data for modeling and characterization. Vault GSL CCS LP will prepare a Pre-operational Narrative that will be submitted to the EPA incorporating the acquired data and updated static and computational models prior to the start of injection.

3. AoR and Corrective Action

The AoR for the Stonewell Project is shown in Figure 1.

Attachment 02: AoR and Corrective Action Plan, (2025) provides a detailed summary of the modeling parameters. After a thorough review of all identified wells in the region, it has been determined that there are no wells within the AoR that penetrate the confining zone, and there are no requirements for corrective action.

AoR and Corrective Action GSDT Submissions
GSDT Module: AoR and Corrective Action ***Tab(s):*** All applicable tabs Please use the checkbox(es) to verify the following information was submitted to the GSDT: ☒ Tabulation of all wells within AoR that penetrate confining zone ***[40 CFR §146.82(a)(4)]*** ☒ AoR and Corrective Action Plan *[40 CFR §146.82(a)(13) and §146.84(b)]* ☒ Computational modeling details ***[40 CFR §146.84(c)]***

4. Financial Responsibility

The financial assurance estimation for the project was divided into four components:

1. Corrective Action,
2. Injection Well Plugging and Abandonment,
3. Post Injection Site Care and Closure, and
4. the Emergency and Remedial Response Plan (ERRP).

Claimed as PBI [redacted]

Internal estimates and external vendor quotes were used to assemble the estimates for the first three components. All appropriate quotes from vendors have been provided with the submittal documentation. The cost estimate for the ERRP was developed in tandem with Industrial Economics (IEc). Their full report is provided with the submittal documentation.

Further detail is provided in the Financial Assurance section of this permit application (Attachment 03: Financial Assurance Plan, 2025).

Financial Responsibility GSDT Submissions
GSDT Module: Financial Responsibility Demonstration ***Tab(s):*** Cost Estimate tab and all applicable financial instrument tabs Please use the checkbox(es) to verify the following information was submitted to the GSDT: ☒ Demonstration of financial responsibility ***[40 CFR §146.82(a)(14) and §146.85]***

5. Injection Well Construction

A stratigraphic well (Stonewell / INJ1, API #: 34-101-2-0223-00-00) will be drilled under the Ohio Department of Natural Resources Division of Oil and Gas Resources Management Permit to Drill a Stratigraphic Well. This stratigraphic well is intended to be used as the injection well (STO INJ1) upon issuance of the final Class VI authorization to inject.

STO INJ1 will be constructed to prevent movement of fluids into or between USDWs or into unauthorized zones; allow the use of testing equipment and workover tools; and permit continuous monitoring of the annulus space between injection tubing and long string casing as per §146.86(a). All well-related construction work will be performed in accordance with EPA guidance documents, approved work plans, and reporting timelines as approved by the EPA. STO INJ1 will be used to collect most of the pre-operational testing data for the project (Attachment 05: Pre-operational Testing Program, 2025) per §146.87.

Materials (casing, cement, etc.) used for the construction of STO INJ1 will conform to §146.82(b) and (c) and be verified by independent third-party sources as suitable for the worst-case corrosive and operational loading expected to occur during the life of the project (Tuboscope - NOV Wellbore Technologies, 2017; Baker Hughes, 2021; Schlumberger, 2021; AMPP, 2023; “API 5CT,” 2023). Documentation verifying the suitability of the selected materials are provided in Appendix 1D-*Suitability of Selected Materials*. This suitability is discussed further in Section 5.5 *Additional Design Parameters*.

STO INJ1 will be drilled through the entirety of the Mt. Simon Sandstone and into the underlying Precambrian rocks to a depth sufficient to allow logging tools to record the Precambrian – Mt. Simon Sandstone contact. STO INJ1 will be constructed with multiple casing strings adhering to §146.82(b). Each string will be smaller in diameter than the previous string and cemented to surface to provide multiple layers of protection for USDWs as per §146.86(b)(2) and (3). After installation of casing strings, the well will be plugged back in manner that will ensure that the CO_2 will not be directly injected into the Precambrian rocks, and perforations will be made into the casing to access the Mt. Simon Sandstone for injection. The wellhead will use appropriately sized components and materials of construction based on the build of the wellbore.

This section of the document details the methods and materials to be used for the construction of the injection well STO INJ1. Schematics of the well that illustrate its construction and wellhead are provided in Attachment 04: Injection Well Construction Plan, (2025). Well schematics are subject to change pending finalization of completion design.

5.1. Proposed Stimulation Program [40 CFR §146.82(a)(9)]

Well stimulation is not expected to be required after initial completion other than to clean out the perforations made in the long string casing.

Intermediate stimulations during the life of the project may be required based on well conditions and performance. For instance, near-wellbore salt precipitation may cause a reduction in well performance that may be remediated using a hot water flush to dissolve and remove the precipitated salt.

The requirements and methods of stimulation will be identified through the evaluation of well performance over time. The EPA will be notified prior to any field mobilization and will include details on the proposed procedure, equipment, and chemicals to be used.

A list of common remediation techniques that may be deployed is listed below. This list is not exhaustive and additional technologies or treatments may be used.

- Matrix acid stimulation,
- Coil tubing chemical stimulation,
- Coil tubing mechanical stimulation,
- Coil tubing stimulation with a saltwater flush,
- Perforations.

All treatments will be performed at or below 90% of the fracture pressure of the Mt. Simon Sandstone to prevent the development of fractures and to ensure that containment is maintained. Calculations to determine safe working pressures during stimulation operations will be determined prior to any work and be strictly enforced while stimulation operations are carried out.

Potential additives to stimulations may include but are not limited to hydrochloric (HCl) acid, dilute mud acid (HCl and hydrofluoric acids), citric acid, scale reducer, defoamers, or saline solution (potassium chloride or other non-reactive mineral solution). Prior to the use of any acids, additives, or other stimulation fluid, analysis of the drill cuttings and/or core will be performed to ensure compatibility between any solutions and the Mt. Simon Sandstone.

5.2. Construction Procedures [40 CFR §146.82(a) and (b)]

Multiple strings of casing consisting of carbon steel, 13-Chrome (13Cr) and 25-Chrome (25Cr) steel alloy will be installed and cemented in place across the entire length of the well to protect the USDWs and other strata overlying the injection zone. 25Cr casing will be installed across the entire injection zone and confining zone to maximize protection from the injection zone fluids. 13Cr will be run from above the confining zone to surface, above the 25Cr, in the long string section. CO_2 will be injected into the Mt. Simon Sandstone using internally coated carbon steel tubing landed in a nickel or chrome-coated packer with a single pup joint of 25Cr tubing below the packer. The Mt. Simon Sandstone will be accessed through[redacted] Table 25 provides a summary of the open-hole sections of the injection well construction including depths and hole size per §146.86(b)(iii).

The injection well is designed to enable monitoring equipment to be accessible and retrievable for maintenance or replacement. Downhole gauges will be landed in a mandrel above the packer. The lines from downhole gauges will be run within the casing-tubing annulus through a port in the wellhead. The mandrel and port will be appropriately rated for the anticipated pressure loading downhole and at the wellhead.

A high-level procedure for the well installation is provided below. A more detailed schedule and procedure will be provided to the EPA prior to spudding the well.

1. Conductor casing will be driven into place.
2. Surface hole section will be drilled to a sufficient depth below the base of the Lockport Dolomite such that the entirety of the Lockport Dolomite can be logged during open and cased hole logs.
3. Open hole logs will be run.
4. Casing will then be run and cemented in place.
5. After allowing sufficient time for the cement to harden, cased hole logs will be run, and the casing will be pressure tested.
6. Intermediate string hole section will be drilled approximately 100 feet into the Trempealeau Formation.
7. Open hole logs will be run.
8. Intermediate casing will be installed and cemented.
9. After allowing sufficient time for the cement to harden, cased hole logs will be run, and the casing will be pressure tested.
10. Long string hole section will be drilled. Core will be acquired in the Rome Formation and Mt. Simon Sandstone. This hole will be drilled into Precambrian Basement.
11. Open hole logs will be run.

12. Casing will then be run and cemented in place with the plugged back depth at the top of the Precambrian Basement.
13. After allowing sufficient time for the cement to harden, cased hole logs will be run, and the casing will be pressure tested.
14. Perforations will be made in the long string casing into the Mt. Simon Sandstone.
15. The tubing, packer, and wellhead will then be installed. The annulus will be filled with a non-corrosive fluid with additives, approximately 8.34 lb/gallon in weight.
    a. The components to be used include, but are not limited to, are:
        i. Freshwater
        ii. Biocide
        iii. Corrosion inhibitor
        iv. Oxygen scavenger

Specifications on the tools, equipment, casing, cement, and other equipment or materials required to install the well are provided in more detail in the following sections. All materials of construction are designed to API standards and are intentionally chosen to maximize protection from corrosive, operational, and installation loading. Each item is suitably rated for the loading it will experience.

5.3. Casing and Cementing

5.3.1. Casing

Table 26 and Table 27 display the design safety factors and the safety factor loads for the proposed well designs as per §146.86(b)(1)(ii). The safety factor is determined by dividing the pipe rating by the calculated load. Three loading scenarios were considered for the casing and tubing analysis: burst analysis scenario, collapse analysis scenario, and tensile analysis scenario. A standard 80% derating factor for new pipe is applied prior to analyses. Material and specification derating based on tensile loading has also been considered for the collapse analysis. Within this section, tensile analysis refers to the axial loading analysis performed on the casing.

The casing burst analysis considers the impact of the plug bump and predetermined holding pressure following the full pumping of cement. The holding pressure is typically 500 psi over the hydrostatic pressure required to pump the cement, or 80% of the burst rating of the pipe, whichever is less.

The tubing burst analysis uses the maximum allowable injection pressure (MAIP) at surface which is where the tubing-annulus differential is greatest (Section 7.1.1 *Determination of Maximum Injection Pressure*).

The casing collapse analysis scenario considers a full column of cement in the annulus following the bleed-off of pressure used to hold the plug in place at the conclusion of cementing. This analysis includes derating the collapse rating of pipe while in tension.

Tubing collapse analysis considers the collapse loading during a modeled annulus pressure test with 1,500 psi on the annulus. In this scenario, the maximum collapse load will be experienced at the packer.

Tensile (axial) analysis for casing evaluates the impact of a 100,000-pound overpull on the casing string, where overpull is the pulling weight less the weight of the pipe. The tubing tensile analysis uses 80,000 pounds for overpull. Note that this scenario will typically occur prior to any cement being pumped, and hydrostatic differences in fluid have not been considered.

Table 27 presents the safety factor loads from these analyses for casing and tubing per §146.86(b)(1)(ii) and §146.86(c)(3)(vii). In addition, operational, cyclic, and temperature loading analyses were performed that are discussed in greater detail in Section 5.5 *Additional Design Parameters*. Further discussion on the suitability of use of the long string casing is provided in Section 5.5.7.1 *Casing*. Further discussion on the suitability of the corrosion resistant cement system to be used in the well per §146.86(b)(5) is provided in Section 5.5.7.3 *Suitability of EverCRETE*.

Table 28 displays the setting depths and specifications of the casing (and tubing) to be used for the well as per §146.86(b)(1)(iv) and §146.86(c)(3)(i) and (vi). All of the casing conforms with API specifications and meets or exceeds Association for Materials Protection and Performance (AMPP) 2023 recommendations (AMPP, 2023). Table 29 shows the design parameters of the casing and tubing to be used for the well. All materials of construction are suitable for the anticipated loading and are not anticipated to decrease in suitability over time. These materials meet or exceed relevant guidance and regulations (40 CFR 146.86(b)).

Details on the cement program are provided in Section 5.3.2 *Cementing*. All cement used will conform with API standards and address §146.86(b)(5). Corrosion resistant cement will be used from the bottom of the long string casing in the Mt. Simon Sandstone to above the top of the Rome Formation.

Mechanical integrity per §146.89 will be demonstrated as part of the initial completion and as needed during injection operations as discussed in (Attachment 05: Pre-operational Testing Program, 2025) and Attachment 06: Testing and Monitoring, (2025).

All materials for the construction will be suitable for the anticipated loading and are not anticipated to decrease in suitability over time.


Claimed as PBI


Claimed as PBI


Claimed as PBI

5.3.2. Cementing

Table 30 provides a summary of the cement systems that will be used during the construction of the injection well. All cement systems used will conform with API standards where applicable.

Cement will be pumped with the following excess:

- Surface: 100% open-hole excess
- Intermediate: 50% open-hole excess
- Long string: 30% open-hole excess

The excess cement pumped will be subject to change pending field results.

The Stonewell Project plans to use CO_2-resistant cement (e.g., EverCRETE from SLB, or an equivalent alternative system) for the lower portion of the long string section per §146.86(b)(viii). These cement systems are stable in extreme acidic conditions, are highly resistant to the CO_2 stream (both wetted and supercritical), and formation fluids in the Mt. Simon Sandstone, and of sufficient quality to maintain integrity over the design life of the injection well per §146.86(b)(5). Further details on the suitability of use for the proposed CO_2-resistant cement are provided in Section 5.5.7.3 *Suitability of EverCRETE*.

No cement will be used for the installation of the conductor casing.

The surface casing cement system will provide the isolation for the Lockport Dolomite, the lowermost USDW, from the drilling process for the remainder of the well installation. The surface cement will serve as an additional layer of protection from potential upward fluid migration from deeper formations. The surface casing cement will utilize a single-stage program comprised of Class A Portland Cement with additives (Table 30).

The intermediate casing cement system will provide isolation from any potential lost circulation zone and serve as an additional layer of protection from potential upward migration of injection zone fluids. It is anticipated that if a lost circulation zone is encountered, it would likely be at the contact of the Gull River and Trempealeau Formations. As such, the intermediate section is planned to be drilled a maximum of 100 feet into the Trempealeau Formation. The intermediate casing cement system will utilize a single stage program comprising of Class H Portland Cement with additives (Table 30).

The long string cement system will provide the primary isolation of USDWs from potential migration of injection zone fluids above the injection zone. The system will use one stage with two types of cement, separated into a lead and tail. The lead cement will contain Class H Portland Cement with additives (Table 30). The tail cement will utilize EverCRETE, a CO_2 resistant cement blend (or equivalent CO_2 resistant cement) (Table 30). This cement system will also be used for STO OBS1.

Single stage cementing will achieve the required zonal isolation as part of the program that ensures quality cement placement per §146.86(b)(4) and (5). Further details on how these practices will be implemented and how they assist with quality cement placement and zonal isolation are provided in Section 5.3.2.1 *Ensuring Quality Cement Placement*.

The quality of the bond between the cement, casing, and borehole for all hole sections, will be verified by the cased hole logs that will be run after each string of casing is cemented in place per §146.86(b)(4) and (5) (Attachment 05: Pre-operational Testing Program, 2025). These cased hole logs may include: CBL with radial arms, Ultrasonic Cement Evaluation, temperature, and pulsed neutron logs.

5.3.2.1. Ensuring Quality Cement Placement §146.86(b)(4)

The proposed cementing program will use single-stage cementing for each casing to attain the required zonal isolation. This method will achieve the required zone isolation through deploying, at minimum, the following techniques:

- Running centralizers,
- Using concentric and properly rated casing,
- Reciprocating the pipe,
- Rotating the pipe,
- Pumping spacers and hole cleaning material, and,
- Rigorous testing and inspection of casing prior to installation.

Centralizers will be run as follows in each of the casing sections per §146.86(b)(3):

- Surface: one bow spring (BS) centralizer per joint
- Intermediate: one BS centralizer every 100 feet
- Long string:
  - 13Cr Section (surface to 2,538 feet): one BS centralizer every other joint
  - 25Cr Section (2,538 feet to 3,063 feet): one BS centralizer per joint

API Specification 10D (API 10D-2, 2004) provides an equation to determine optimal centralizer separation for a 2D wellbore. The wellbore is planned to be vertical (zero inclination), but it is probable that the wellbore will have some minor inclination. The plan to measure well inclination is provided in the Pre-operational Testing Program (Attachment 05: Pre-operational Testing Program, 2025). An average inclination of the wellbore of 1.5 degrees has been conservatively assumed for the calculations presented below.

As an example, the long-string casing was evaluated using Equation 1 below at the bottom of the 13Cr section, which terminates above the top of the confining zone (Table 28).

$$l_c = \sqrt[4]{\frac{d_{max} \times 384 \times E \times I}{W_b \times \sin\theta}} \qquad (1)$$

Where,

lc is the optimum centralizer spacing, in inches
d_{max} is the maximum deflection of the casing between centralizers, in inches
E is casing modulus of elasticity in psi (defined as 2.92 E06 psi for 13Cr steel alloy)
I is the casing moment of inertia, in inches4
W_b is the buoyant weight of the casing, in pounds per inch
θ is the inclination of the well, in degrees

To determine d_{max}, the following equation was used:

$$d_{max} = e_c - e_s \qquad (2)$$

Where,

e_c is defined as the stand off at the centralizer, in inches
e_s is defined as the stand off at the sag point, in inches
e_s was determined by multiplying the standoff ratio (standard 66.7% was utilized, per API recommendations) by the maximum annual clearance for perfectly centered pipe.

Utilizing long-string parameters in Equation 2, the d_{max} was determined to be 0.291 inches.

The moment of inertia was determined using Equation 3 to be 37.24 inches^4.

$$I = \frac{\pi \times (OD^4 - ID^4)}{64} \qquad (3)$$

The buoyant weight of the casing was determined by multiplying the buoyancy factor by the weight of the casing in air. The buoyancy factor (f_b) was evaluated at two different scenarios. The first is when the entire casing string is full of cement. In this scenario, the casing will fall to the bottom of the hole, and the deflection will be assessed at the bottom of the hole. In the second scenario, the annulus is full of cement, and the casing string is full of the displacement fluid. In this scenario, the casing floats to the top of the hole and the deflection is assessed at the top of the hole. Within this scenario, the buoyant weight of the pipe is negative, consistent with the pipe floating. The absolute value of the weight of the pipe was utilized to determine the centralizer separation.

Using Equation 4, a cement weight of 15.6 pounds per gallon (ppg), a displacement fluid weight of 8.5 ppg, and the casing weight and cross-sectional area for the 13Cr portion of the long string section, the buoyancy factors for both scenarios were calculated.

$$f_b = \frac{\left(1 - \frac{\rho_e}{\rho_s}\right) - \left(\frac{ID}{OD}\right)^2 \times \left(1 - \frac{\rho_i}{\rho_s}\right)}{1 - \left(\frac{ID}{OD}\right)^2} \qquad (4)$$

Where,

ρ_e is the density of the external fluid, in ppg
ρ_s is the density of the casing, in ppg
ρ_i is the density of the internal fluid, in ppg

The weight of the casing was determined to be 4.80 pounds per inch (pounds/in) and 3.74 pounds/in for scenarios one and two, respectively.

Using the determined inputs in Equation 1, optimal centralizer separation for scenarios one and two were determined to be 80 feet and 85 feet, respectively. The minimum value was taken to determine the optimal spacing.

Based on this analysis an 80-foot centralizer separation (nominally every other joint) will be utilized in the 13Cr section. A 40-foot centralizer spacing (approximately one centralizer per joint) will be used in the 25Cr section, which covers the injection and confining zones, and is consistent with published guidance and publicly available sources (API 10D-2, 2004)
.

The same analysis was used to determine optimum centralizer separation of approximately 100 feet in the intermediate section. To maximize casing centralization, Vault GSL CCS LP will conservatively run one centralizer per joint in the surface section, although analysis indicates centralizer spacing of approximately 130 feet would be sufficient.

The centralizer program will be run as detailed in Table 31 for the injection well.

Claimed as PBI

The centralizer spacing analysis also was performed for each of the monitoring wells and the results are provided in Attachment 06: Testing and Monitoring,(2025).

In addition to effective centralizer separation, while cement is being pumped the pipe will be reciprocated (moved up and down) and rotated. Once the cement has reached the backside of the casing, reciprocation will cease, but rotation will continue. These actions will help to agitate any remaining mud cake or debris in the backside of the casing following the spacer and hole cleaning buffer fluids, improving the overall quality of cement. These actions will be employed for each cementing system for each well.

5.4. Tubing and Packer §146.86(c)

Tubing will be used to inject CO_2 into the injection zone beneath a packer set at approximately 2,785 feet opposite a cemented interval as per §146.86(c)(2). The tubing will be internally coated 2 7/8-inch L-80 pipe designed for CO_2 service per §146.86(c)(1). An example of a CO_2 service coating is National Oilwell Varco (NOV) Tuboscope™, TK15XT, which is used in CO_2 floods for enhanced oil recovery. Material specifications and suitability for use were determined from material provided by NOV (*Tuboscope Coatings Spec Sheet*, 2022).

The injection packer will use CO_2 resistant materials for the CO_2-wet surfaces per §146.86(c)(1). An example of this type of packer is the Baker Hughes' Signature F™ Injection packer system. The packer can be used with either a retrievable or permanent configuration and will be made of 25Cr or a nickel alloy to resist corrosion effects of the CO_2 stream (Baker Hughes, 2021). Tubing and packer setting depths and materials of construction are detailed in Table 32 per §146.86(c)(3).

Claimed as PBI

5.5. Additional Design Parameters

This section discusses the application of the design ratings to ensure the suitability of the construction materials for this project in addition to the analysis performed in Section 5.3 *Casing and Cementing.*

Consistent with Section 5.3 *Casing and Cementing*, all tubulars have been derated to 80% of their initial ratings. All comparative evaluations detailed in this section are in reference to these derated values.

The injection packer will have a differential rating of 10,000 psi and a max load rating of 80,000 pound-force.

5.5.1. Temperature

Claimed as PBI

5.5.2. Injection Pressure

Claimed as PBI

Claimed as PBI

5.5.3. Annulus Pressure

Claimed as PBI

Claimed as PBI

5.5.4. Formation Pressure

Claimed as PBI

5.5.5. Tensile Loading

5.5.6. Cyclic Loading

5.5.7. Corrosion Loading

Claimed as PBI

5.5.7.1. Casing

Claimed as PBI

Claimed as PBI

5.5.7.2. Tubing and Packer

Claimed as PBI

Claimed as PBI

5.5.7.3. Suitability of EverCRETE

Claimed as PBI

Claimed as PBI

5.5.8. Operational Considerations

Emergency shut-down equipment will be used for this project. Details on this equipment, the set points to trigger alarms and shut-downs, as well as testing are provided in Attachment 06: Testing and Monitoring (2025), Attachment 09: Emergency and Remedial Response Plan (2025), and Section 7 *Well Operation*.

Surface monitoring equipment will be connected to the surface SCADA system (Attachment 06: Testing and Monitoring, 2025 and Section 7 *Well Operation*).

Permanent downhole gauges will be used to monitor pressure and temperature at the packer. These gauges will be landed in a gauge nipple above the packer in STO INJ1 and STO OBS1 and will be hung from wire strapped to the tubing in STO ACZ1. These gauges will transmit data through a wire that is run up the annulus to the SCADA system.

Tubulars have been designed such that logging tools and other equipment needed for routine annual monitoring will be able to pass through with no restrictions.

6. Pre-operational Logging and Testing

Details on the pre-operation testing plan are provided in the relevant section of this permit application (Attachment 05: Pre-operational Testing Program, 2025).

Pre-Operational Logging and Testing GSDT Submissions
GSDT Module: Pre-Operational Testing ***Tab(s):*** Welcome tab Please use the checkbox(es) to verify the following information was submitted to the GSDT: ☒ Proposed pre-operational testing program ***[40 CFR §146.82(a)(8) and §146.87]***

7. Well Operation

This section provides a brief overview of the well operation conditions. The operational parameters for STO INJ1 are provided in Table 33 will be monitored continuously. All gauges and sensors will record and transmit data to the SCADA system. These data will be provided semi-annually (twice per year) as part of regular reporting per 40 CFR §146.91.

Downhole pressure gauges will be installed to help prevent the maximum allowable bottomhole pressure (BHP) from being exceeded. The maximum allowable BHP is 90% of the fracture pressure (40 CFR 146.88 (a)). The downhole pressure gauge will not be the primary monitoring point for injection pressure but will be used to validate the surface pressure gauges (primary monitoring point) and help to calibrate the conversion from BHP to surface pressure at the beginning of the project. The downhole temperature gauges will be installed in the same package as the downhole pressure gauge.

The pressure and temperature gauges will also be used to calculate the injected volume of CO_2 at reservoir conditions and will allow the project to identify potential mechanical integrity, or formation integrity issues in real-time. The downhole gauges will be programed to record data at the intervals outlined in Table 33. The data collected from these measurement systems will be collected continuously and sent to a surface SCADA system. Data collected by this system will be transferred and maintained permanently in a secure database. This data will be provided biannually (twice per year) as part of regular reporting as per 40 CFR 146.91.

The downhole pressure gauges will be used primarily to prevent the maximum allowable bottomhole pressure from being exceeded

7.1. Operational Procedures [40 CFR §146.82(a)(10)]

Table 34 displays the parameters that will be used during injection operations that will be discussed in this portion of the document. Details on the methods of calculations and inputs for these values are provided in Section 7.1.1 *Determination of Maximum Injection Pressure.* The presented values are based on regional data and will be updated as a result of the Pre-operational Testing Program (Attachment 05: Pre-operational Testing Program, 2025).

Injection pressures will remain below 90% of the fracture pressure (40 CFR §146.988(a)). It is not anticipated that significant deviation from these values will occur during the life of the project.

7.1.1. Determination of Maximum Injection Pressure

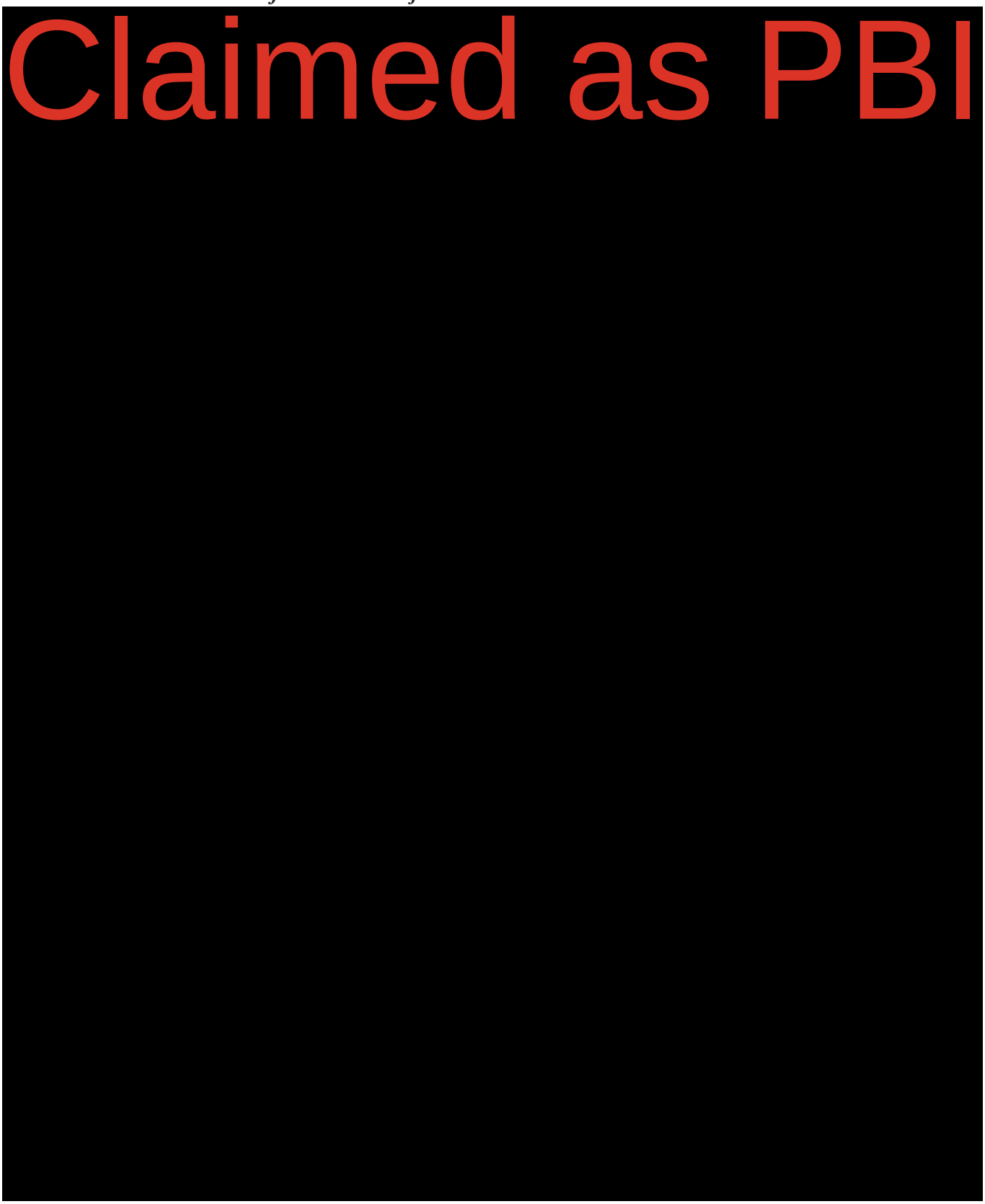


Claimed as PBI

Claimed as PBI

7.1.2. Determination of Operational Annulus Pressure

Claimed as PBI


Claimed as PBI

Claimed as PBI

The annular pressure operations will be performed as follows:

1. The fluids in the annulus will be managed to mitigate the effects of thermal expansion or contraction during start-up and shutdown conditions. Annulus fluids will be required to be bled off during any injection start-ups following the initial completion or subsequent workovers. Nitrogen will be added to the annulus in order to maintain minimum pressure during shutdowns or when the injection rate is reduced.
2. Under steady-state injection operations, pressure alarm set points will be at:
    a. 1,250 psi for the high alarm
    b. 1,500 psi for the high-high automatic shutdown
    c. 300 psi for the low alarm
    d. 100 psi for the low-low automatic shutdown
    e. 100 psi differential for the automatic shutdown.
3. Should a high or low alarm occur, the occurrence will be noted in daily logs.
4. Should a shut-down event occur, the well will be shut-in, and the cause of the shut-down event will be investigated by the operator.

Any time the annulus is blown down and fluid is removed, the volume of fluid removed from the annulus will be measured.

7.1.3. Potential Future Variation in Operational Parameters

The Stonewell Project does not anticipate any variations from the current operational parameters outlined in Section 7.1 *Operational Procedures*. Should variations occur which would necessitate any changes to those parameters, EPA Region 5 would be consulted prior to making any such changes.

7.2. Proposed CO_2 Stream [40 CFR §146.82(a)(7)(iii) and (iv)]

The CO_2 injection stream will be sourced from an ethanol production facility located in Marion County, Ohio and is anticipated to have the fluid composition as shown in Table 36.

Vault GSL CCS LP will analyze the CO_2 stream during the injection phase of the project to provide data representative of its chemical characteristics and to meet the requirements of 40 CFR §146.90 (a). Quarterly sampling and analysis of the CO_2 injection stream will be performed to track the composition of the stream (Attachment 06: Testing and Monitoring, 2025). Additional details on technical standards, QA/QC policy, sample collection and storage policies, and analytical methods are provided in Attachment 10: Quality Assurance and Surveillance Plan, (2025).

The CO_2 stream produced from an ethanol production facility will be of high purity based on the nature of the ethanol fermentation process. The CO_2 stream from ethanol fermentation typically exceeds 99 % CO_2 (mole basis), with minor impurities including common atmospheric gases (ex: O_2, N_2) and H_2O. The stream will be dehydrated to a low water content prior to entering the pipeline to the injection well.

7.3. Planned Shutdowns and Well Interventions

Through the injection phase of the project, Vault GSL CCS LP anticipates that the project wells will need to be shut down for maintenance or have intermediate stimulations performed on them. These scenarios were considered when evaluating the materials, the design of the wells, and through the development of the operational procedures in order to minimize and mitigate risk of damage to well materials.

7.4. Well Maintenance

Through the life of the project, it is anticipated that the project wells may require well maintenance or a workover to modify the injection interval. Should there be a need to pull tubing, several steps will be taken to minimize potential contact of the casing with CO_2 or brine from the injection zone.

- Prior to removing the tubing or packer, the well will be killed using a brine of sufficient weight to displace CO_2 in the well and near wellbore CO_2. A minimum of two casing volumes (cased hole interval plus the tubing string) will be pumped to kill the well at a rate sufficient to achieve plug flow.
- During a workover, the rig crew will have CO_2 detectors to monitor for CO_2 influx or migration from the injection zone and re-kill the well if necessary.
- Blow out preventors will be installed during all workover to act as a second barrier to flow.
- If the well is left without the tubing and packer for an extended period of time, a retrievable bridge plug will be run in the well and set above the perforations. This plug will be made of sufficient materials to resist corrosion. The wellbore above the bridge plug will be filled with corrosion inhibited fluid.

At the end of the operational life of the project, the wells will be worked over to fully replace the tubing string and downhole gauges to minimize the likelihood of the need to workover the wells within the PISC period.

8. Testing and Monitoring

Testing and Monitoring GSDT Submissions
GSDT Module: Project Plan Submissions **Tab(s):** Testing and Monitoring tab Please use the checkbox(es) to verify the following information was submitted to the GSDT: ☒ Testing and Monitoring Plan [40 CFR §146.82(a)(15) and §146.90]

This section is meant to provide a brief overview of the Testing and Monitoring Plan. Further details on the well operation program are provided in Attachment 06: Testing and Monitoring, (2025).

The Stonewell Project uses a risk-based Testing and Monitoring Plan that includes operational, verification, and environmental assurance components that meet the regulatory requirements of 40 CFR §146.90. This Testing and Monitoring Plan is based on experience gained from other approved Class VI projects, as well as extensive geologic evaluation and computational modeling.

Goals of the monitoring strategy include, but are not limited to:

- Fulfillment of the regulatory requirements of 40 CFR §146.90,
- Protection of underground sources of drinking water (USDW),
- Risk mitigation over the life of the project,
- Confirmation that STO INJ1 is operating as planned while maintaining mechanical integrity,
- Acquisition of data to validate and calibrate the models used to predict the distribution
  of CO_2 within the injection zone, and
- Support AoR re-evaluations over the course of the project.

The Testing and Monitoring Plan will be adaptive over time, and is subject to alteration should one of the following potential scenarios occur:

- Project risks evolve over the course of the project outside of those envisioned at the beginning of the project,
- Significant differences between the monitoring data and predicted computational modeling results are identified,
- Key monitoring techniques indicate anomalous results related to well integrity or the loss of containment.

The monitoring activities fall within three categories based on project objectives: operational, verification, and assurance monitoring Table 37.

- ***Operational monitoring*** focuses on day-to-day injection operations such as system performance.
- ***Verification monitoring*** confirms that the injected CO_2 remains contained within the selected storage zone. The CO_2 plume and pressure front development are tracked over time to provide data for model calibration. Integration of verification monitoring data into project models allows the project to demonstrate conformance between the computational modeling and the testing and monitoring data collected during the operations and post injection phases of the project's lifecycle.
- ***Assurance monitoring*** is performed at surface and near-surface (i.e., soil, shallow groundwater, USDWs, etc.) to monitor for any changes from baseline sample data that might indicate CO_2 or injection zone fluid migration towards surface.

The three monitoring categories encompass:

- Well operations,
- Containment,
- Non-endangerment of USDWs,
- Capacity,
- Injectivity,
- Injection pressure, and
- Conformance.

Table 37 provides a summary of the general monitoring strategy with subcategories.

9. Injection Well Plugging

During the PISC period the injection well will be permanently plugged and abandoned (Attachment 08: Post-injection Site Care and Site Closure, 2025). Details on the methods of these operations are provided in (Attachment 07: Injection Well Plugging Plan, 2025). The methods and procedures presented in the attachment are consistent with industry standards and the requirements detailed in 40 CFR §146.92. All materials to be used for the plugging and abandonment are suitable for the anticipated corrosive loading below the top of the Conasauga Formation. Above the top of the Conasauga Formation, the materials are standard construction materials, conforming the API specifications.

Injection Well Plugging GSDT Submissions
GSDT Module: Project Plan Submissions ***Tab(s):*** Injection Well Plugging tab Please use the checkbox(es) to verify the following information was submitted to the GSDT: ☒ Injection Well Plugging Plan [40 CFR §146.82(a)(16) and §146.92(b)]

10. Post-injection Site Care and Closure

The requested documents listed below have been included in the file submission (Attachment 08: Post-injection Site Care and Site Closure, 2025). These documents address the rule requirements for the EPA citations. The Stonewell Project is not requesting an alternative PISC timeframe.

PISC and Site Closure GSDT Submissions
GSDT Module: Project Plan Submissions ***Tab(s):*** PISC and Site Closure tab Please use the checkbox(es) to verify the following information was submitted to the GSDT: ☒ PISC and Site Closure Plan [40 CFR §146.82(a)(17) and §146.93(a)]
GSDT Module: Alternative PISC Timeframe Demonstration ***Tab(s):*** All tabs (only if an alternative PISC timeframe is requested) Please use the checkbox(es) to verify the following information was submitted to the GSDT: ☐ Alternative PISC timeframe demonstration ***[40 CFR §146.82(a)(18) and §146.93(c)]***

11. Emergency and Remedial Response

The requested documents listed below have been included in the file submission (Attachment 09: Emergency and Remedial Response Plan, 2025). These documents address the rule requirements for the above EPA citations.

Emergency and Remedial Response GSDT Submissions
GSDT Module: Project Plan Submissions ***Tab(s):*** Emergency and Remedial Response tab Please use the checkbox(es) to verify the following information was submitted to the GSDT: ☒ Emergency and Remedial Response Plan *[40 CFR §146.82(a)(19) and §146.94(a)]*

12. Injection Depth Waiver and Aquifer Exemption Expansion

Vault GSL CCS LP does not intend to apply for a Depth Waiver or Aquifer Exemption. As such, no supplemental documents have been filed.

Injection Depth Waiver and Aquifer Exemption Expansion GSDT Submissions
GSDT Module: Injection Depth Waivers and Aquifer Exemption Expansions ***Tab(s):*** All applicable tabs Please use the checkbox(es) to verify the following information was submitted to the GSDT: ☐ Injection Depth Waiver supplemental report ***[40 CFR §146.82(d) and §146.95(a)]*** ☐ Aquifer exemption expansion request and data ***[40 CFR §146.4(d) and §144.7(d)]***

13. Optional Additional Project Information

The National Wild and Scenic River System database indicates that no designated wild and scenic rivers exist in Marion County, Ohio. Within the state of Ohio, there are three rivers designated as national wild and scenic river, all of which are located well away from the project area. Big & Little Darby Creeks are located in the central portion of the state west of Columbus, Little Beaver Creek is in the eastern portion of the state near Calcutta, and the Little Miami River is located in the southwest corner of the state traversing from Cincinnati to Fairborn. (National Information Services Center and National Park Service, 2023; National Wild and Scenic Rivers System).

A review of Nationwide Rivers Inventory (NRI) river segments was undertaken to identify nearby NRI river segments that are potential candidates for inclusion in the National Wild and Scenic River System. Scioto River, a NRI river located in Marion County, runs from Kenton to Bellepoint (National Park Service). Although located in Marion County, Scioto River is located over 6 miles south from the injection well. Another NRI river in the area, the Sandusky River, is

located over 7 miles north from the injection well. Neither NRI river is located within the AoR so the project will have no effect on the identified rivers.

The Stonewell Project is located inland Ohio, far from coastal zones, therefore project activities will not affect any coastal zones.

The Stonewell Project well site will be located on private land. The Ohio State Historic Preservation Office conducted a cultural resources desktop review in the area surrounding the AoR to determine known archaeological, historic, and cultural properties that could potentially be affected by the Stonewell Project. The desktop review identified several previously surveyed areas, 13 previous archaeological inventories (12 pending review), five historic inventories, and four cemeteries located within the AoR (Table 38, Tetra Tech, 2024)). No National Register Historic Districts or National Register Historic Sites were identified within the Stonewell Project AoR. (Tetra Tech, 2024; National Park Service). None of the identified archaeological or historic inventory sites or cemeteries are expected to be disturbed, as they are located outside of the proposed wellsite and pipeline disturbance areas.

Table 38: Cemeteries within the AoR, identified by Ohio State Historic Preservation Office (SHPO) during desktop review (Tetra Tech, 2024)

OGS ID	Description
7338	Kannel Cemetery
7339	Pleasant Hill Cemetery
7341	Union Cemetery
7437	Neff Cemetery

On August 20, 2025, a review of the US Fish and Wildlife Service (USFWS) Information for Planning and Consultation (IPaC) system identified threatened, endangered, candidate, or proposed species that may potentially be affected by the Stonewell Project (Table 39).

Table 39: Federal threatened or endangered, candidate, or proposed species potentially affected by the Stonewell Project (USFWS, 2025)

Name	Federal Status	Critical Habitat
Indiana Bat	Endangered	Project location does not overlap critical habitat
Whooping Crane	Experimental non-essential	No critical habitat designated
Eastern Massasauga	Threatened	No critical habitat designated
Rayed Bean	Endangered	Project location does not overlap proposed critical habitat
Salamander Mussel	Proposed Endangered	Project location does not overlap proposed critical habitat
Monarch Butterfly	Proposed Threatened	Project location does not overlap proposed critical habitat

IPaC indicates bald and/or golden eagles are in the Stonewell Project area. Bald and golden eagles are protected under the Bald and Golden Eagle Protection Act and the Migratory Bird Treaty Act. Migratory birds of particular concern that may be present in the AoR include the USFWS Birds of Conservation Concern (BCC) listed in Table 40.

Table 40: Migratory birds of conservation concern potentially affected by the Stonewell Project (USFWS, 2025). BCC=Birds of Conservation Concern, BCR=Bird Conservation Regions.

Name	Level of Concern	Breeding Season
American Golden-plover	BCC Rangewide [1]	Breeds elsewhere
Bald Eagle	Non-BCC Vulnerable [2]	Breeds Oct 15 to Aug 31
Black-billed Cuckoo	BCC Rangewide	Breeds May 15 to Oct 10
Bobolink	BCC Rangewide	Breeds May 20 to Jul 31
Cerulean Warbler	BCC Rangewide	Breeds Apr 21 to Jul 20
Chimney Swift	BCC Rangewide	Breeds Mar 15 to Aug 25
Golden Eagle	Non-BCC Vulnerable	Breeds elsewhere
Grasshopper Sparrow	BCC Bird Conservation Regions (BCR)[3]	Breeds Jun 1 to Aug 20
Henslow's Sparrow	BCC Rangewide	Breeds May 1 to Aug 31
Hudsonian Godwit	BCC Rangewide	Breeds elsewhere
Kentucky Warbler	BCC Rangewide	Breeds Apr 20 to Aug 20
King Rail	BCC Rangewide	Breeds May 1 to Sep 5
Lesser Yellowlegs	BCC Rangewide	Breeds elsewhere
Pectoral Sandpiper	BCC Rangewide	Breeds elsewhere
Prothonotary Warbler	BCC Rangewide	Breeds Apr 1 to Jul 31
Red-headed Woodpecker	BCC Rangewide	Breeds May 10 to Sep 10
Ruddy Turnstone	BCC - BCR	Breeds elsewhere
Rusty Blackbird	BCC - BCR	Breeds elsewhere
Semipalmated Sandpiper	BCC - BCR	Breeds elsewhere
Short-billed Dowitcher	BCC Rangewide	Breeds elsewhere
Upland Sandpiper	BCC - BCR	Breeds May 1 to Aug 31
Wood Thrush	BCC Rangewide	Breeds May 10 to Aug 31

[1] BCC Rangewide birds are of concern throughout their range anywhere within the USA.

[2] Non-BCC Vulnerable birds are not BCC species in the project area but are listed because of Eagle Act requirements.

[3] BCC-BCR birds are of concern only in particular BCRs in the continental USA.

There is potential to encounter threatened or endangered (T&E) flora or fauna within the project AoR. The Ohio State Listed Species includes 20 T&E animal species and 10 T&E plant species within Marion County (Table 41, Table 42, Ohio Natural Heritage Database, 2023a, 2023b).

Table 41: Threatened and endangered fauna of Marion County, Ohio (Ohio Natural Heritage Database, 2023a).

Species Name	Common Name	State Status
Antigone canadensis	Sandhill Crane	Threatened [1]
Aythya americana	Redhead	Special Interest [2]
Bartramia longicauda	Upland Sandpiper	Endangered [3]
Botaurus lentiginosus	American Bittern	Endangered
Cygnus buccinator	Trumpeter Swan	Threatened
Ixobrychus exilis	Least Bittern	Threatened
Oxyura jamaicensis	Ruddy Duck	Special Interest
Porzana carolina	Sora Rail	Species of Concern [4]
Rallus elegans	King Rail	Endangered
Rallus limicola	Virginia Rail	Species of Concern
Spatula clypeata	Northern Shoveler	Special Interest
Erimyzon claviformis	Western Creek Chubsucker	Species of Concern
Taxidea taxus	American Badger	Species of Concern
Alasmidonta marginata	Elktoe	Species of Concern
Alasmidonta viridis	Slippershell Mussel	Threatened
Epioblasma triquetra	Snuffbox	Endangered
Lasmigona compressa	Creek Heelsplitter	Species of Concern
Uniomerus tetralasmus	Pondhorn	Threatened
Villosa fabalis	Rayed Bean	Endangered
Villosa iris	Rainbow	Species of Concern

[1] A threatened species is not in immediate jeopardy, but a threat exists. Continued or increased stress may result in the species becoming endangered.

[2] Special interest species are capable of breeding in Ohio but are at the edge of their range.

[3] An endangered species is threatened with extirpation from the state resulting from one or more causes.

[4] A species of concern may become threatened under continued or increased stress.

Table 42: Threatened and endangered flora of Marion County, Ohio (Ohio Natural Heritage Database, 2023b). U=Undetermined, P=Potentially Threatened, T=Threatened, E=Endangered.

Common Name	Scientific Name	Last Observed	State Status
Prairie False Indigo	Baptisia lactea	2019	P
False Aster	Boltonia asteroides	1999	T
Wheat Sedge	Carex atherodes	1993	P
Leiberg's Panic Grass	Dichanthelium leibergii	1995	E
Flat-stemmed Spike-rush	Eleocharis compressa	1998	P
Greene's Rush	Juncus greenei	2005	T
Large Blazing-star	Liatris scariosa	2009	T
Prairie Rattlesnake-root	Nabalus racemosus	2015	P
Royal Catchfly	Silene regia	2010	T
Prairie Ironweed	Vernonia fasciculata	2011	T

14. References

AMPP, 2023, Guideline for Materials Selection and Corrosion Control for CO2 Transport and Injection, AMPP Guide 21532–2023.

American Petroleum Institute 5CT, 11th Edition, Casing and Tubing, 2023: American Petroleum Institute.

API 10D-2, 2004, API 10D-2 Recommended Practice for Centralizer Placement and Stop-collar Testing, API Recommended Practice 10D–2: American Petroleum Institute (API).

Attachment 02: AoR and Corrective Action Plan, 2025, Underground Injection Control Class VI Permit Application: Stonewell.

Attachment 03: Financial Assurance Plan, 2025, Underground Injection Control Class VI Permit Application: Stonewell.

Attachment 04: Injection Well Construction Plan, 2025, Underground Injection Control Class VI Permit Application: Stonewell.

Attachment 05: Pre-operational Testing Program, 2025, Underground Injection Control Class VI Permit Application: Stonewell.

Attachment 06: Testing and Monitoring, 2025, Underground Injection Control Class VI Permit Application: Stonewell.

Attachment 07: Injection Well Plugging Plan, 2025, Underground Injection Control Class VI Permit Application: Stonewell.

Attachment 08: Post-injection Site Care and Site Closure, 2025, Underground Injection Control Class VI Permit Application: Stonewell.

Attachment 09: Emergency and Remedial Response Plan, 2025, Underground Injection Control Class VI Permit Application: Stonewell.

Attachment 10: Quality Assurance and Surveillance Plan, 2025, Underground Injection Control Class VI Permit Application: Stonewell.

Baker Hughes, 2021, Signature Series F Retainer Production Packer Brochure: Baker Hughes Company.

Banjade, B., 2011, Subsurface Facies Analysis of the Cambrian Conasauga Formation and Kerbel Formation in East - Central Ohio: Geology.

Baranoski, M. T., 2002, Structure contour map on the Precambrian unconformity surface in Ohio and related basement features: Ohio Division of Geological Survey, and 18-page text.

Baranoski, M. T., 2013, Structure Contour Map on the Precambrian Unconformity Surface in Ohio and Related Basement Features, Version 2.0: Columbus, OH, Department of Natural Resources, Division of Geological Survey, Digital Map Series PG-23, 17 p. text.

Baranoski, M. T., S. L. Dean, J. L. Wicks, and V. M. Brown, 2009, Unconformity-bounded seismic reflection sequences define Grenville-age rift system and foreland basins beneath the Phanerozoic in Ohio: Geosphere, v. 5, no. 2, p. 140–151, doi:10.1130/GES00202.1.

Barlet-Gouedard, V., G. Rimmele, B. Goffe, and O. Porcherie, 2007, Well Technologies for CO_2 Geological Storage: CO2-Resistant Cement: Oil and Gas Science and Technology, v. 62, no. No. 3, p. 325–334, doi:10.2516.

Barree, R. D., M. W. Conway, and J. V. Gilbert, 2009, Stress and Rock Property Profiling for Unconventional Reservoir Stimulation: SPE Hydraulic Fracturing Technology Conference, no. SPE-118703-MS, doi:https://doi.org/10.2118/118703-MS.

Berger, P. M., and W. R. Roy, 2011, Potential for iron oxides to control metal releases in CO2 sequestration scenarios: Energy Procedia, v. 4, p. 3195–3201, doi:10.1016/j.egypro.2011.02.235.

Bergstrom, S., and C. Mitchell, 1992, The Ordovician Utica Shale in the eastern midcontinent region: Age, lithofacies, and regional relationships: Oklahoma Geological Survey Bulletin, v. 14, p. 67–89.

Bethke, C. M., 1998, The Geochemist's Workbench Users Guide: University of Illinois.

Bickford, M. E., W. R. Van, and I. Zietz, 1986, Proterozoic history of the midcontinent region of North America: Geology, v. 14, no. 6, p. 492–496, doi:10.1130/0091-7613(1986)14%3C492:PHOTMR%3E2.0.CO;2.

Bloxson, J., and A. Valdez, 2024, Far–field tectonic controls on deposition in the Appalachian Basin – A case study of Late Cambrian–Late Ordovician strata in Morrow County, Ohio: Results in Earth Sciences, v. 2, doi:https://doi.org/10.1016/j.rines.2024.100035.

Bowen, B. B., R. I. Ochoa, N. D. Wilkens, J. Brophy, T. R. Lovell, N. Fischietto, C. R. Medina, and J. A. Rupp, 2011, Depositional and diagenetic variability within the Cambrian Mount Simon Sandstone: Implications for carbon dioxide sequestration: Environmental Geosciences, v. 18, no. 2, p. 69–89, doi:10.1306/eg.07271010012.

Byerlee, J. D., 1978, Friction of Rock: Pure and Applied Geophysics, v. 116, p. 615–626.

Calvert, W., 1962, Sub-Trenton rocks from Lee County, Virginia to Fayette County, Ohio: Ohio Division of Geological Survey.

Casey, G. D., 1994, Preliminary matrix permeability and porosity variation in the Silurian and Devonian carbonates of the Indiana and Ohio parts of the Midwestern Basins and Arches Region: Columbus, Ohio, The Ohio State University, 82 p.

Conner, A., E. Howat, I. Fukai, and S. Mishra, 2016, Analysis and Integration of Advanced Logs and Core Data: Characterization of the Copper Ridge Dolomite in Morrow County, Ohio, *in* Lexington, KY: AAPG.

Crowell, K., 1979, Ground-water resources of Marion County: Ohio Division of Water.

Dart, R. L., and M. C. Hansen, 2008, Earthquakes in Ohio and Vicinity 1776-2007: U.S. Geological Survey, Open-File Report 2008-1221.

Denison, R. E., E. G. Lidiak, M. E. Bickford, and E. G. Kisvarsanyi, 1984, Geology and geochronology of Precambrian rocks in the Central Interior Region of the United States: U.S: Geological Survey Professional Paper, v. 1241– C, p. 20.

Dickas, A. B., M. G. Mudrey Jr., R. W. Ojakangas, and D. L. Shrake, 1992, A possible southeastern extension of the Midcontinent Rift System located in Ohio: Tectonics, v. 11, no. 6, p. 1406–1414, doi:10.1029/91TC02903.

Drahovzal, J. A., D. C. Harris, L. H. Wickstrom, D. Walker, M. T. Baranoski, B. Keith, and L. C. Furer, 1992, The East Continent Rift Basin: A New Discovery, Special Publication 18: Kentucky Geological Survey, Series XI.

Droste, J. B., and J. B. Patton, 1985, Lithostratigraphy of the Sauk Sequence: Bloomington: Indiana Geological Survey, Occasional Paper, v. 47, p. 24.

Eberts, S.M. and George, L.L., 2000, Regional groundwater flow and geochemistry in the Midwestern basins and arches aquifer system in parts of Indiana, Ohio, Michigan, and Illinois, No. 1423-C: US Geological Survey.

Fakhari, M., 2016, Revisiting the Structural Geology of Northwestern Ohio, *in* Champaign, IL: doi:10.1130/abs/2016NC-275634.

FEMA, National Flood Hazard Layer: <https://www.fema.gov/flood-maps/national-flood-hazard-layer> (accessed April 27, 2023).

Fisher, D., and S. Nightengale, 2006, The rise and fall of the Taconic Mountains: A geological history of eastern New York: Nensonville, New York, Black Dome Press, 184 p.

Freeman, L., 1953, Regional subsurface stratigraphy of the Cambrian and Ordovician in Kentucky and vicinity: Kentucky Geological Survey, 12,352 p.

Freiburg, J. T., R. W. Ritzi, and K. S. Kehoe, 2016, Depositional and diagenetic controls on anomalously high porosity within a deeply buried CO2 storage reservoir—The Cambrian Mt. Simon Sandstone, Illinois Basin, USA: International Journal of Greenhouse Gas Control, v. 55, p. 42–54, doi:10.1016/j.ijggc.2016.11.005.

Gaus, I., M. Azaroual, and I. Czernichowski-Lauriol, 2005, Reactive transport modelling of the impact of CO2 injection on the clayey cap rock at Sleipner (North Sea): Chemical Geology, v. 217, no. 3, p. 319–337, doi:10.1016/j.chemgeo.2004.12.016.

Gollakota, S., and S. McDonald, 2014, Commercial-scale CCS Project in Decatur, Illinois - Construction Status and Operational Plans for Demonstration: Energy Procedia, p. 5986–5993.

Green, M. R., 2018, Geophysical Exploration of the Upper Crust Underlying North-Central Indiana: New Insight into the Eastern Granite-Rhyolite Province: Wright State University.

Greenberg, S. E., 2021, Illinois Basin-Decatur Project Final Report: An Assessment of Geologic Carbon Sequestration Options in the Illinois Basin: Phase III: United States Department of Energy.

Gundogan, O., E. Mackay, and A. Todd, 2011, Comparison of numerical codes for geochemical modelling of CO2 storage in target sandstone reservoirs: Chemical Engineering Research and Design, v. 89, no. 9, p. 1805–1816, doi:10.1016/j.cherd.2010.09.008.

Gupta, N. et al., 2017, Integrated Sub-Basin Scale Exploration for Carbon Storage Targets: Advanced Characterization of Geologic Reservoirs and Caprocks in the Upper Ohio River Valley: Energy Procedia, v. 14, p. 2781–2791.

Haneberg-Diggs, D. M., 2015, The “Clinton” Oil-And-Gas Play in Ohio, GeoFacts 30: Ohio Department of Natural Resources, Division of Geological Survey.

Hansen, M.C., 1998, GEOLOGY OF OHIO—THE SILURIAN.

Hansen, Michael C., 1998, The Geology of Ohio—The Cambrian, GeoFacts No. 20: Ohio Department of Natural Resources, Division of Geological Survey.

Harris, D. C., and M. T. Baranoski, 1997, CAMBRIAN PRE-KNOX GROUP PLAY: State of Ohio Information Circular, v. 60, p. 31.

Heidbach, O., M. Rajabi, K. Reiter, M. Ziegler, and WSM Team, 2016, World Stress Map Database Release 2016: GFZ Data Servies.

Hickman, J., C. Eble, and D. Harris, 2015, A geologic play book for Utica Shale Appalachian basin exploration, Final report of the Utica Shale Appalachian basin exploration consortium, *in* Patchen, D.G. and Carter, K.M.: Lithostratigraphy, p. 19–21.

Hurd, O., and M. Zoback, 2012, Intraplate earthquakes, regional stress and fault mechanics in the Central and Eastern U.S. and Southern Canada: v. 581, p. 182–192.

INEOS Nitriles, 2016, Underground Injection Control Permit to Operate Class I Hazardous Well; Ohio Permit UIC 03-02-005-PTO-I, Ohio Permit UIC 03-02-005-PTO-I: Ohio Environmental Protection Agency Division of Drinking and Ground Waters.

Jaeger, J. C., and N. G. W. Cook, 1971, Fundamentals of Rock Mechanics: London, Chapman and Hall.

Janssens, A., 1973, Stratigraphy of the Cambrian and lower Ordovician in Ohio,1973 Ohio Div: Geol. Survey Bull, v. 64.

Knight, W. V., 1969, Historical and Economic Geology of Lower Silurian Clinton Sandstone of Northeastern Ohio1: AAPG Bulletin, v. 53, no. 7, p. 1421–1452, doi:10.1306/5D25C85D-16C1-11D7-8645000102C1865D.

Kolata, D. R., and W. J. Nelson, 1990, Tectonic History of the Illinois Basin, *in* Interior Cratonic Basins: American Association of Petroleum Geologists, doi:10.1306/M51530C19.

Kolata, D. R., and C. K. Nimz (eds.), 2010, Geology of Illinois: Illinois State Geological Survey.

Komara, K., 2017, Lithologic and Well Log Analysis of a Four Well Case Study, in Morrow County, Ohio: Senior Independent Study Theses, v. 7653.

Korose, C., 2022, Wabash CarbonSAFE, Final Report, Final Report, DE-FE0031626-FINAL, 1874030: DE-FE0031626-FINAL, 1874030 p., doi:10.2172/1874030.

Labotka, D. M., S. V. Panno, R. A. Locke, and J. T. Freiburg, 2015, Isotopic and geochemical characterization of fossil brines of the Cambrian Mt. Simon Sandstone and Ironton–Galesville Formation from the Illinois Basin, USA: Geochimica et Cosmochimica Acta, v. 165, p. 342–360, doi:10.1016/j.gca.2015.06.013.

Lacy, L., 1997, Dynamic Rock Mechanics Testing for Optimized Fracture Design: doi:SPE%20Annual%20Technical%20Conference%20and%20Exhibition.

Leetaru, H., C. Blakley, C. Carman, D. Garner, and C. Korose, 2019, Carbon Storage Assurance Facility Enterprise (CarbonSAFE): Integrated CCS Pre-Feasibility CarbonSAFE Illinois East Sub-Basin Final Report, Final Report, DOE-FE0029445, 1576199: Prairie Research Institute, DOE-FE0029445, 1576199 p., doi:10.2172/1576199.

Leetaru, H. E., and J. H. McBride, 2009, Reservoir uncertainty, Precambrian topography, and carbon sequestration in the Mt. Simon Sandstone, Illinois Basin: Environmental Geosciences, v. 16, no. 4, p. 235–243, doi:10.1306/eg.04210909006.

Medina, C. R., and J. A. Rupp, 2012, Reservoir characterization and lithostratigraphic division of the Mount Simon Sandstone (Cambrian): Implications for estimations of geologic sequestration storage capacity: Environmental Geosciences, v. 19, no. No. 1, p. 1–15, doi:10.1306/eg.07011111005.

Meyer, James P., 2007, Summary of Carbon Dioxide Enhanced Oil Recovery Injection Well Technology: American Petroleum Institute.

Mohamed, I. M., J. He, and H. A. Nasr-El-Din, 2012, Carbon Dioxide Sequestration in Dolomite Rock: European Association of Geoscientists & Engineers, p. cp, doi:10.3997/2214-4609-pdb.280.iptc14924_noPW.

National Information Services Center, and National Park Service, 2023, National Wild and Scenic Rivers System Map: Harpers Ferry Center, National Wild and Scenic Rivers System, originally published in September 2018.

National Park Service, National Register of Historic Places Database and Research: <https://www.nps.gov/subjects/nationalregister/database-research.htm>.

National Park Service, Nationwide Rivers Inventory: <https://www.nps.gov/maps/full.html?mapId=8adbe798-0d7e-40fb-bd48-225513d64977>.

National Wild and Scenic Rivers System, Find a River: <https://www.rivers.gov/find-a-river>.

Nelson, R., 2001, Geologic Analysis of Naturally Fractured Reservoirs: Elsevier, 353 p.

Norris, S. E., and R. E. Fidler, 1973, Availability of ground water from limestone and dolomite aquifers in southwest Ohio and the relation of water quality to the regional flow system: U.S. Geological Survey Water Resource Investigation, 17–73 p.

NORSOK/EG D, 2024, Well integrity in drilling and well operations, NORSOK Standard NORSOK D-010:2021+AC2:2024: Standards Norway.

ODNR, ODNR Oil & Gas Well Viewer: Ohio Department of Natural Resources, Division of Oil & Gas.

ODNR, ODNR Water Well Database: Ohio Department of Natural Resources, Division of Geological Survey.

Ohio Division of Geologic Survey, 2004, Oil and Gas Fields Map of Ohio: Ohio Department of Natural Resources, Division of Geological Survey Map PG-1,.

Ohio Division of Geologic Survey, 2017, Shaded drift-thickness map of Ohio: Ohio Department of Natural Resources, Division of Geological Survey, Ohio Department of Natural Resources, Division of Geological Survey Map.

Ohio Division of Geological Survey, 2014, A Brief Summary of the Geologic History of Ohio.

Ohio EPA, Ambient Ground Water Monitoring Network: Ohio Environmental Protection Agency, Division of Drinking and Ground Waters.

Ohio Natural Heritage Database, 2023a, Marion County State Listed Animal Species: Division of Natural Heritage, Ohio Department of Natural Resources.

Ohio Natural Heritage Database, 2023b, Marion County State Listed Plant Species: Division of Natural Heritage, Ohio Department of Natural Resources.

The Ohio Seismic Network (OhioSeis) Earthquake Database, 2025: Ohio Department of Natural Resources, Division of Geological Survey.

Onasch, C., 2007, Structural evolution of the bowling green fault.

Panno, S. V., K. C. Hackley, R. A. Locke, I. G. Krapac, B. Wimmer, A. Iranmanesh, and W. R. Kelly, 2013, Formation waters from Cambrian-age strata, Illinois Basin, USA: Constraints on their origin and evolution: Geochimica et Cosmochimica Acta, v. 122, p. 184–197, doi:10.1016/j.gca.2013.08.021.

Parkhurst, D. L., and C. A. J. Appelo, 2013, USGS - Description of Input and Examples for PHREEQC Version 3—A Computer Program for Speciation, Batch-Reaction, One-Dimensional Transport, and Inverse Geochemical Calculations, *in* U.S. Geological Survey Techniques and Methods: Book 6 Chapter A43, p. 497.

Qafoku, N., L. Zheng, D. H. Bacon, A. R. Lawter, and C. F. Brown, 2015, A Critical Review of the Impacts of Leaking CO_2 Gas and Brine on Groundwater Quality, PNNL--24897, 1347881: PNNL--24897, 1347881 p., doi:10.2172/1347881.

Riley, R. A., J. McDonald, and D. R. Martin, 2012, Elevation contours on the base of the deepest underground sources of drinking water in Ohio: Columbus, OH, Department of Natural Resources, Division of Geological Survey, Map EG_6.

Riley, R. A., J. Wicks, and J. Thomas, 2002, Cambrian-Ordovician Knox Production in Ohio: Three Case Studies of Structural-Stratigraphic Traps: AAPG Bulletin, v. 86, no. 4, p. 539–555, doi:10.1306/61EEDB3E-173E-11D7-8645000102C1865D.

Ruff, L., R. LaForge, R. Thorson, T. Wagner, and F. Goudaen, 1994, Geophysical Investigations of the Western Ohio-Indiana Region: Final Report for the U.S. Nuclear Regulatory Commission, October 1986-September 1992, NUREG/CR-3145, Vol. 10: The University of Michigan Department of Geological Sciences.

Saeed, A., and J. E. Evans, 2012, Subsurface Facies Analysis of the Late Cambrian Mt. Simon Sandstone in Western Ohio (Midcontinent North America), 2: Open Journal of Geology, v. 2, no. 2, p. 35–47, doi:10.4236/ojg.2012.22004.

Schlumberger, 2021, EverCRETE CO_2-resistant cement system: Schlumberger.

Shrake, D. L., E. Venteris, G. Larsen, M. Angle, R. Pavey, and D. Powers, 2009, Surficial geology of the Marion 30 X 60-minute quadrangle: Ohio Department of Natural Resources, Division of Geological Survey Map SG-2 MAR.

Sminchak, J., 2012, SIMULATION FRAMEWORK FOR REGIONAL GEOLOGIC CO2 STORAGE ALONG ARCHES PROVINCE OF MIDWESTERN UNITED STATES: United States, Battelle Memorial Institute, Columbus, OH (United States), doi:10.2172/1110321.

Smith, Dr. L, 2012, Establishing and Maintaining the Integrity of Wells used for Sequestration of CO2.: NACE.

S&P Global, S&P Global Energy Portal: <https://my.ihs.com/Energy/Products> (accessed May 5, 2023).

Sutton, E., 1965, Trempealeau Reservoir Performance, Morrow County Field, Ohio: Journal of Petroleum Technology, v. 17, no. 12, p. 1391–1395, doi:10.2118/1208-PA.

Syed, T., R. Sweatman, and G. Benge, 2018, Well Engineering and Injection Regularity in CO_2 Storage Wells, Technical Report 2018–08: IEAGHG, IEA Greenhouse Gas R&D Programme, 415 p.

Tetra Tech, 2024, Critical Issues Analysis - Carbon Sequestration Project in Marion County, Ohio.

Trémosa, J., C. Castillo, C. Q. Vong, C. Kervévan, A. Lassin, and P. Audigane, 2014, Long-term assessment of geochemical reactivity of CO2 storage in highly saline aquifers: Application to Ketzin, In Salah and Snøhvit storage sites: International Journal of Greenhouse Gas Control, v. 20, p. 2–26, doi:10.1016/j.ijggc.2013.10.022.

Tuboscope - NOV Wellbore Technologies, 2017, TK-15XT Specifications: National Oilwell Varco.

Tuboscope Coatings Spec Sheet, 2022: National Oilwell Varco.

USFWS, 2025, IPaC: Information for Planning and Consultation Resource List, Stonewell Project.

USGS, 2024, USGS Earthquake Catalog Search: <https://earthquake.usgs.gov/earthquakes/search/> (accessed September 24, 2024).

USGS, 2025, USGS Earthquake Catalog Search: <https://earthquake.usgs.gov/earthquakes/search/> (accessed July 3, 2025).

Vickery Environmental, Inc., 1989, Petrography report.

Vickery Environmental Inc., 2020, Vault 4401 - Renewal Application for UIC Permits 3-5-2020.pdf - All Documents.

Whittaker, S., 2022, Illinois Storage Corridor, *in* NETL, ed.: NETL Annual Review Meeting 2022.

Whittaker, S., and C. Carman, 2022, CarbonSAFE Illinois - Macon County Final Report.

Wickstrom, L. H. et al., 2005, Characterization of Geologic Sequestration Opportunities in the MRCSP Region Phase I, Open-File Report 2005–1: Midwest Regional Carbon Sequestration Partnership (MRCSP).

Wickstrom, L., J. Gray, and R. Stieglitz, 1992, Stratigraphy, structure, and production history of the Trenton Limestone (Ordovician) and adjacent strata in northwestern Ohio, Report of

Investigations No. 143: Columbus, Ohio, Department of Natural Resources, Division of Geological Survey.

Wilson, K., 1987, Ground-water flow and water quality in northeastern Union County, Ohio, 87: Department of the Interior, U.S. Geological Survey.

Zhao, H., R. Dilmore, D. E. Allen, S. W. Hedges, Y. Soong, and S. N. Lvov, 2015, Measurement and Modeling of CO2 Solubility in Natural and Synthetic Formation Brines for CO2 Sequestration: Environmental Science & Technology, v. 49, no. 3, p. 1972–1980, doi:10.1021/es505550a.

Zoback, M. D., 2010, Reservoir Geomechanics: Cambridge University Press, 505 p.

15. Figures

Claimed as PBI

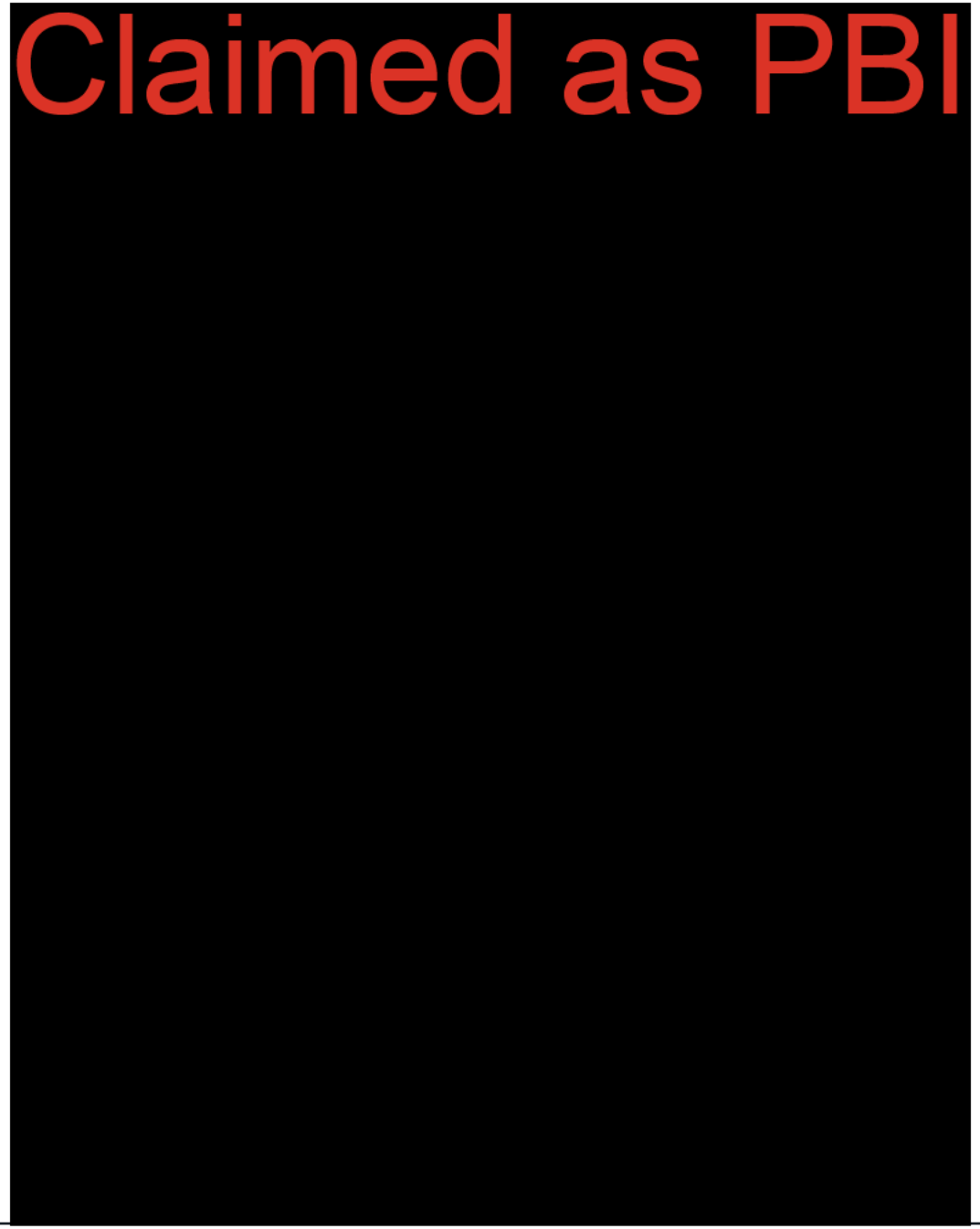

Map of the Stonewell Project location that shows the proposed location of the injection and deep observation wells, simulated extent of CO_2 plume 50-years post-injection (Year 62), maximum extent of the critical pressure front, and the AoR with required information per 40 CFR 40 CFR §146.82(a)(2). Map base adapted from Esri.

PBI

Figure 1

Claimed as PBI

Proposed locations of the injection, deep observation, above confining zone monitoring, and the underground source of drinking water (USDW) monitoring wells for the Stonewell Project. Map base adapted from Esri.

PBI

Figure 2

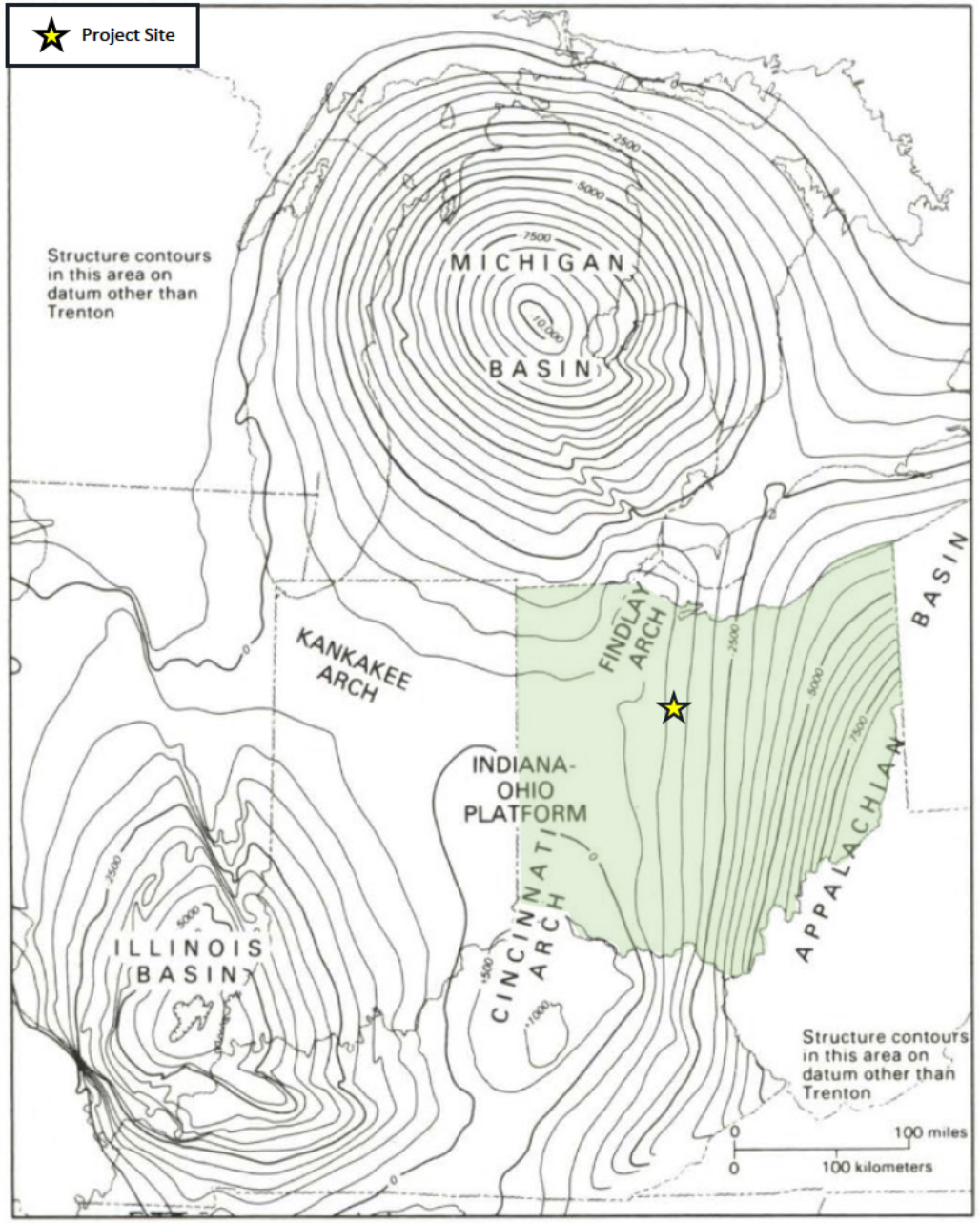

Regional structural contour map (top of Trenton Limestone) showing the location of the Arches Province, the arches within the province, and surrounding sedimentary basins. The state of Ohio is shaded green, and the Stonewell Project site is a yellow star. Modified from Wickstrom et al. (1992).

Figure 3

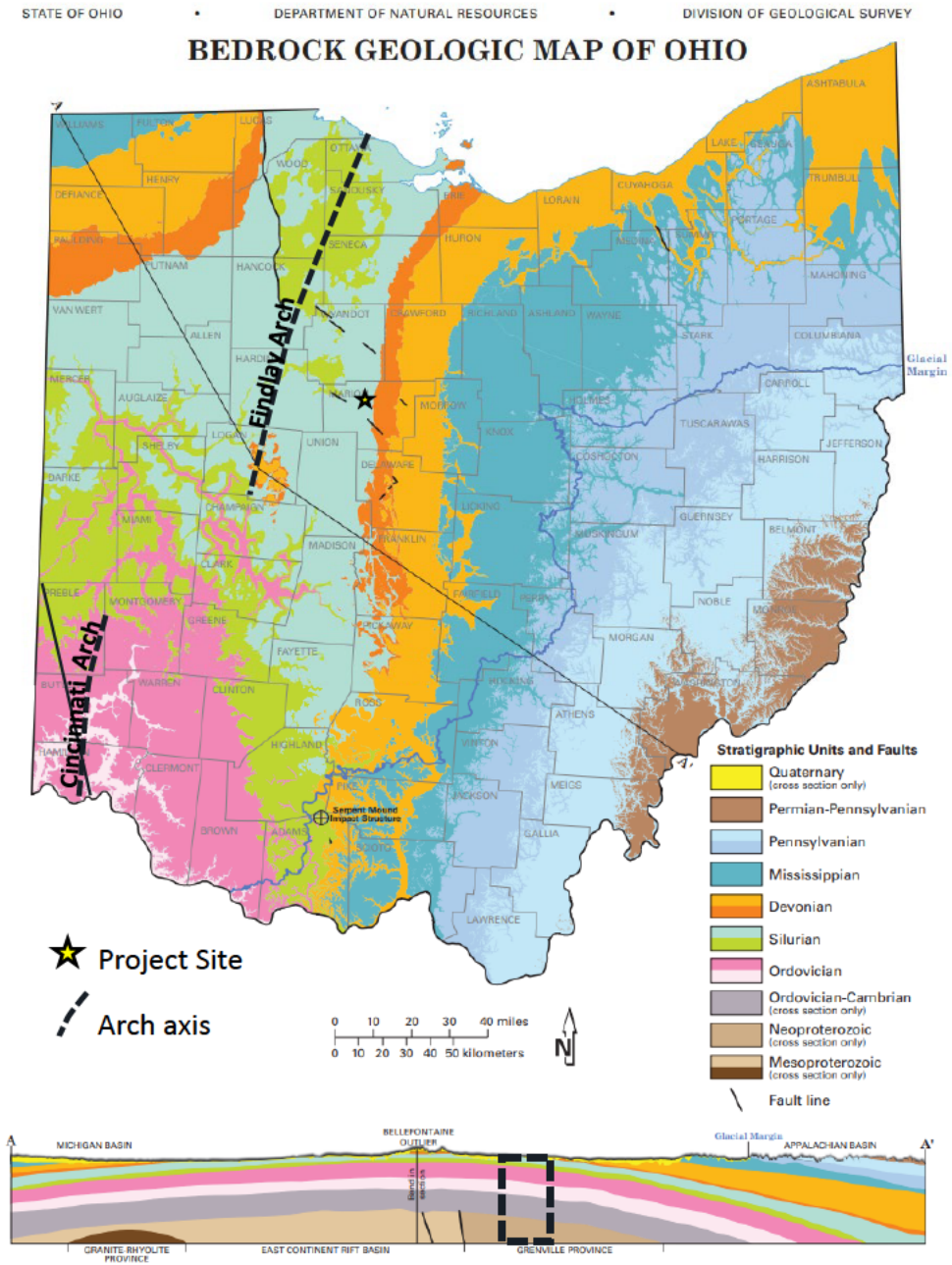

Bedrock geologic map of Ohio with a vertical section through the bedrock geology showing the broad nature of Findlay Arch, and the structural position of the Stonewell Project site on the east limb of the arch. The approximate surface location of the Stonewell Project site (yellow star) and projected underlying geology (black dashed rectangle) are shown. Modified from the Ohio Department of Natural Resources (2006).

Figure 4

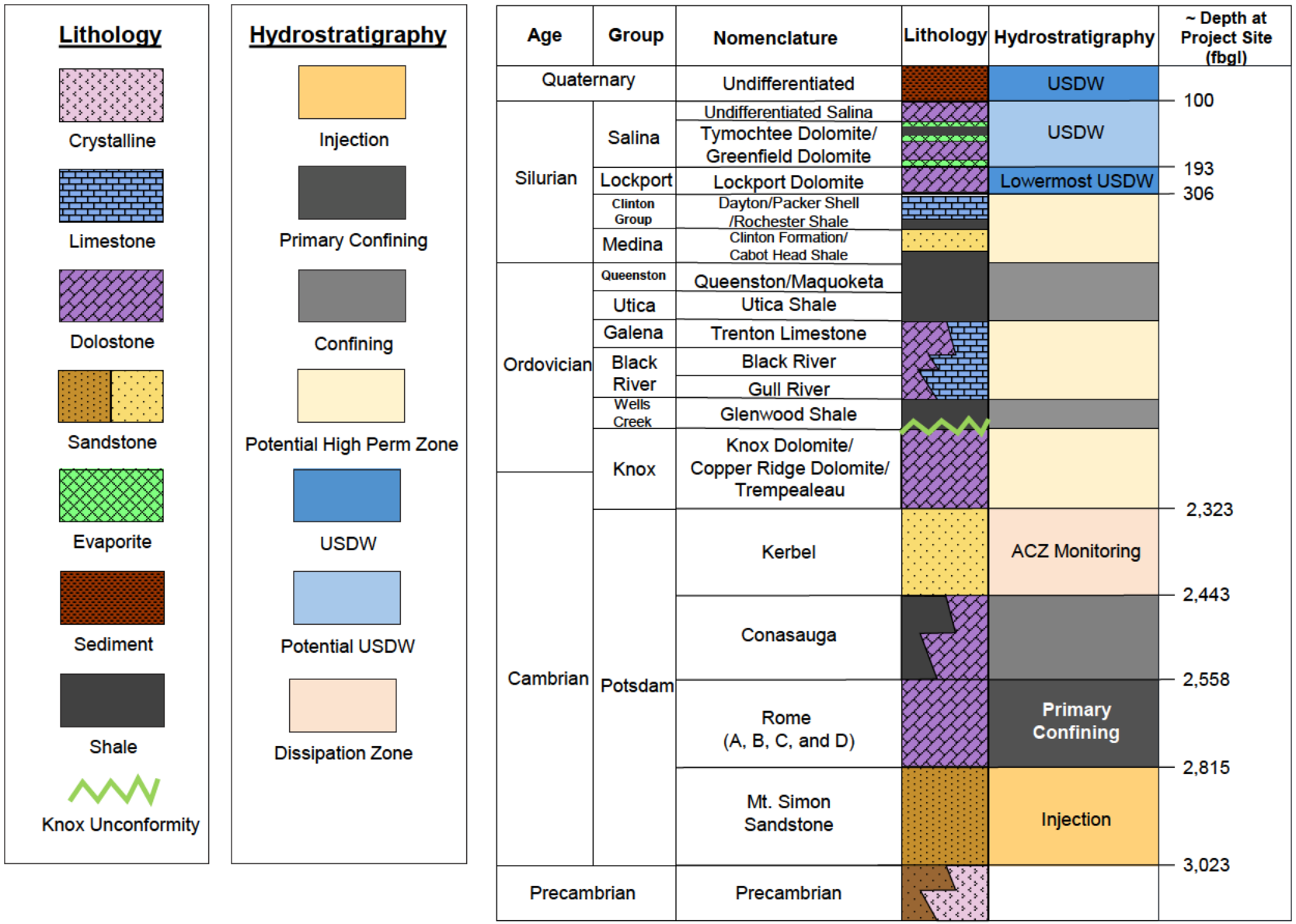

Stonewell Project site-specific stratigraphic column with age, nomenclature, generalized lithology, and formation depths at the injection well.

Figure 5

A) West to east regional cross section A-A' and B) north to south regional cross section B-B' through the project site (see inset map) with AoR. The injection well is projected onto both cross sections. The dashed box on cross section A-A' is shown in Figure 54. Vertical exaggeration = 10X

PBI

Figure 6

Wells that penetrate the Mt. Simon Sandstone within a 50-mile radius (black circle) of the injection well. The AoR is represented by the blue circle. Structural features are represented by red lines.

PBI

Figure 7

Regional cross section C-C' demonstrates the regional continuity of the Rome Formation and the Mt. Simon Sandstone. Gamma Ray Logs (GR_TOT) are color filled, effective porosity is color filled, and density (RHOB) is green, sandstone neutron porosity is black, density porosity is yellow, and sonic is blue. Well locations are shown on the inset map. Project location shown as well as yellow star. The cross section is flattened on the Rome Formation top.

PBI

Figure 8

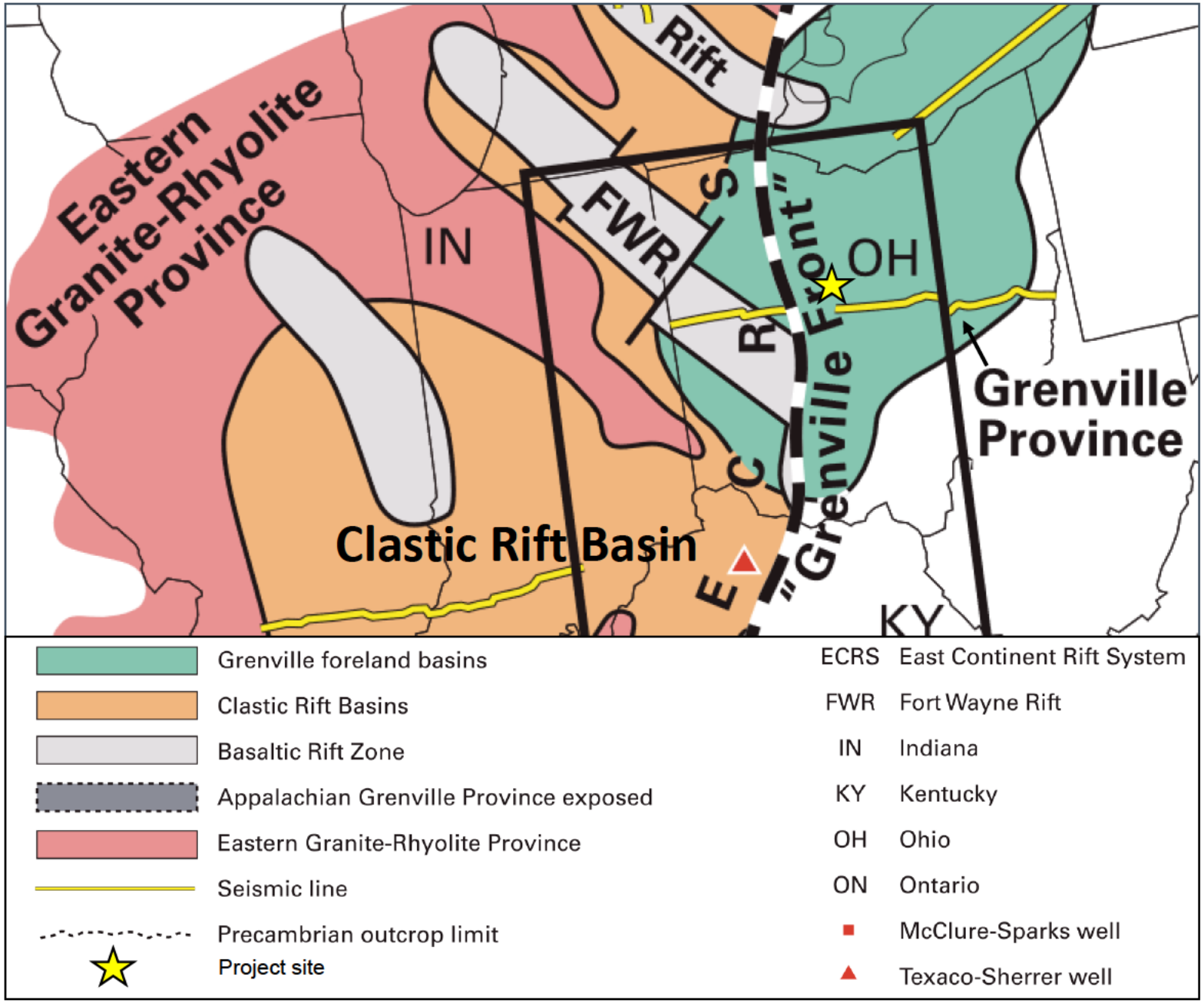

Map showing the Precambrian EGRP, ECRS, and the Grenville Province. The Grenville Front and regional seismic lines are also shown (modified from Baranoski et al., 2009).

Figure 9

Map of wells identifying Precambrian rock type in the Arches Province.

Modified from (Drahovzal et al., 1992).

PBI

Figure 10

Elevation map in feet below sea level (fbsl) of the Precambrian Basement. Wells shown penetrate the Precambrian Basement top. The project location is also shown.

PBI

Figure 11

Elevation map in fbsl of the Mt. Simon Sandstone. Wells shown penetrate the Mt. Simon Sandstone top. Project location is also shown.

PBI

Figure 12

Thickness map (feet) of the Mt. Simon Sandstone. Wells shown penetrate the Mt. Simon Sandstone. Project location is also shown.

PBI

Figure 13

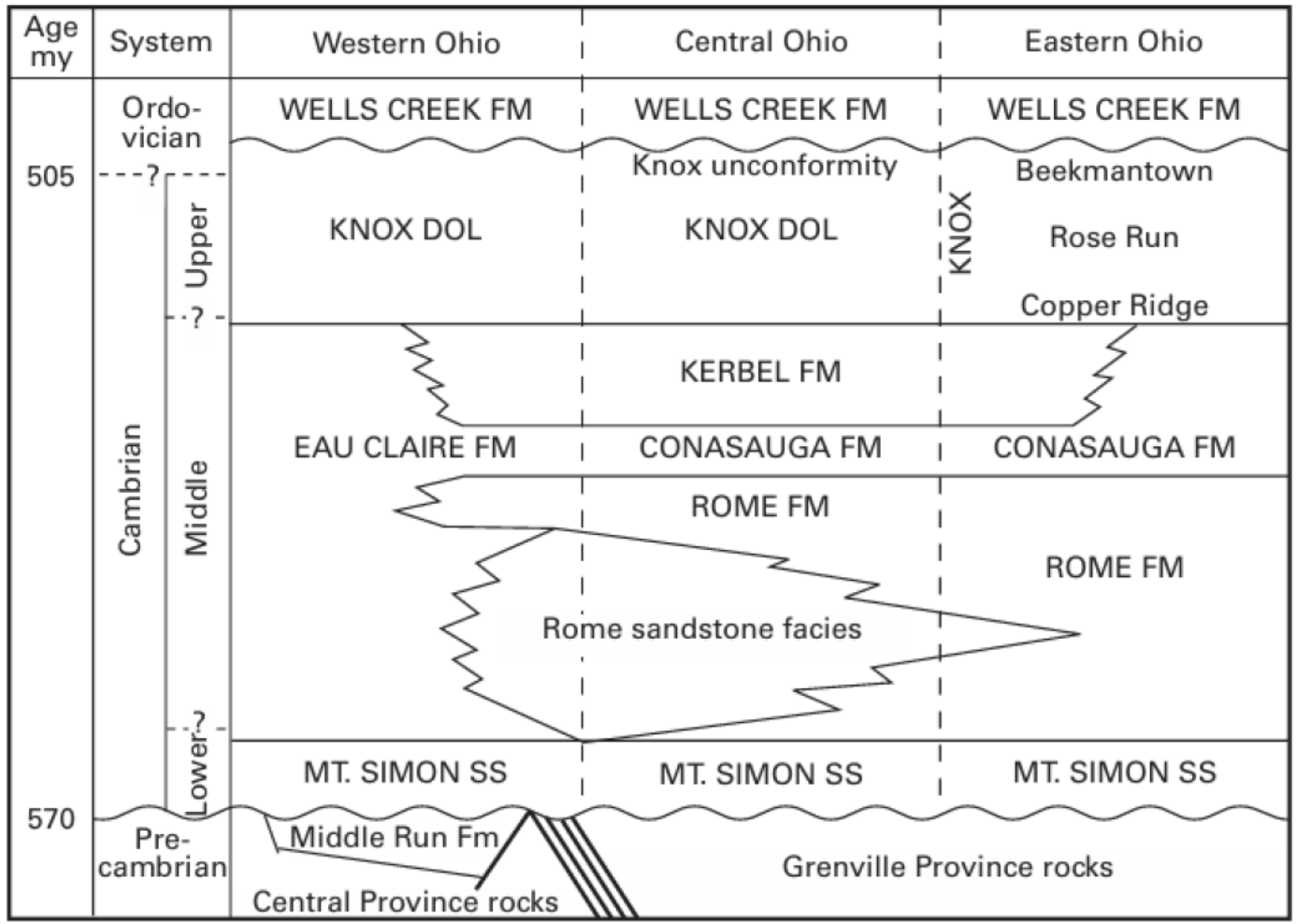

GF20_Hansen_1998.pdf (ohiodnr.gov)

Relationships of Cambro-Ordovician rocks of Ohio. The project site is east of where the Eau Claire Shale grades into the Rome Formation and Conasauga Formation. Modified from Janssens (1973).

Figure 14

Elevation map in fbsl of the Rome Formation. Wells shown penetrate the Rome Formation top. Project location is also shown.

PBI

Figure 15

Thickness map (feet) of the Rome Formation. Wells shown penetrate the formation. Project location is also shown.

PBI

Figure 16

Regional structural features in western Ohio. Inset map highlights the detailed mapped area. Faults are depicted as red lines. The Fort Wayne Rift and Grenville Front are also shown. The vertical black line on the left shows the state boundaries and the yellow star indicates the location of the Stonewell Project site.

Modified from Baranoski et al. (2002)

PBI

Figure 17

All water wells (167) and expired oil and gas well permit (1) within the Stonewell AoR. There are no existing wells that penetrate the primary confining zone in the AoR at the Stonewell Project site. The STO INJ1 and STO OBS1 wells are also shown.

PBI

Figure 18

Map of the ten 2D seismic lines (1, 2, 3, 26, 27, 63, 83, 231N, 231S, 309) acquired for the Stonewell Project. Interpreted faults transecting the Mt. Simon Sandstone and nearby wells are also shown. The fault positions are at the top of the Mt. Simon Sandstone. The Marion Fault Zone is derived from Baranoski 2002). The Stonewell Project AoR is also shown.

PBI

Figure 19

Well logs and synthetic seismograms from the Gracely Farms 1 (UWI 34101201680000) and Forry Evelyn (34101202070000; Figure 19) wells. The stratigraphy at the UWE Gracely Farms 1 and Forry Evelyn wells is equivalent to the Stonewell Project site and was used to tie the 2D seismic data for seismic interpretation.

PBI

Figure 20

East-West 2D seismic line 26 of the Stonewell Project site with interpreted stratigraphy and possible structures. See Figure 19 for location.

PBI

Figure 21

Western half of east-west 2D seismic line 27 with interpreted stratigraphy. See Figure 19 for location.

PBI

Figure 22

Eastern half of east-west 2D seismic line 27 with interpreted stratigraphy, faults MR-5 and MR-6, and possible structures. See Figure 19 for location.

PBI

Figure 23

West-east 2D seismic line 1 with interpreted stratigraphy and possible structures. See Figure 19 for location.

PBI

Figure 24

Western half of northwest-southeast seismic line 309 with interpreted stratigraphy and possible structures. See Figure 19 for location.

PBI

Figure 25

Eastern half of northwest-southeast seismic line 309 with interpreted stratigraphy and possible structures. See Figure 19 for location.

PBI

Figure 26

North-south seismic line 63 with interpreted stratigraphy and fault MF-1. See Figure 19 for location.

PBI

Figure 27

Northern half of north-south seismic line 83 with interpreted stratigraphy. See Figure 19 for location.

PBI

Figure 28

North-south seismic line 2 with interpreted stratigraphy and possible structures. See Figure 19 for location.

PBI

Figure 29

Southern half of north-south seismic line 83 with interpreted stratigraphy and possible structures. See Figure 19 for location.

PBI

Figure 30

West-east seismic line 231 with interpreted stratigraphy and faults MR-1, MR-2, MR-3, and MR-4, and possible structures. This seismic line is not within the AoR. See Figure 19 for location.

PBI

Figure 31

North-south seismic line 231S with interpreted stratigraphy, faults MR-5 and MR-6, and possible structures. This seismic line is not within the AoR.

See Figure 19 for location.

PBI

Figure 32

Northwest-southeast seismic line 3 with interpreted stratigraphy and the MSF fault

PBI

Figure 33

Interpretation of fault MF-1 on A) seismic line 309 B) seismic line 63, and C) trace of fault plane between line 309 and 63 on fence diagram. See Figure 19 seismic line and fault locations.

PBI

Figure 34

Interpretation of faults MR-1, MR-2, MR-3 and MR-4 on seismic line 231N. See Figure 19 seismic line and fault locations.

PBI

Figure 35

Interpretation of fault MR-2 on seismic lines A) 231S and B) 231N, and C) trace of fault plane between lines 231S and 231N. Figure 19seismic line and fault locations.

PBI

Figure 36

Interpretation of fault MR-5 and MR-6 on seismic lines A) 27 and B) 231S. C) Trace of fault planes between lines 231S and 27 on fence diagram. See Figure 19 for seismic line and fault locations.

PBI

Figure 37

Thickness (feet) of the Mt. Simon Sandstone injection zone in the AoR.

PBI

Figure 38

Thickness (feet) of the Rome Formation primary confining zone in the AoR.

PBI

Figure 39

Precambrian unconformity structural map modified from Baranoski (2013), Fakhari (2016), and (Bloxson and Valdez, 2024) with published fault interpretations. Solid green line is the border of Marion County, and the blue circle is the project AoR. U=up and D=down with respect to vertical displacement along faults.

PBI

Figure 40

Frequency plot of fault strike and the fault number from both regional data (Baranoski, 2002; Fakhari, 2016; Bloxson and Valdez, 2024) and local seismic interpretation.

PBI

Figure 41

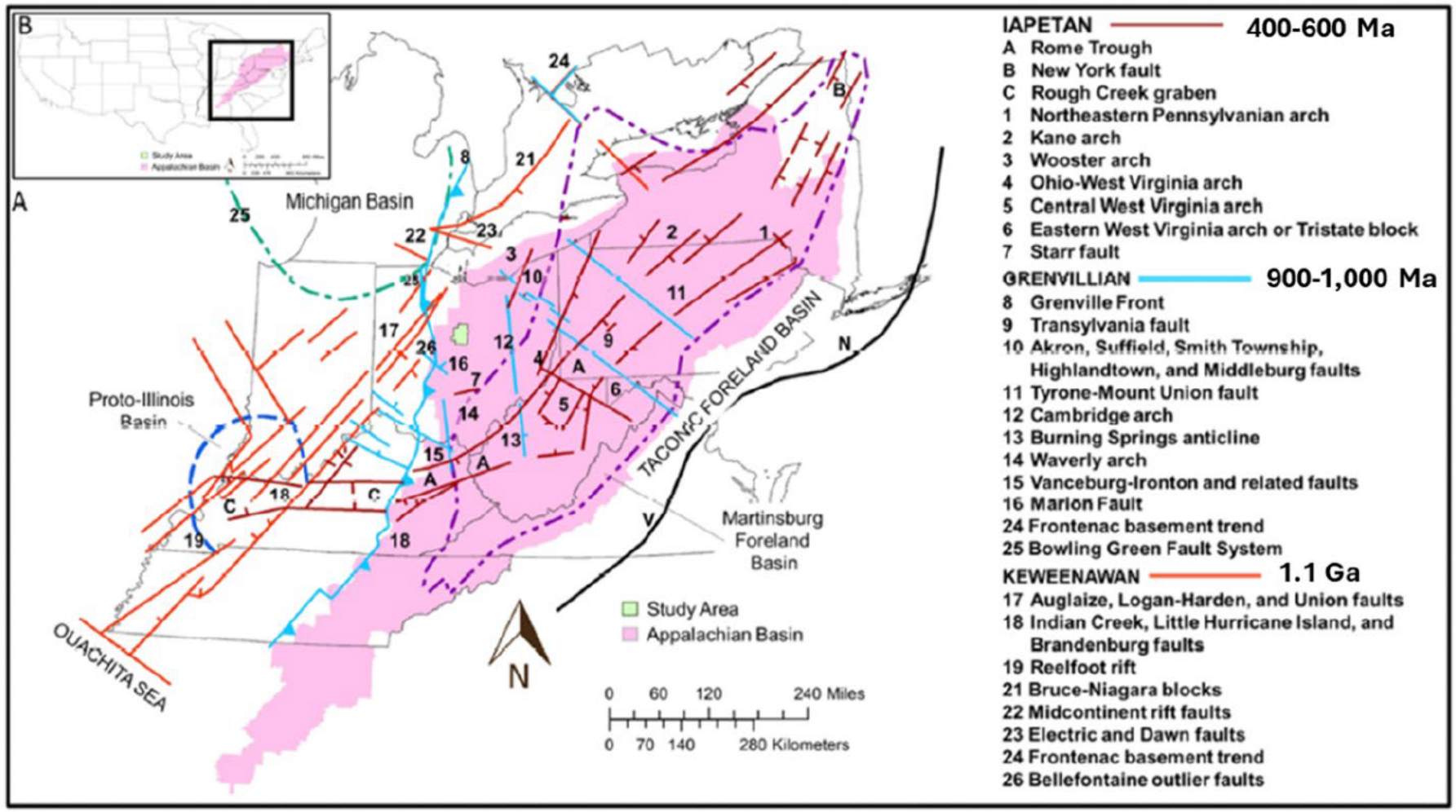

Map showing tectonic elements and orientations of basement structures adapted from Ettensohn and Lieman (2012) by Bloxom and Valdez (2024).

Figure 42

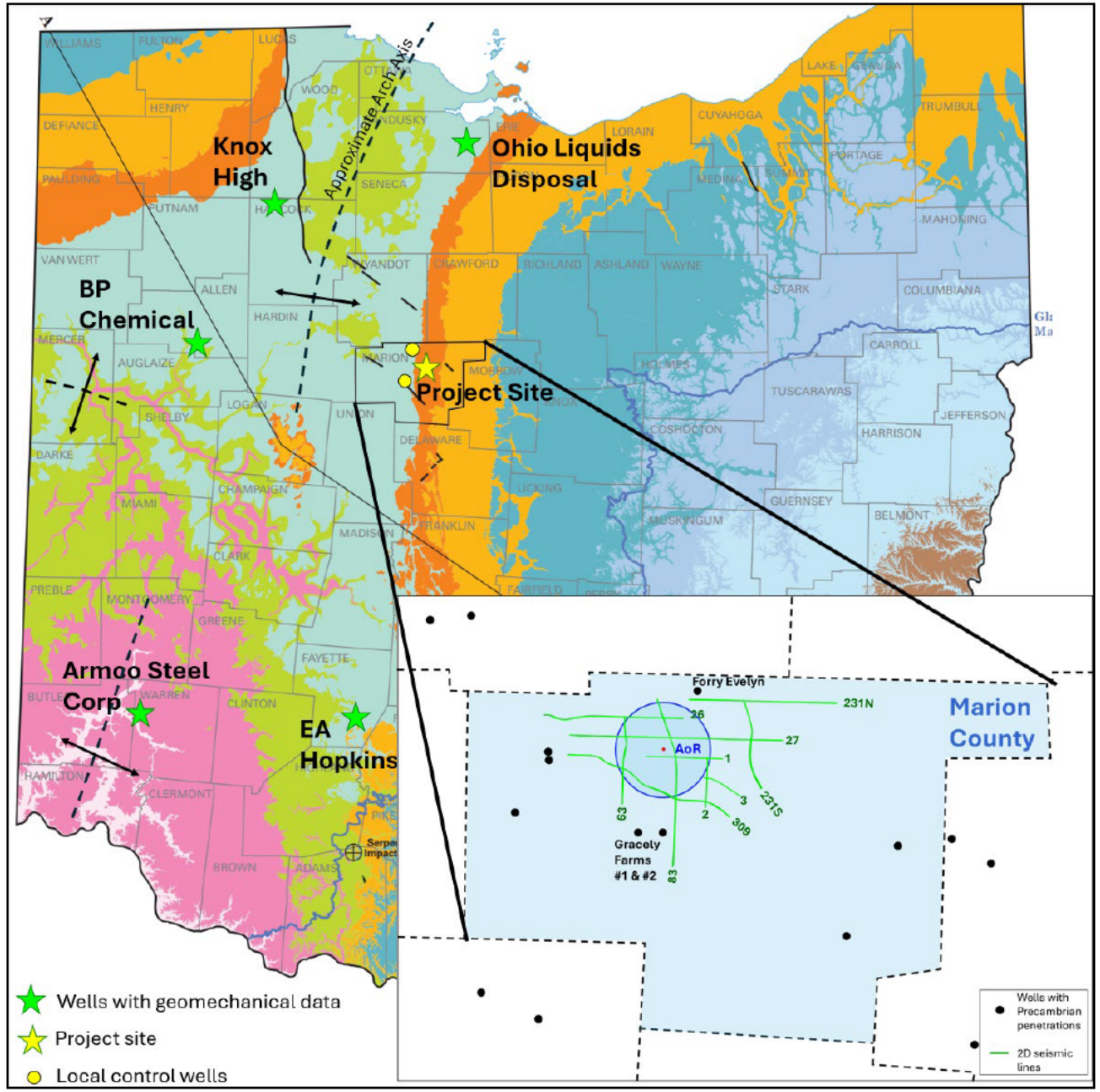

Location of regional wells with geomechanical information. The inset map shows Marion County, the 2D seismic survey, and nearby wells. Modified from the Ohio Department of Natural Resources (2006).

Figure 43

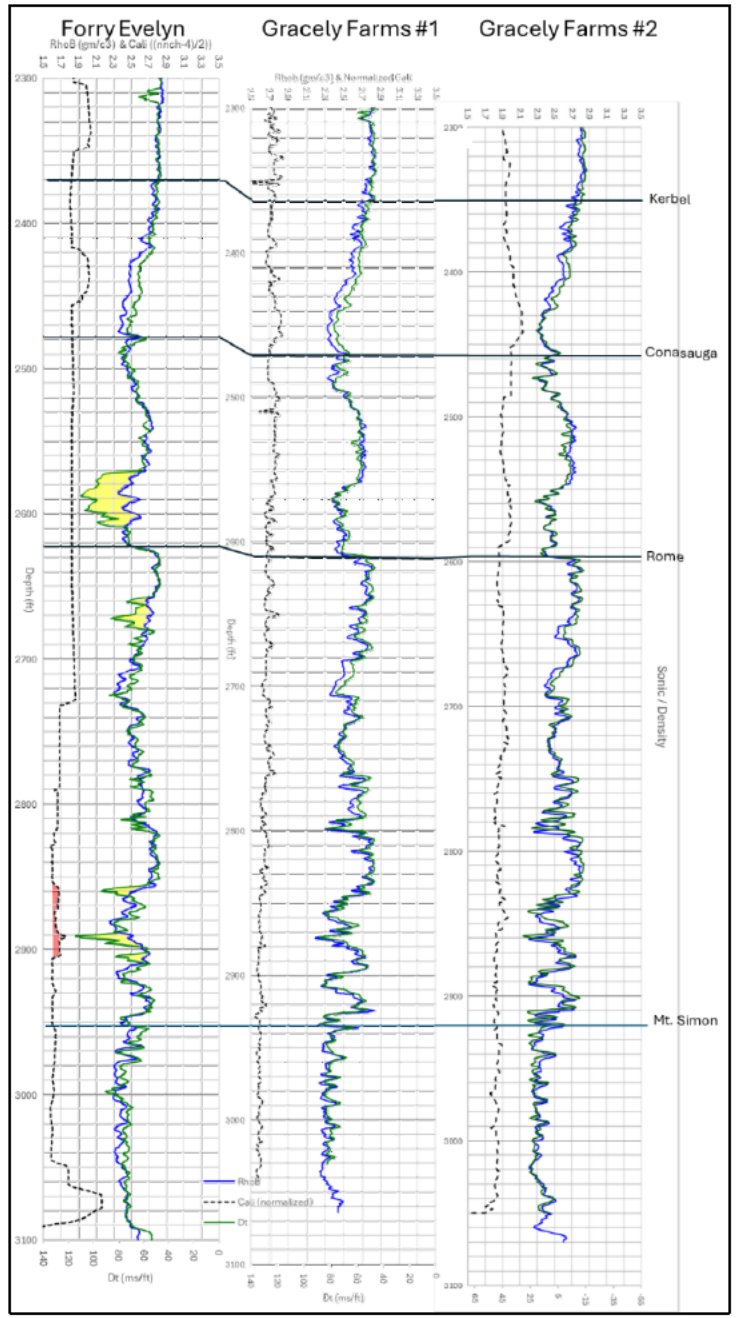

Normalized overlay of density and sonic geophysical for the Forry Evelyn and Gracely Farms 1 and 2 wells. The yellow shading indicates sonic and density log excursions, and the red shading shows abnormal caliper measurements due to borehole enlargement.

Figure 44

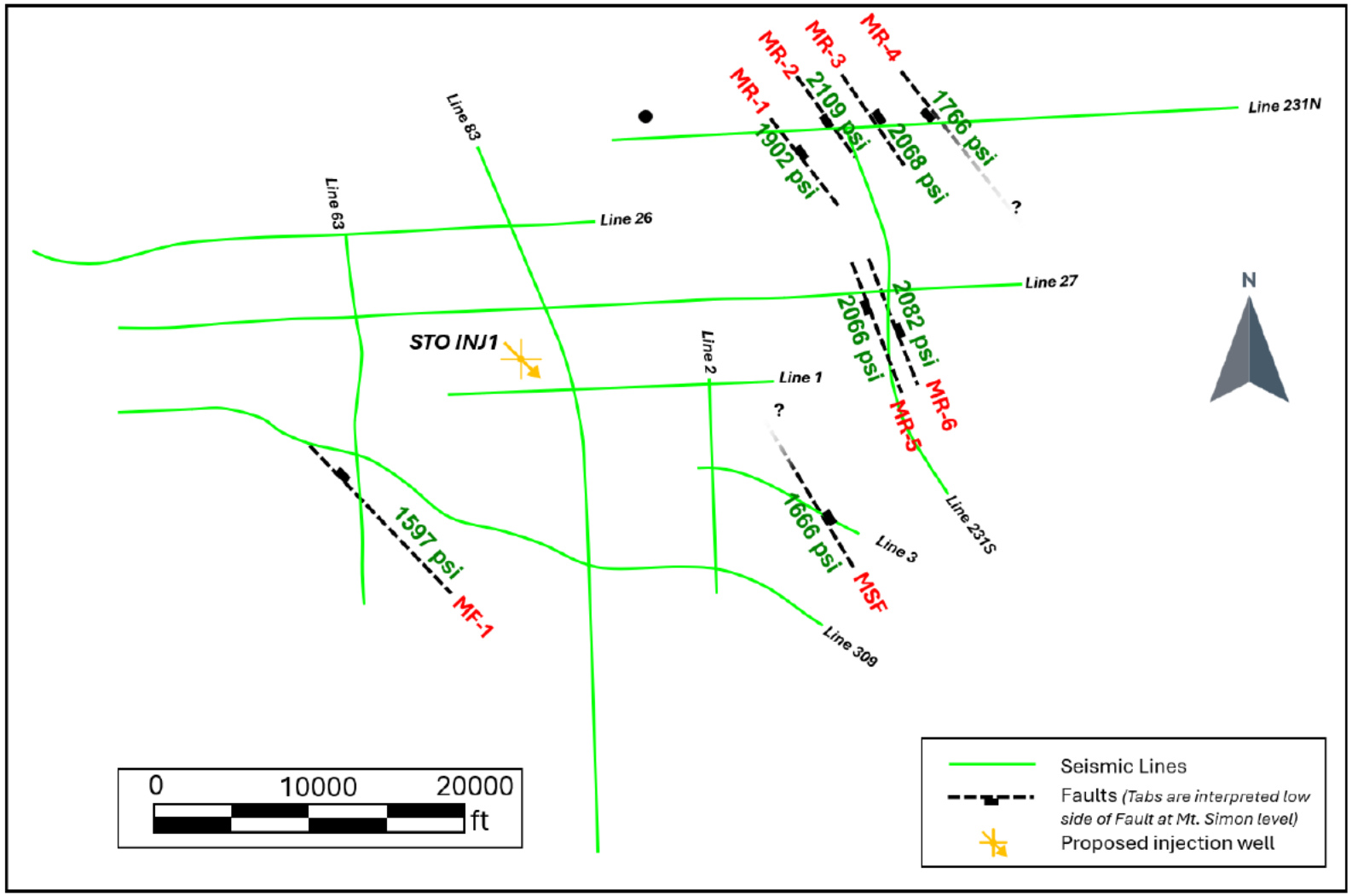

Location of interpreted faults in the 2D seismic survey and the increase in pore pressure (psi) required to critically stress the fault.

Figure 45

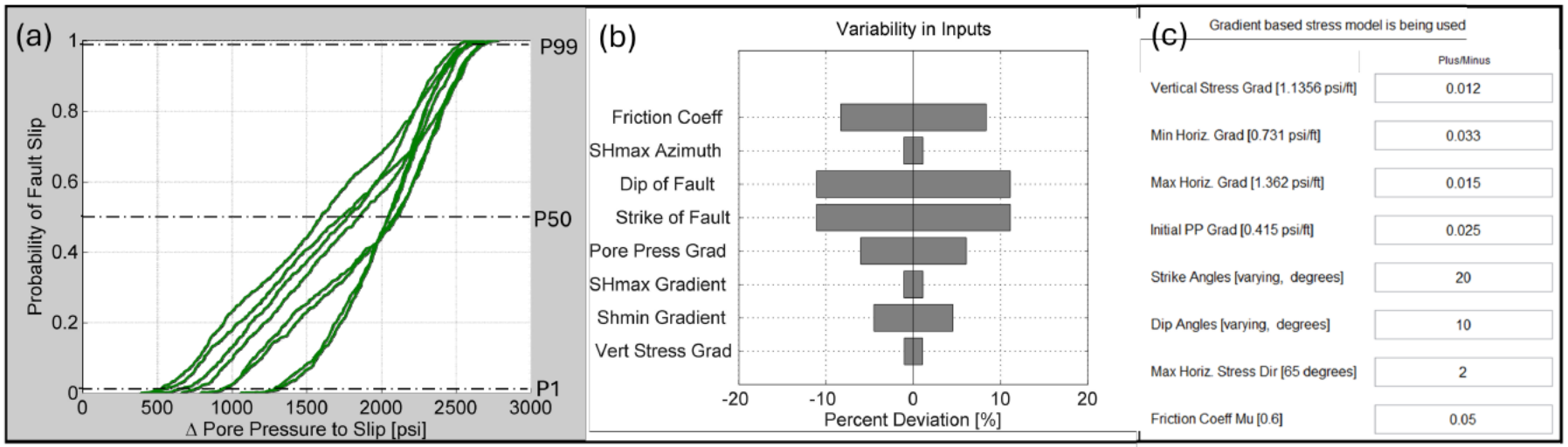

Fault slip potential for the interpreted faults on the 2D seismic survey. A) Graphical response showing the range of values from the Monte Carlo analysis, B) the variability of inputs used in the analysis as a percentage of the total value, and C) numeric inputs for the analysis.

Figure 46

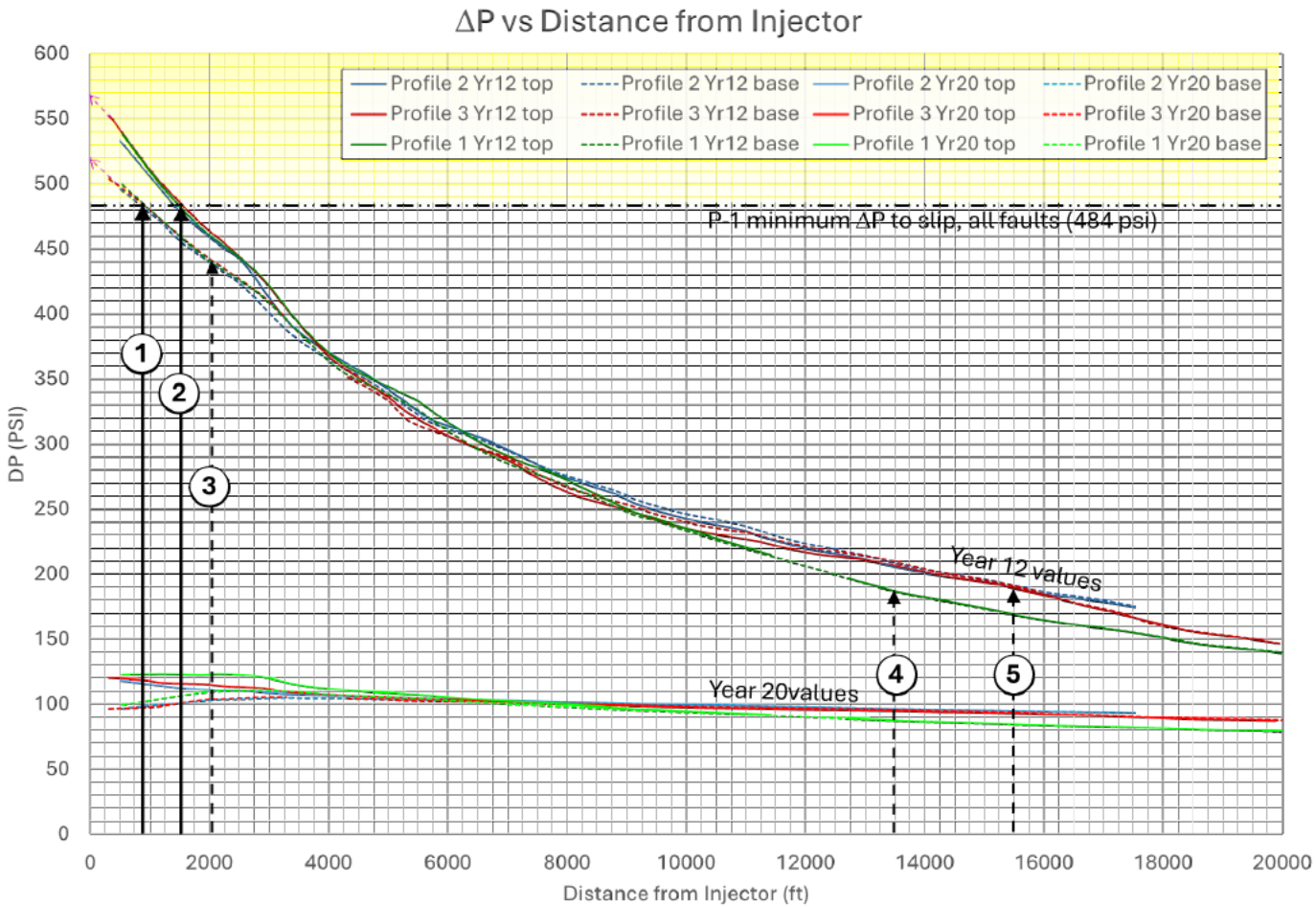

Pressure versus distance profiles for both the top and base of the Mt. Simon Sandstone at years 12 years (end of injection) and year 20. The delta pressure P-1 value is the lowest pressure to cause failure for all faults and is the dashed black line at the top of the graph. Line 1 (solid black vertical line) indicates the closest distance to the injector that a fault at the base of the Mt. Simon Sandstone could become critically stressed under the injection scheme, which occurs at ~850 feet from the injector. Line 2 (solid black vertical line) indicates the closest distance to the injector that a fault at the top of the Mt. Simon Sandstone could become critically stressed under the injection scheme, which occurs at ~1,500 feet from the injector. Line 3 (dashed black vertical line) is the nearest interpreted structure in the Precambrian Basement (base of Mt. Simon Sandstone). Line 4 (dashed black vertical line) is the distance to fault MF-1 that corresponds to a maximum delta pressure of ~185 psi at the top of the Mt. Simon Sandstone along profile 1 (Figure). Line 5 (dashed black vertical line) is the distance to the Merrit Fault corresponding to a maximum delta pressure of ~185 psi at the top of the Mt. Simon Sandstone along profile 3 (Figure). It should be noted that the lowest deterministic (~P50) value for delta pressure to critically stress (possibly causing slip) a fault is 1,597 psi (Table 4), which is not reached by this injection scheme. The difference in delta pressures between top of Mt. Simon Sandstone and base of Mt. Simon Sandstone is due to the buoyancy affect of the injected CO2 overriding the pressure gradient.

Figure 47

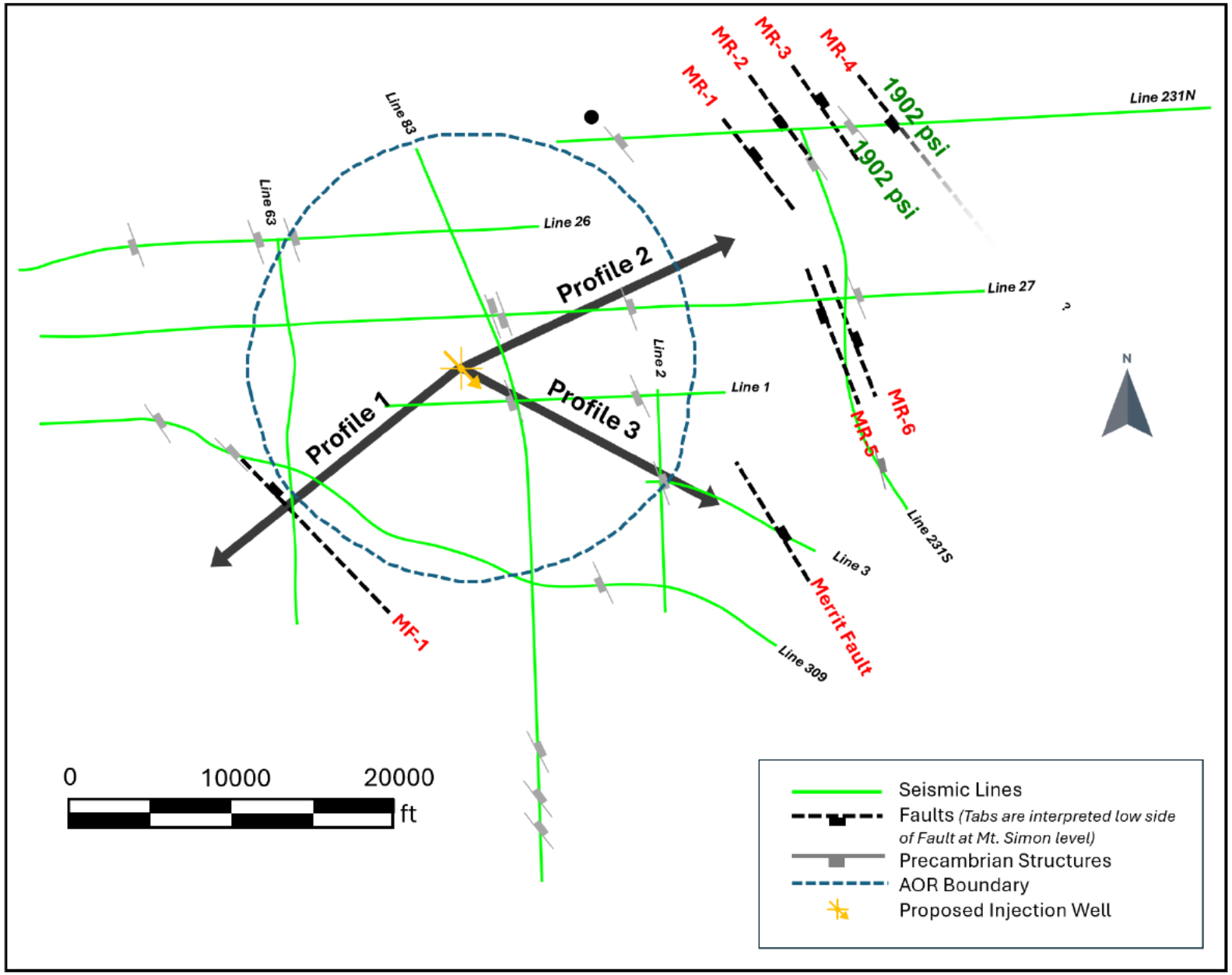

Pressure profiles 1, 3, and 4 (solid black lines), 2D seismic surveys (solid green lines), and interpreted faults (dashed black lines).

Figure 48

A

Fracture Orientation		ΔP to Critically stressed (psi)				
Strike(deg)	Dip(Deg)	P-1	P-10	P-50	P-90	P-99
120	80	469.45	575.23	709.9	831.87	931.73
125	80	715.24	819.37	956.99	1080.5	1156.5
130	80	999.14	1094.5	1223.1	1350.5	1434.2
135	80	1318.2	1392.1	1516	1631.9	1714
140	80	1615.3	1693.9	1810.7	1927.6	2006.9
145	80	1906.4	1977.7	2093.7	2217.5	2314
150	80	2139.5	2222.9	2363.8	2496.9	2590.5
155	80	2272.6	2346.1	2510.3	2668.6	2758.8
160	80	2143	2227	2356.2	2496.4	2599.4
165	80	1901.6	1982.8	2098.1	2227.4	2305.4
170	80	1585.7	1686.2	1809.5	1923.9	2000.5
175	80	1309.5	1385.3	1512.9	1634.1	1730.7
180	80	994.48	1091.4	1227.6	1359.8	1429.7
185	80	719.09	814.93	954.78	1076.4	1155.8
190	80	469.3	566.76	709.63	837.93	923.26

B

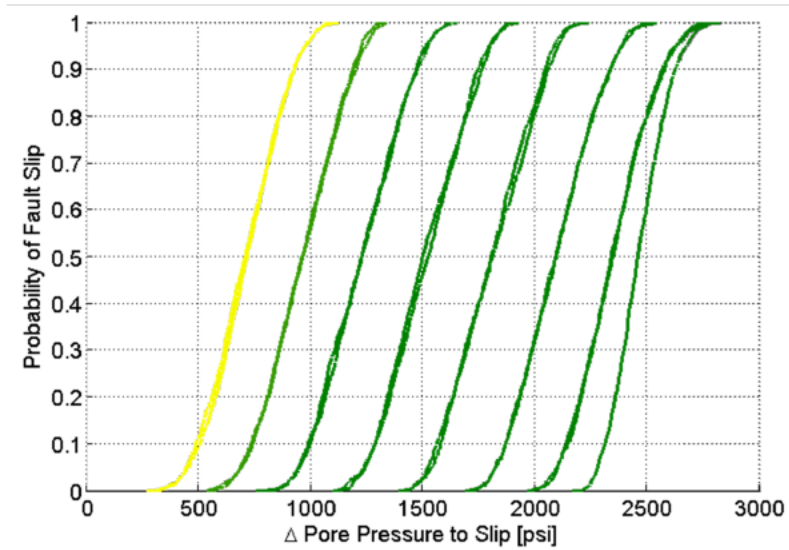

A) Table and B) graphical representation of fracture orientations related to paleo-stress from regional faults. These ranges are expanded from expected orientation by ±35° to include potential conjugate orientations.

Figure 49

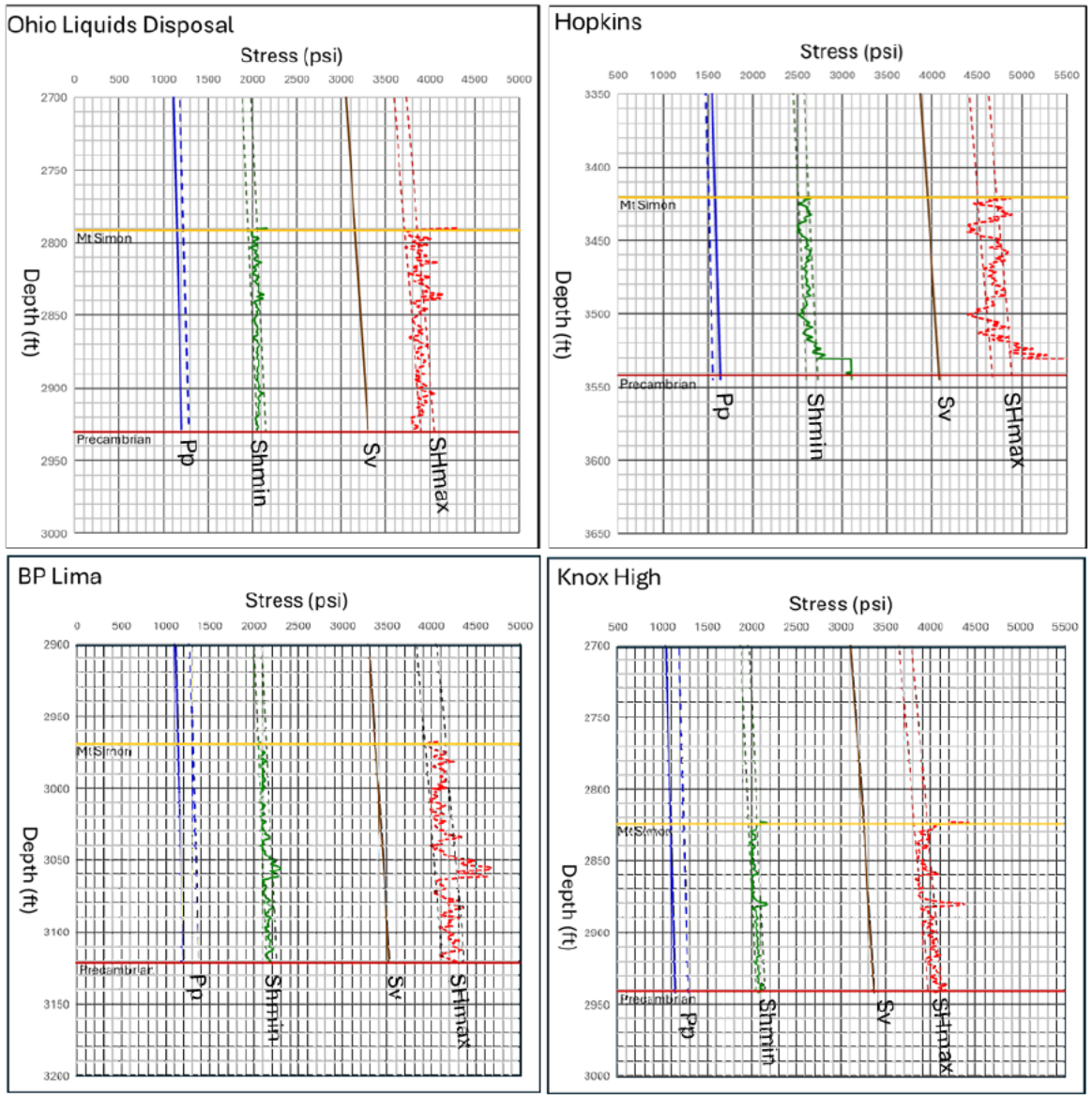

Stress values for wells in region. The solid blue line is measured pore pressure (Pp) and the dashed blue line is 0.44 psi/ft (hydrostatic pore pressure gradient). The solid green is log-derived minimum stress (SHmin) and the dashed green lines are minimum and maximum excursions used for the range of Shmin values. The brown solid line is vertical stress (Sv). The solid red line is calculated SHmax and dashed red lines are minimum and maximum excursions used for the range of SHmax values.

Figure 50

Wells used for petrophysical analysis of the Stonewell injection and confining zones.

PBI

Figure 51

Claimed as PBI

Ohio Liquids Disposal A) well logs and core photos of the B) Rome Formation and C) Mt. Simon Sandstone.

PBI

Figure 52

Forry Evelyn (UWI 34101202070000) geophysical logs with measured depth (MD), formation tops well log average effective porosity (%), and intrinsic permeability (mD) values.

GR_TOT=total gamma ray log, RHOB =density; DPHI_SS=sandstone density porosity, NPHI_SS=sandstone neutron porosity, PHIE=effective porosity, Perm =permeability in mD.

PBI

Figure 53

Gracely Farms 1 (UWI 3410120168000) geophysical logs with measured depth (MD), formation tops, well log average effective porosity (%), and intrinsic permeability (mD) values. GR_TOT=total gamma ray log; RHOB =density, DPHI_SS=sandstone density porosity, NPHI_SS=sandstone neutron porosity, PHIE=effective porosity, Perm=permeability in mD, and black circles=core porosity.

PBI

Figure 54

BP Chemical 2 (UWI 34003200670000) geophysical logs with measured depth (MD), formation tops, well log average effective porosity (%), and intrinsic permeability (mD) values. GR_TOT=total gamma ray log; RHOB =density, DPHI_SS=sandstone density porosity, NPHI_SS=sandstone neutron porosity, PHIE=effective porosity, Perm=permeability in mD, and black circles=core porosity.

PBI

Figure 55

Geomechanical parameters calculated from the Ohio Liquids Disposal (UWI 34143202370000) well. Res=reservoir, VPVS=compressional to shear wave velocity ratio, BIOT=Biot's Factor, Press=pressure, Grads=gradients, Min=mineralogy

PBI

Figure 56

Effective porosity (PHIE) and permeability cross plots with core plug values (grey squares) for the A) Mt. Simon Sandstone, B) Rome A and D subunits, and C) Rome B and C subunits.

PBI

Figure 57

Claimed as PBI

Effective porosity (PHIE) histograms of the key petrophysical wells. The plots are divided into the A) the Rome Formation A and D subunits, B) the Rome Formation B and C subunits, and C) the Mt. Simon Sandstone injection zone.

PBI

Figure 58

Permeability (mD) histograms of the key petrophysical wells. The plots are divided into the A) the Rome Formation A and D subunits, B) the Rome Formation B and C subunits, and C) the Mt. Simon Sandstone injection zone.

PBI

Figure 59

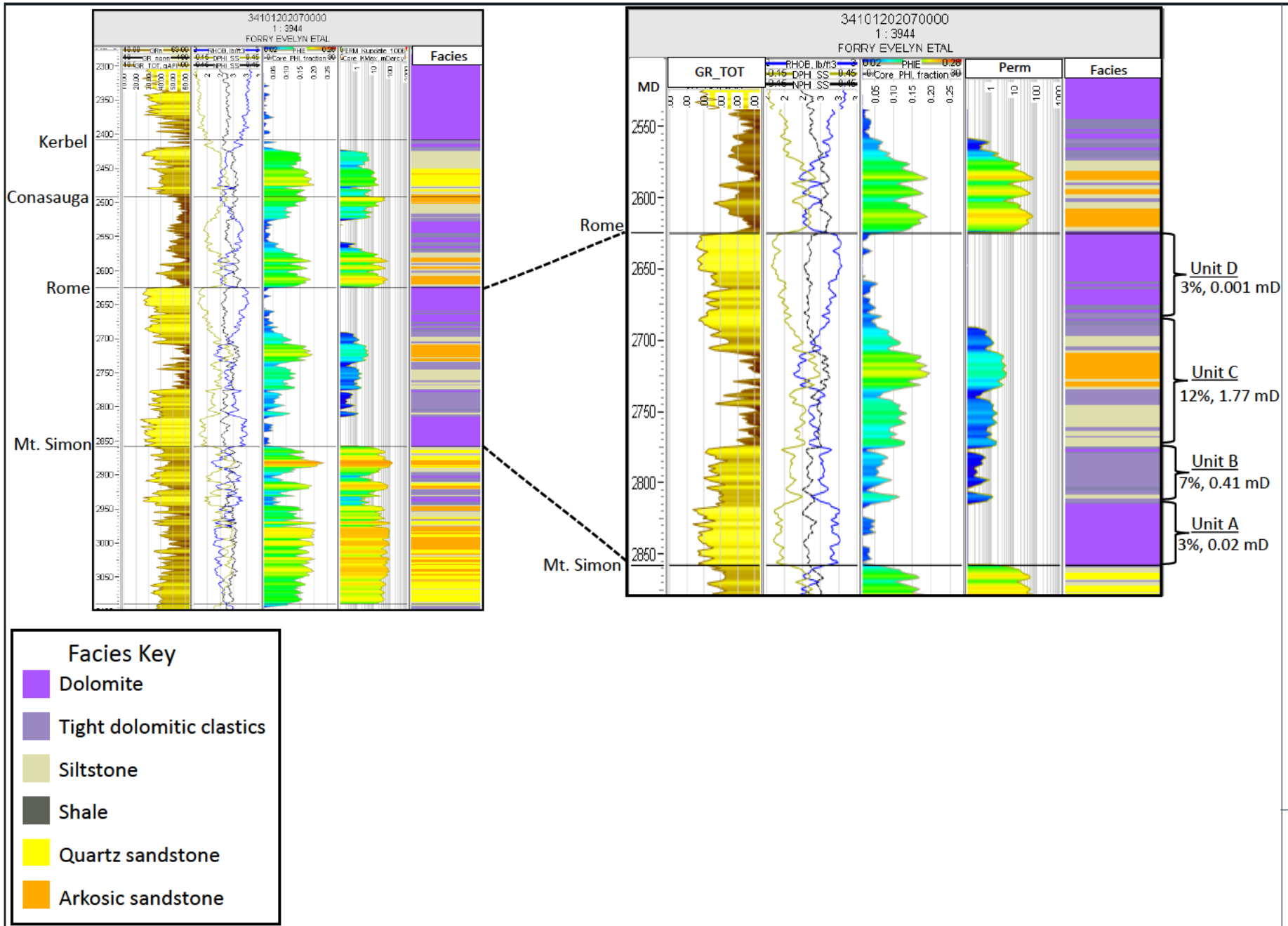

Forry Evelyn (UWI 34101202070000) geophysical logs and petrophysical results. Gamma-ray API (GR_TOT), density (RHOB) and porosity (DPHI, NPHI) logs are shown. Effective porosity (PHIE), permeability (Perm), and facies.

Figure 60

Gracely Farms 1 (UWI 34101201680000) geophysical logs and petrophysical results. Gamma-ray API (GR_TOT), density (RHOB) and porosity (DPHI, NPHI) logs are shown. Effective porosity (PHIE), permeability (Perm),and facies.

PBI

Figure 61

Cross section C-C' of key petrophysical wells showing the lateral continuity of the Rome A, Rome B, Rome C, and Rome D. Gamma-ray API (GR_TOT), density (RHOB), sandstone porosity (DPHI_SS, NPHI_SS), effective porosity (PHIE), permeability (PERM), core points (circles), and facies are shown.

PBI

Figure 62

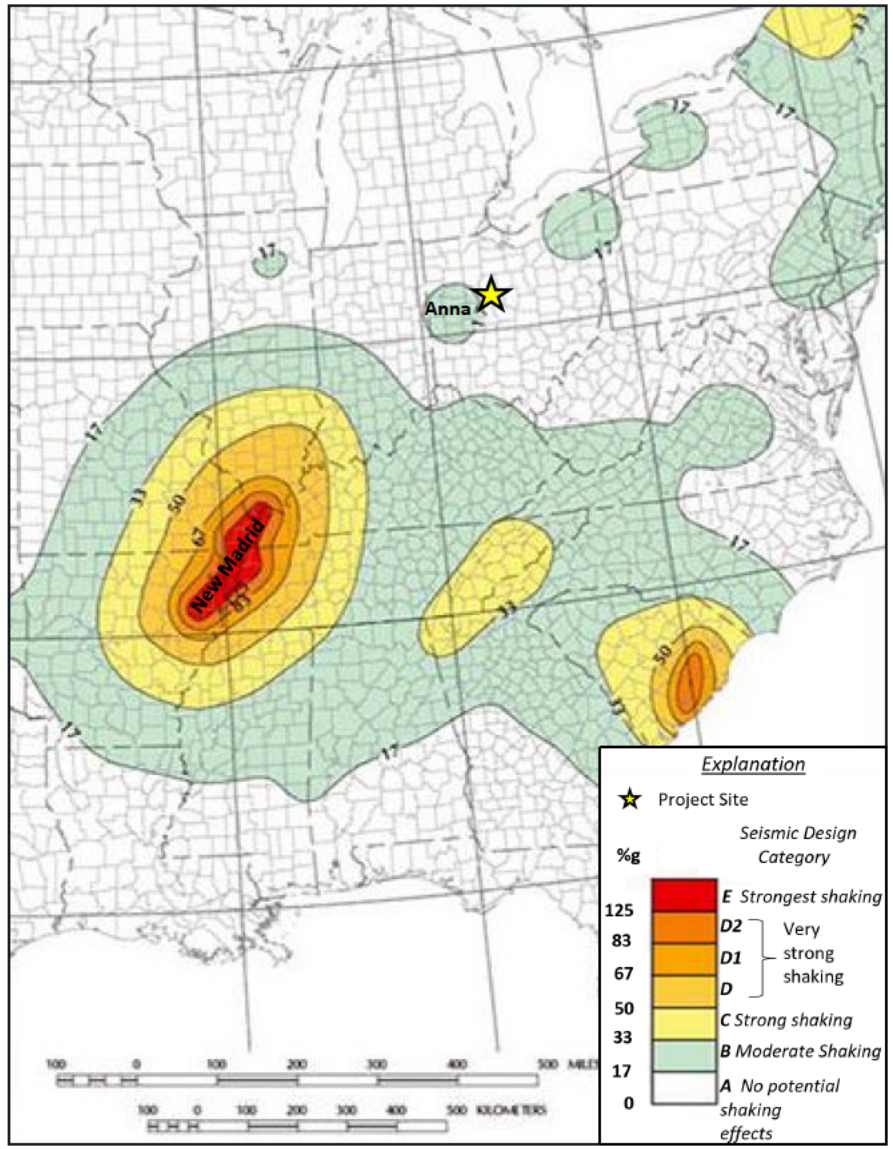

Cross section C-C' of key petrophysical wells showing the lateral continuity of the Rome A, Rome B, Rome C, and Rome D. Gamma-ray API (GR_TOT), density (RHOB), sandstone porosity (DPHI_SS, NPHI_SS), effective porosity (PHIE), permeability (PERM), core points (circles), and facies are shown.

Figure 63

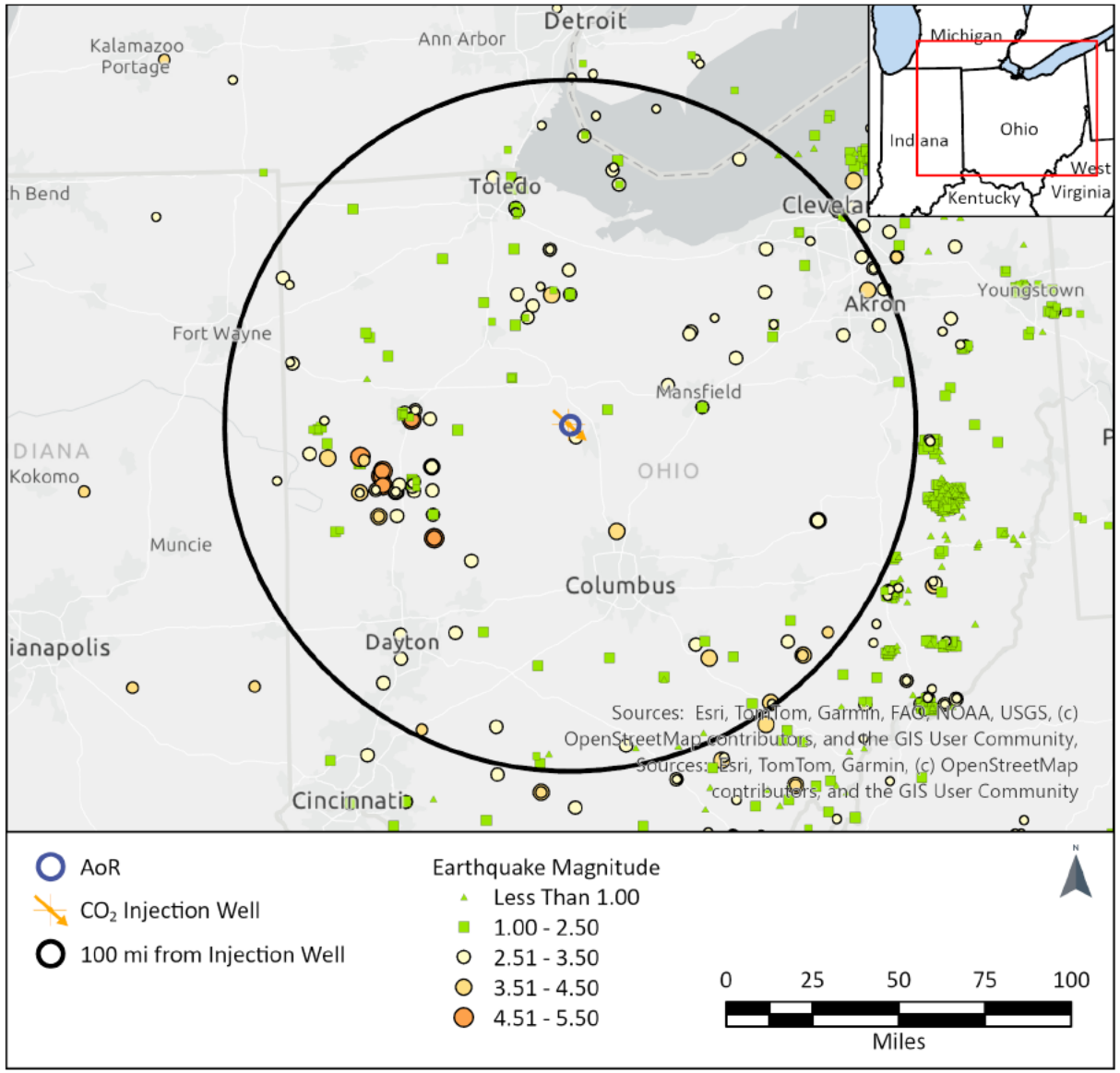

Map of earthquake epicenters that occurred between 1 January 1800 to 3 July 2025 within 100 miles (black circle) of the Stonewell injection well.

Figure 64

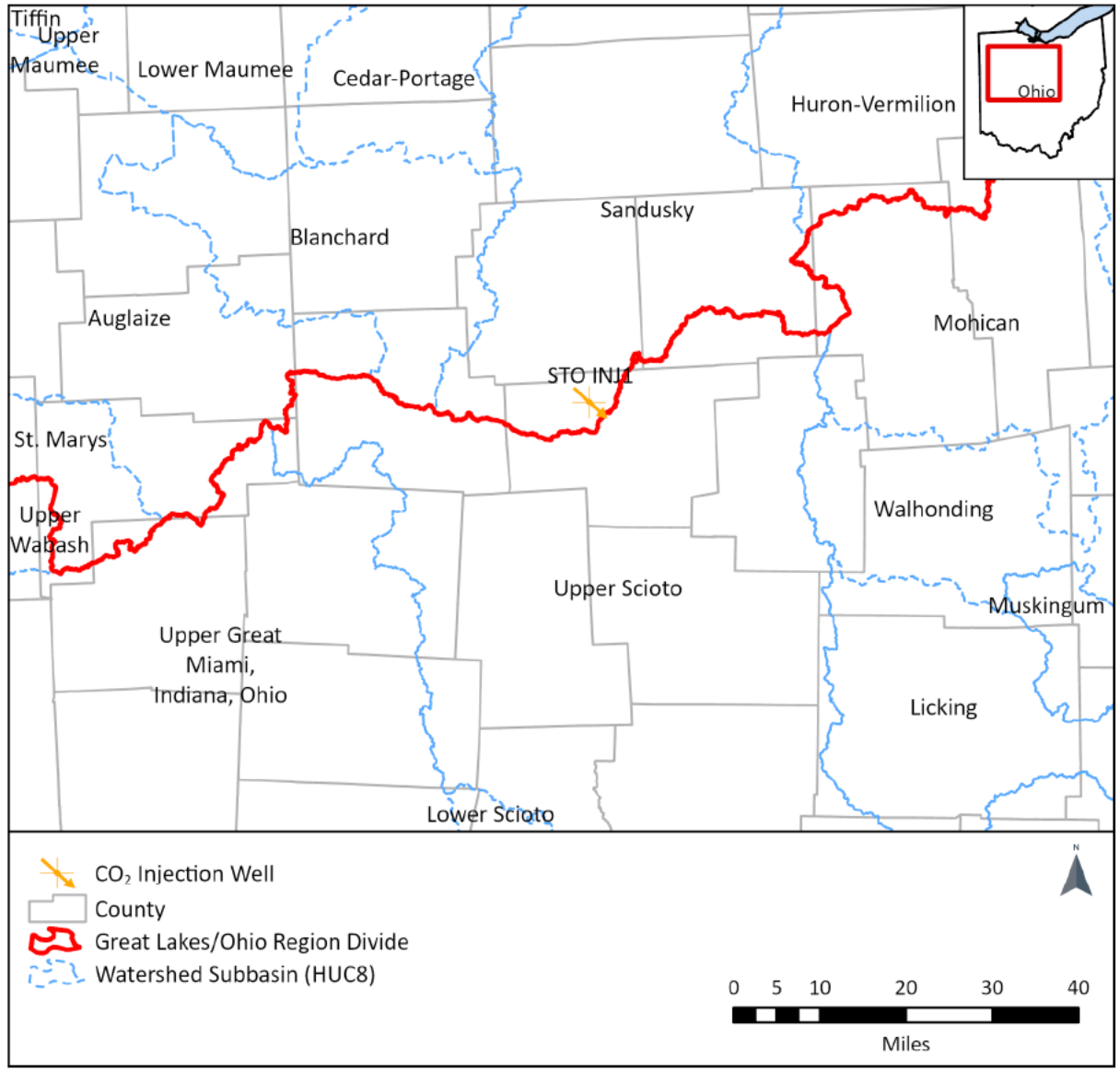

Map of the Ohio River watershed with individual drainage basins within the watershed. The Stonewell Project is located within the Sandusky sub-basin.

Figure 65

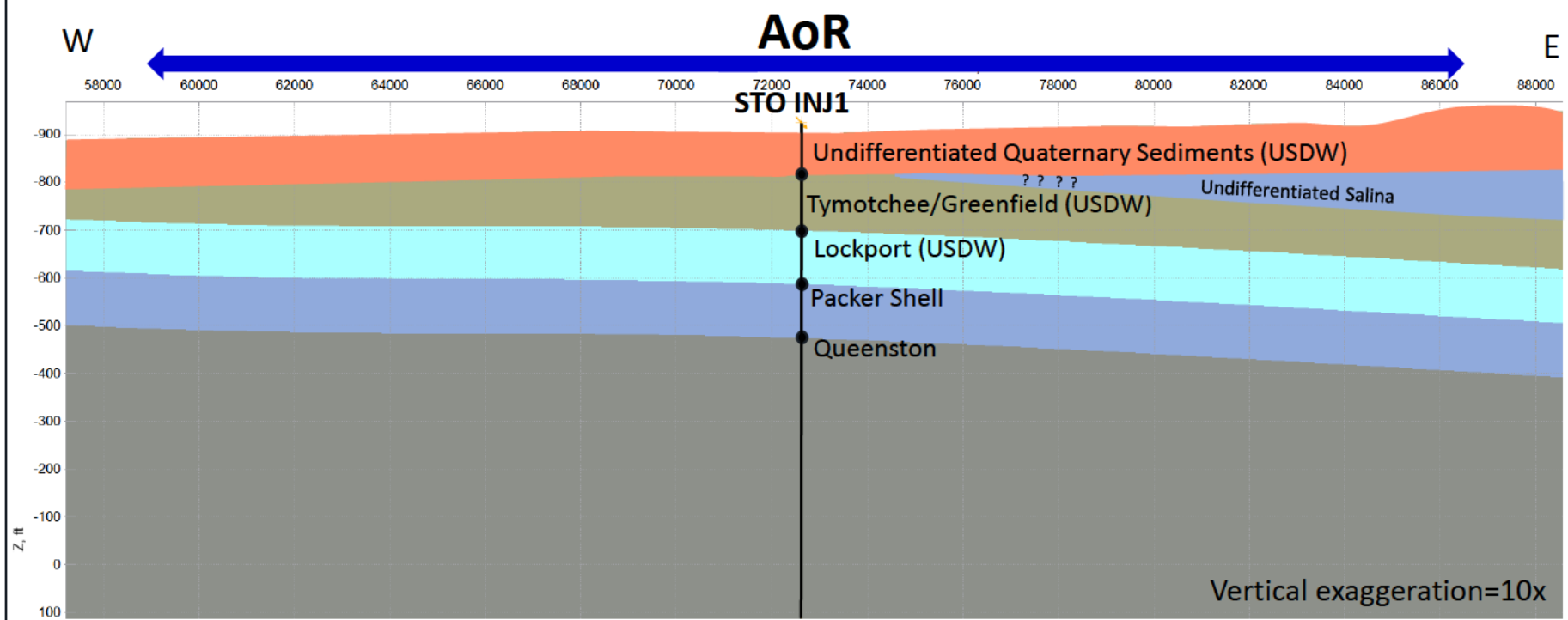

West to east cross section of the shallow hydrostratigraphy in the AoR. See Figure 6 for location. Depth is in fbsl and vertical exaggeration= 10x

Figure 66

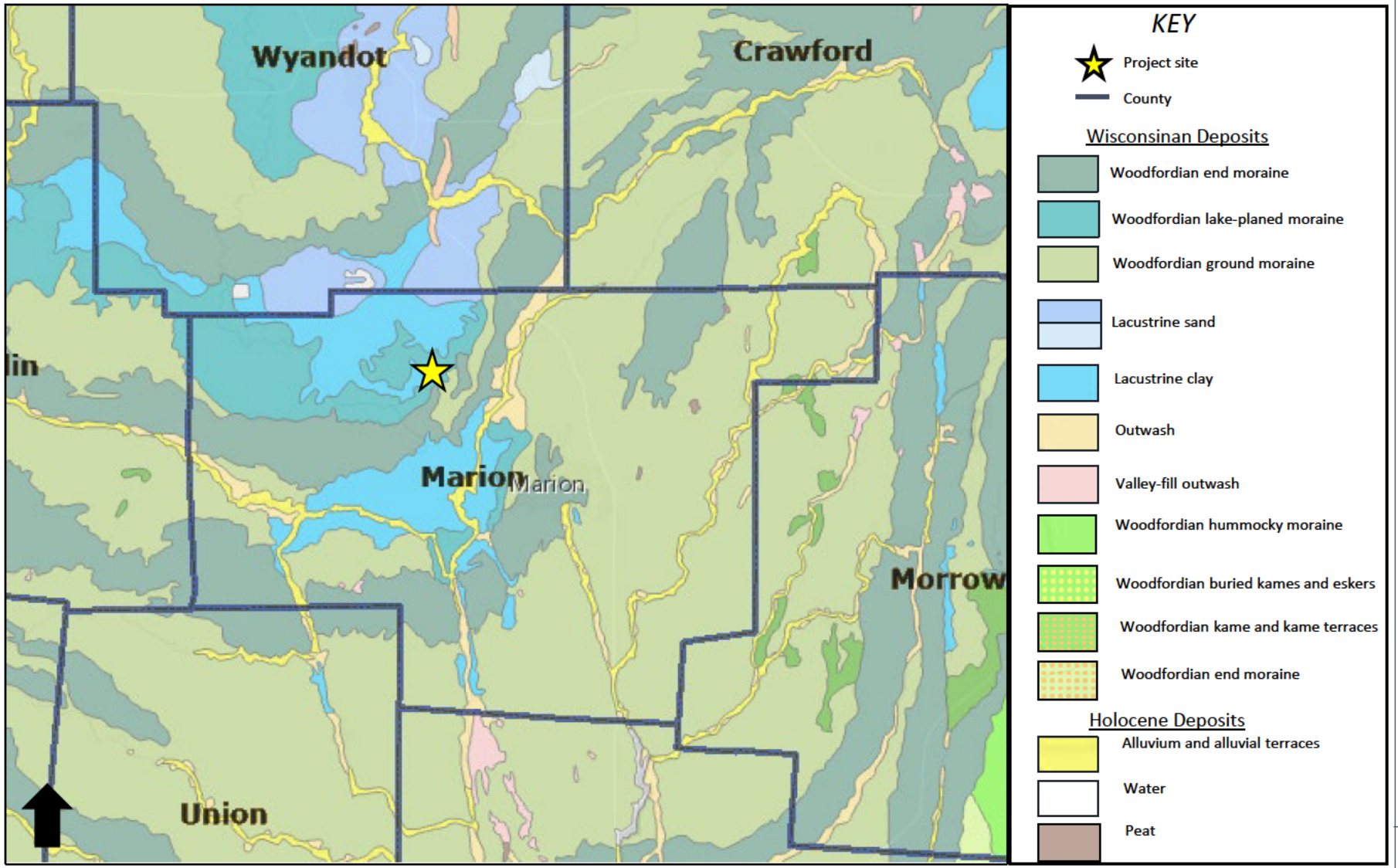

Map of Ohio glacial deposits shows that the Stonewell Project site is located on glacial deposits composed of Wisconsinan Woodfordian lake-planed moraine deposits and lacustrine clay. Modified from ODNR Ohio Geology Interactive Map (ohiodnr.gov).

Figure 67

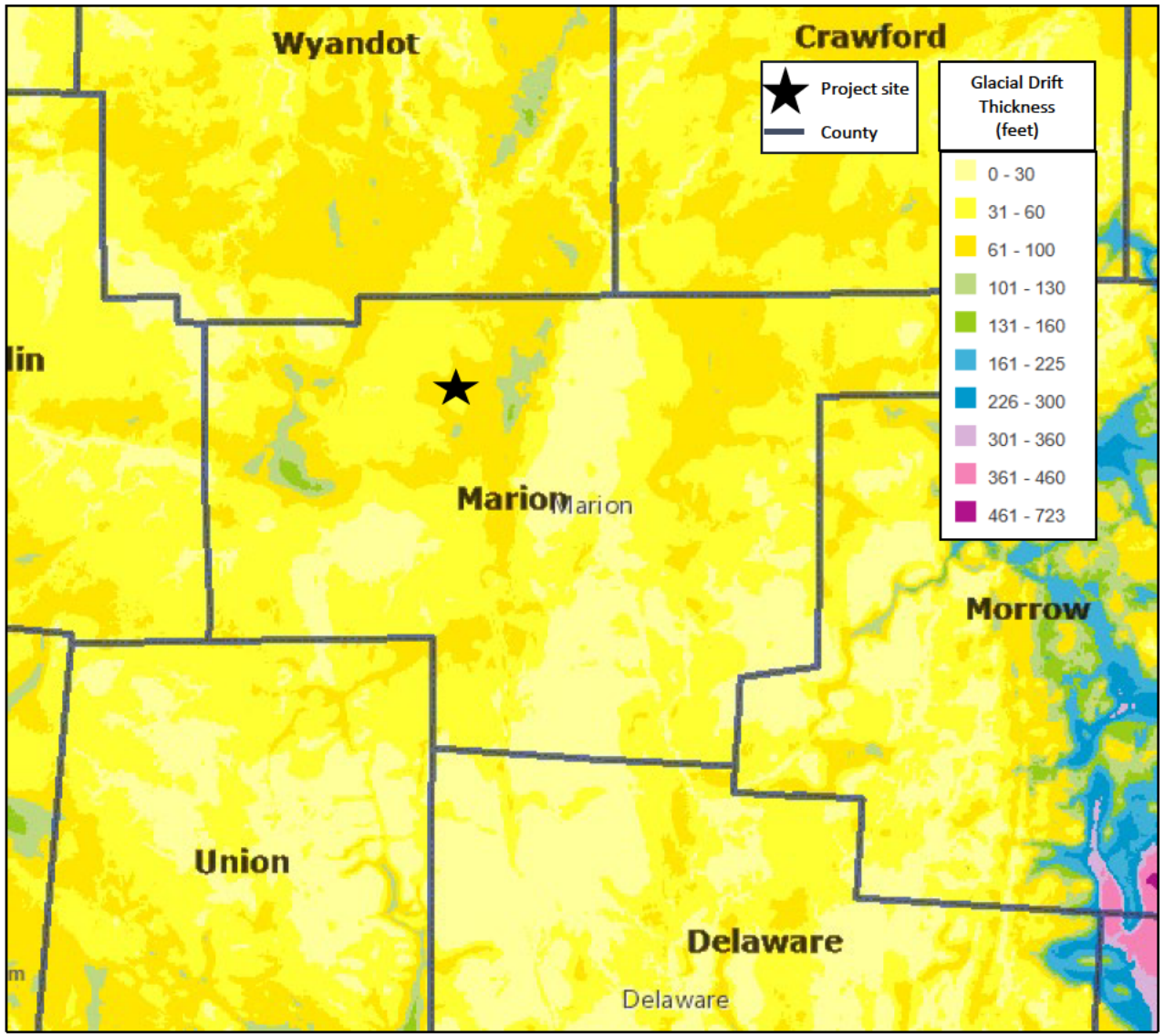

Map of glacial drift thickness in feet. At the project site, less than thirty feet of glacial sediments are expected. Modified from ODNR [Ohio Geology Interactive Map (ohiodnr.gov)]

Figure 68

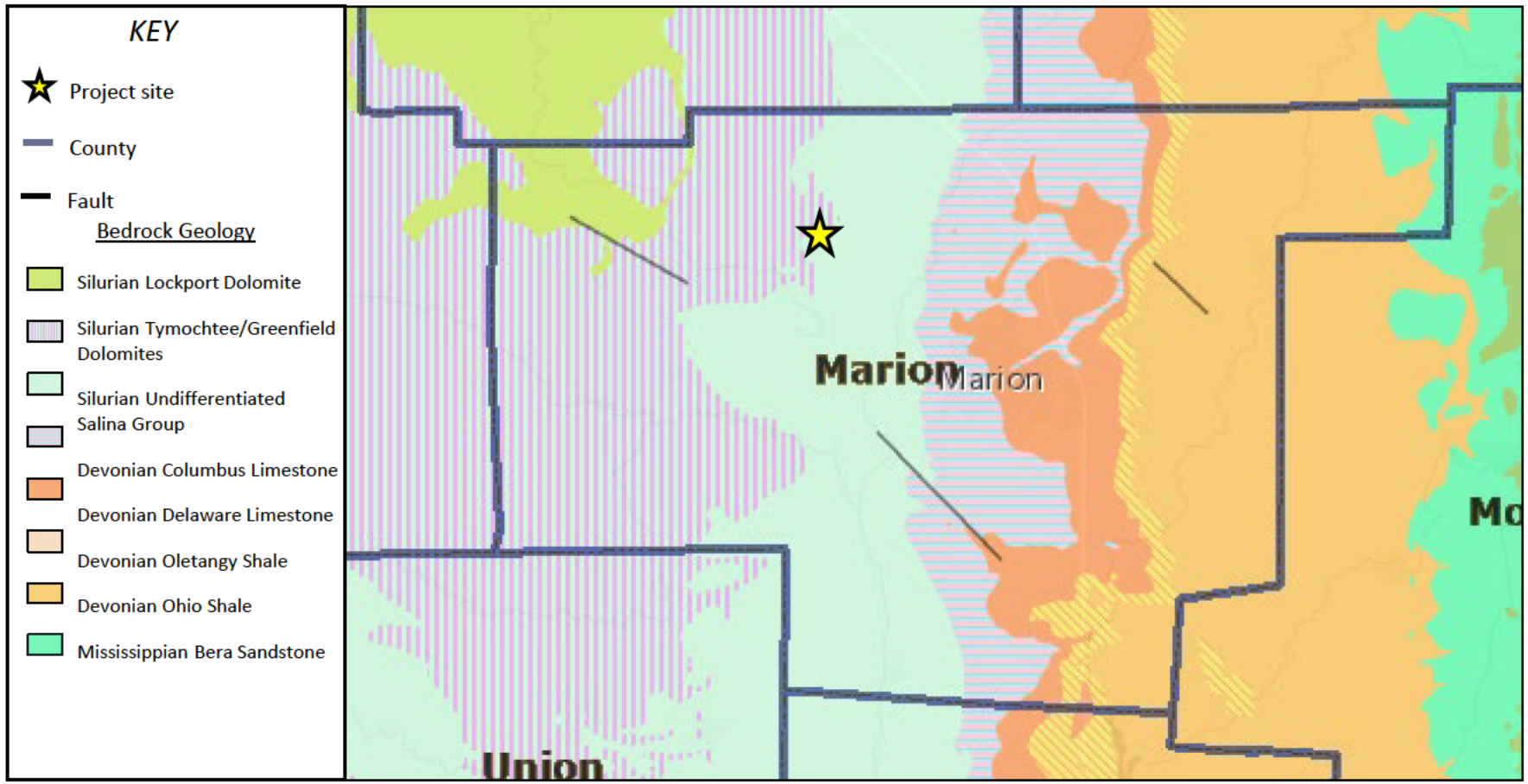

Bedrock geology underlying unconsolidated glacial deposits. The Stonewell Project site, indicated by the yellow star, is located at the contact of the undifferentiated Salina Group and the Tymochtee/Greenfield Dolomites. Modified from ODNR Ohio Geology Interactive Map (ohiodnr.gov)

Figure 69

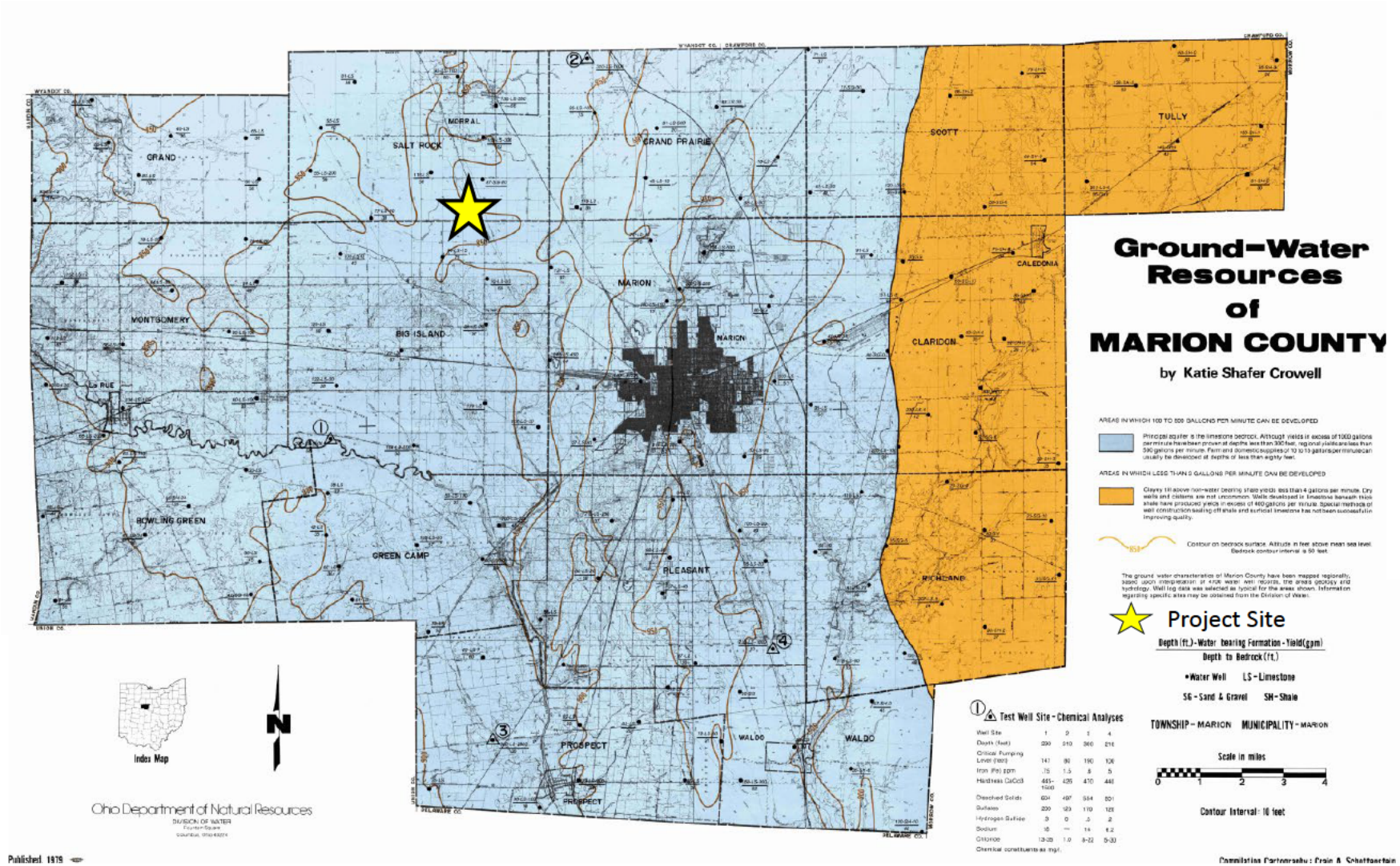

Aquifer map of Marion County, Ohio.

Modified from Cromwell (1979)

Figure 70

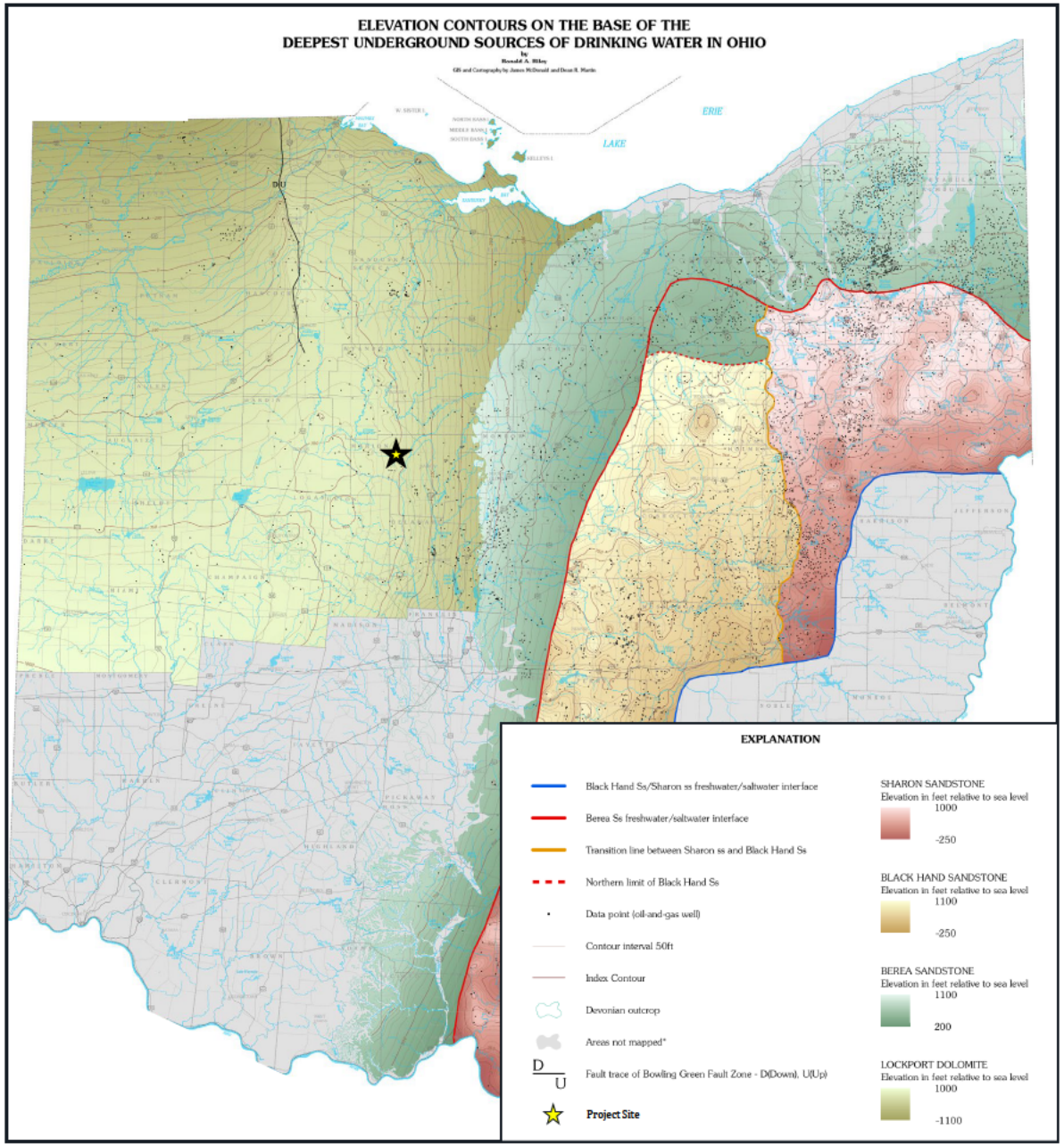

Map of the base of the lowermost USDW in Ohio. The Silurian Lockport Dolomite is the lowermost USDW at the Stonewell project site. Modified from (Riley et al., 2012)

Figure 71

Claimed as PBI

Map of TDS concentration contours in the Mt. Simon Sandstone brine. The project site is represented with a yellow star. (Modified from Mehnert and Weberling, 2014)

PBI

Figure 72

National Flood Hazard Layer from FEMA. Zone A (100 Yr) flood hazard is located along Little Sandusky River within the Stonewell Project AoR. The STO INJ1 and STO OBS1 wells are shown.

PBI

Figure 73

Evolution of pH at the base of the primary confining zone over the 62-year modeling time duration. The shift from gas injection to post-injection conditions is indicated on the plots by the dashed line.

PBI

Figure 74

Reaction pathway modeling results showing mineral reactions in the primary confining zone. The shift from gas injection to post-injection conditions is indicated on the plots by the dashed line.

PBI

Figure 75

Reaction pathway modeling results showing mineral reactions in the arkosic-dominated lithology of the injection zone. The shift from gas injection to post-injection conditions is indicated on the plots by the dashed line.

PBI

Figure 76

Reaction pathway modeling results showing mineral reactions in the quartz-dominated lithology of the injection zone. The shift from gas injection to post-injection conditions is indicated on the plots by the dashed line.

PBI

Figure 77

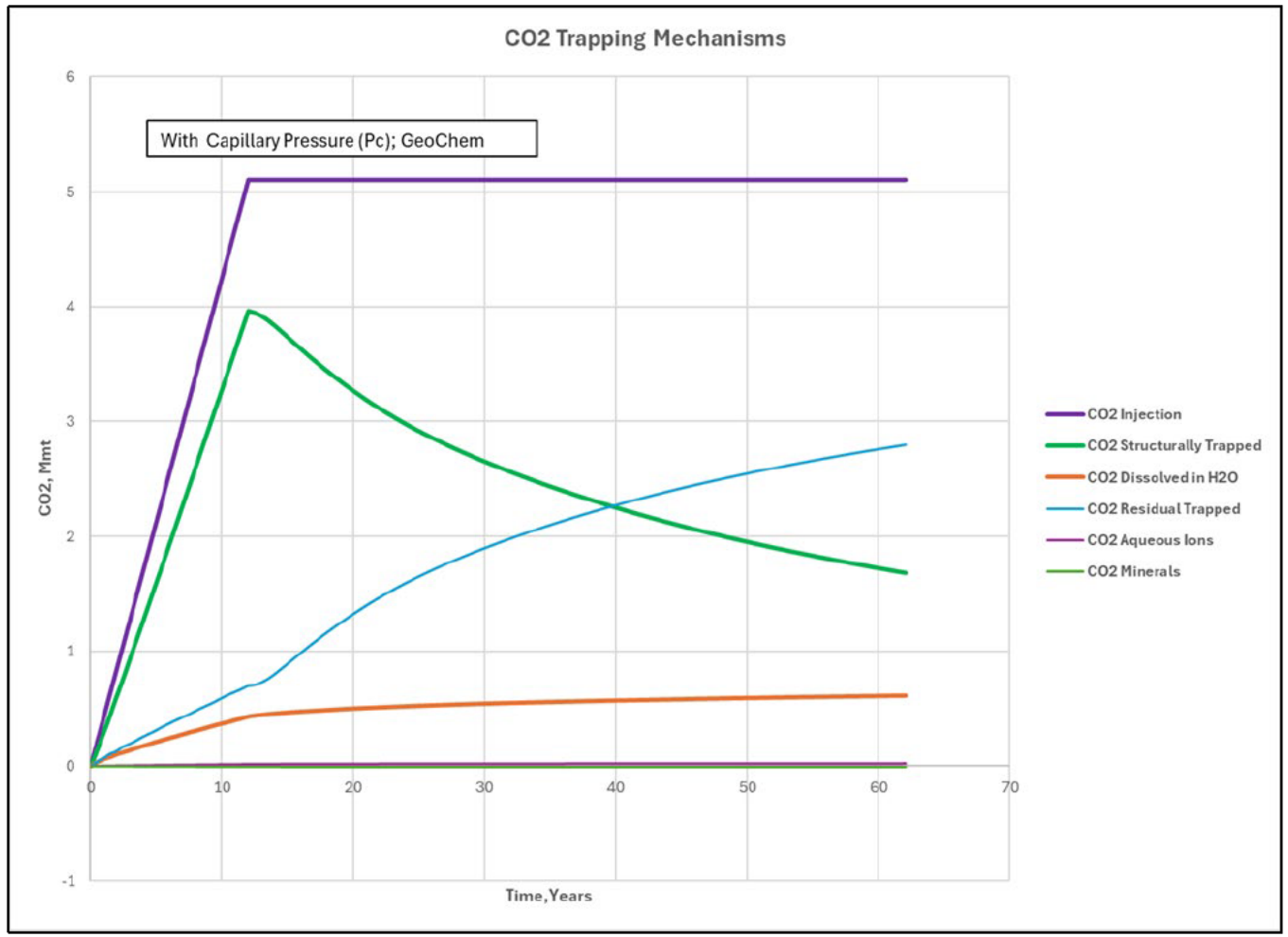

Graph of the relationships and evolution of CO2 trapping mechanism during 12 years of CO2 injection followed by a 50-year PISC period at the Stonewell Project site.

Figure 78

16. PBI Appendix 1A-List of Landowners Within the AoR

Claimed as PBI

Claimed as PBI

Claimed as PBI

Claimed as PBI

Claimed as PBI

Claimed as PBI

Claimed as PBI

Claimed as PBI

Claimed as PBI

Claimed as PBI

Claimed as PBI

Claimed as PBI

Claimed as PBI

Claimed as PBI

Claimed as PBI

Claimed as PBI

Claimed as PBI

Claimed as PBI

Claimed as PBI

Claimed as PBI

Claimed as PBI

Claimed as PBI

Claimed as PBI

Claimed as PBI

Claimed as PBI

Claimed as PBI

Claimed as PBI

Claimed as PBI

Claimed as PBI

Claimed as PBI

Claimed as PBI

17. Appendix 1B-Wells used for Geologic Evaluation

UWI	Permit License Number	Wel Name	Bottomhole Latitude	Bottomhole Longitude	Kelly Bushing Elevation (feet above sea level)	Ground Surface Elevation (feet above sea level)	Max TD	Current Status	Spud Date	Permit License Date	Completion Date	Abandonment Date	Current Operator	Formation at TD	Hole Direction	Current Class	Plot Symbol Description
34175202590000	259	Kuenzli C W & L M	40.8270165	-83.1902655	890	876	3149	Dry & Abandoned	1982-11-05	1982-10-26	1982-11-21		Berea Oil & Gas Corp	Granite	Vertical	New Field Wildcat-Dry (Including Temporarily Abandoned Well)	Dry And Abandoned
34175600010000	0001	Martin G W & M	40.7037889	-83.1343234		951	2471	Dry & Abandoned	1919-02-21	1919-02-11	1919-04-10		Logan Natural Gas&Fuel	Trenton /LM/	Vertical	Development Well-Dry (Including Temporarily Abandoned Well)	Dry And Abandoned
34083238650000	3865	Daniels-Weller Unit	40.5114737	-82.6192525	1179	1168	4400	Dry & Abandoned	1989-07-28	1989-07-18	1990-08-06		Smail James R	Kerbel	Vertical	New Field Wildcat-Dry (Including Temporarily Abandoned Well)	Dry And Abandoned
34083214680001	1468	G D Larimore	40.3256659	-82.5644442		1194	5376	Dry & Abandoned-Old Well Worked Over	1963-01-01	1962-12-22	1963-02-04		Ohio Fuel Gas	Basal/SD/	Vertical	New Field Wildcat-Dry (Including Temporarily Abandoned Well)	Dry And Abandoned
34143200770000	77	V Haff	41.3542782	-82.9126811		643	3123	Dry & Abandoned-Gas Shows	1960-01-01	1959-12-22	1960-11-17		East Ohio Gas Co, The	Precambrian	Vertical	New Field Wildcat-Dry (Including Temporarily Abandoned Well)	Dry And Abandoned
34173203670000	367	Breneman Donelda	41.2177956	-83.5117109		719	2200	Dry & Abandoned	1980-03-15	1980-03-05	1980-04-26		Allerton Resources	Conasauga	Vertical	Deeper Pool Wildcat-Dry	Dry And Abandoned
34041200500000	50	J B Rupple	40.2799222	-83.0733809	915	889	3487	Dry & Abandoned	1964-05-12	1964-05-02	1964-06-07		Texas Coastal Oil Co	Mount Simon /SD/	Vertical	New Field Wildcat-Dry (Including Temporarily Abandoned Well)	Dry And Abandoned
34149201030000	103	Borland	40.2712794	-84.0600345	1074	1063	3227	Dry & Abandoned	1985-01-24	1985-01-14	1985-03-24		Funk Exploration Inc	Mount Simon /SD/	Vertical	New Field Wildcat-Dry (Including Temporarily Abandoned Well)	Dry And Abandoned
34159200710000	71	Black	40.2763072	-83.2768567	987	971	3396	Dry & Abandoned	1984-08-25	1984-08-15	1984-09-01		Funk Exploration Inc	Mount Simon /SD/	Vertical	New Field Wildcat-Dry (Including Temporarily Abandoned Well)	Dry And Abandoned
34147202140000	214	Hoover Stanley	41.1654494	-83.2493860	764	755	2600	Temporarily Abandoned - Gas	1979-08-18	1979-08-08	1980-01-25		A & S Energy LLC	Basement	Vertical	Development Well-Gas	Suspended Gas
34041203580000	358	Longshore R Etal Unit	40.2438314	-82.8036422	1071	1060	4272	Abandoned Oil Producer	1993-02-16	1993-02-06	1993-02-25	2001-12-07	Cgas Exploration	Granite	Vertical	New Field Wildcat-Discovery	Abandoned Oil
34041203540000	354	Cockrell-Godshall Unit	40.2617574	-82.7701322	1118	1112	4873	Temporarily Abandoned	1991-01-10	1990-11-09	1995-04-26		Poling Richard C	Precambrian	Vertical	Deeper Pool Wildcat-Dry	Dry And Abandoned
34091201010000	101	Wish Trust	40.4045578	-83.7487561	1275	1270	3258	Dry & Abandoned-Gas Shows	2002-05-16	2001-04-02	2002-05-22		Bakerwell Inc	Mount Simon /SD/	Vertical	New Field Wildcat-Dry (Including Temporarily Abandoned Well)	Dry And Abandoned
34069201390000	20139	Shidler James SWIW #2	41.3284829	-83.9592311	692	682	3375	Salt Water Disposal	2005-02-17	2004-10-25	2005-04-03		Aurora Energy Ltd	Granite	Vertical	Injection	Disposal
34117237330000	3733	Fry-Morris Unit	40.5644096	-82.6898408	1318	1299	4700	Oil Producer	1986-12-28	1986-12-18	1987-03-08		Maram Energy	Rome	Vertical	Development Well-Oil	Oil
34101200610000	61	M G Kennedy	40.6803912	-83.0901252		961	2565	Dry & Abandoned	1964-07-16	1964-07-06	1964-09-01		Mitchell & Donelson	Trempealeau	Vertical	New Field Wildcat-Dry (Including Temporarily Abandoned Well)	Dry And Abandoned
34101200710000	0071	Ferguson B S	40.6456610	-83.3057191		889	1933	Dry & Abandoned	1964-09-23	1964-08-21	1964-11-05	1964-11-18	Petroleum Services Inc	Unknown	Vertical	New Field Wildcat-Dry (Including Temporarily Abandoned Well)	Dry And Abandoned
34003200670000	67	Standard Oil Company	40.7162036	-84.1277752	872	866	3133	Salt Water Disposal	1968-01-20	1968-01-10	1968-01-27		Vistron Corp	Mount Simon	Vertical	Injection-Water	Disposal
34041203560000	356	Sheets Lula Mae	40.3278570	-82.9154774	987	965	4013	Dry & Abandoned	1993-03-30	1993-03-20	1993-04-05		Ngo Development Corp	Granite	Vertical	New Field Wildcat-Dry (Including Temporarily Abandoned Well)	Dry And Abandoned
34041202420000	242	H & H Smith	40.3520305	-82.9871524	992	974	4035	Dry & Abandoned	1965-02-24	1965-02-14	1965-03-07		McClure Oil Co	Precambrian	Vertical	New Field Wildcat-Dry (Including Temporarily Abandoned Well)	Dry And Abandoned
34101600180000	0018	Brown L C Brush Ridge	40.6862520	-83.1632486		951	2490	Dry & Abandoned					Unknown	St Peter /SD/	Vertical	Development Well-Dry (Including Temporarily Abandoned Well)	Dry And Abandoned
34173202310000	231	Peek Lillian L	41.2548386	-83.6634898	698	689	2770	Dry & Abandoned	1964-09-03	1964-08-27	1964-09-14	1964-09-14	Oneill Joseph I Jr	Precambrian	Vertical	Development Well-Dry (Including Temporarily Abandoned Well)	Dry And Abandoned
34101201440001	144	Kyle J & J	40.5188335	-83.1190853	997	988	3485	Dry & Abandoned-Old Well Worked Over	1982-11-18	1982-11-08	1982-11-22		Ohio Natural Fuel	Mount Simon /SD/	Vertical	Deeper Pool Wildcat-Dry	Dry And Abandoned
34101200080000	8	H T & M E Mitchell	40.5812733	-83.0028819	1001	988	3672	Dry & Abandoned	1962-02-23	1962-02-13	1962-03-14		United Producing Co Inc	Precambrian	Vertical	Development Well-Dry (Including Temporarily Abandoned Well)	Dry And Abandoned
34005239380000	3938	Fingulin	41.0130000	-82.3923032	1083	1073	5163	1 Oil & 1 Gas Well	1991-12-18	1991-12-08	1993-09-01	2007-11-15	Bass Energy Inc	Granite	Vertical	Deeper Pool Wildcat-Discovery	Oil And Gas
34077202330000	233	Walcher/Gray	41.1185153	-82.5622486	970	955	4445	Dry & Abandoned	1993-03-09	1993-02-27	1993-03-19		Ngo Development Corp	Basement	Vertical	New Field Wildcat-Dry (Including Temporarily Abandoned Well)	Dry And Abandoned
34063201400000	0140	Harris Bessie	40.9367971	-83.5126302	833	824	2798	Dry & Abandoned	1964-05-25	1964-05-01	1964-06-06	2007-01-24	Cowen Michael T	Precambrian	Vertical	New Field Wildcat-Dry (Including Temporarily Abandoned Well)	Dry And Abandoned
34041203290000	329	Case	40.3431858	-83.0600559	919	909	3569	Dry & Abandoned	1985-02-09	1985-01-30	1985-02-20		Funk Exploration Inc	Granite	Vertical	New Field Wildcat-Dry (Including Temporarily Abandoned Well)	Dry And Abandoned
34143202350000	0235	Ohio Liquid Disposal Inc	41.3715003	-82.9823478	616	610	2980	Water Injection	1979-09-10	1979-09-05	1979-09-27		Ohio Liquid Disposal	Precambrian	Vertical	Injection	Water Injector
34173204230000	423	Kramer	41.3425844	-83.6817178		686	2880	Dry & Abandoned-Oil Shows	1984-05-13	1984-05-03	1984-07-20		Anschutz Corp	Precambrian	Vertical	New Field Wildcat-Dry (Including Temporarily Abandoned Well)	Dry And Abandoned
34143201460000	146	E Ray Aleshire	41.3725345	-83.3421852	705	696	2762	Dry & Abandoned-Oil Shows	1965-09-30	1965-09-20	1965-10-04		Maguire Russell	Precambrian	Vertical	Deeper Pool Wildcat-Dry	Dry And Abandoned
34147608400000	0840	M & B Asphalt Co	41.2264537	-83.1988296		696	2870	Observation Well-No Shows	1984-12-17	1984-12-07	1985-01-01		Dnr Geological Survey	Precambrian	Vertical	Unclassified	Service
34117216810000	1681	Shaver-Neff Unit	40.3941940	-82.8700273	1007	994	4215	Oil Producer	1964-06-10	1964-05-31	1964-07-16		Kin-Ark Oil Co	Granite	Vertical	Development Well-Oil	Oil
34159200840000	84	Hutchins	40.3414734	-83.5079286	1079	1070	2765	Dry & Abandoned-Gas Shows	1992-05-09	1992-04-29	1992-05-17		Majestic Oil & Gas Inc	Rome	Vertical	New Field Wildcat-Dry (Including Temporarily Abandoned Well)	Dry And Abandoned
34101201760000	176	Gracely Farms	40.5881499	-83.2551163	926	915	3078	Dry & Abandoned	1984-11-10	1984-10-31	1984-11-18		Texas Gas Exploration Corp	Granite	Vertical	New Field Wildcat-Dry (Including Temporarily Abandoned Well)	Dry And Abandoned
34043200190000	20019	Herman A et Al Unit	41.3110563	-82.3517368	830	820	4466	Salt Water Disposal	1966-09-09	1966-08-30	1967-05-01		Sun Oil Co	Precambrian	Vertical	Injection-Water	Disposal
34039200280000		Pearl A Haver	41.3244444	-84.5939131		715	3609	Dry & Abandoned	1962-10-22	1962-10-12	1963-01-04		Brown S E Trustee	Granite	Vertical	New Field Wildcat-Dry (Including Temporarily Abandoned Well)	Dry And Abandoned

UWI	Permit License Number	Wel Name	Bottomhole Latitude	Bottomhole Longitude	Kelly Bushing Elevation (feet above sea level)	Ground Surface Elevation (feet above sea level)	Max TD	Current Status	Spud Date	Permit License Date	Completion Date	Abandonment Date	Current Operator	Formation at TD	Hole Direction	Current Class	Plot Symbol Description
34091200930000	93	State Of Ohio	40.3039240	-83.5618607	1103	1093	3140	Dry & Abandoned	1985-01-02	1984-12-23	1985-01-11		Texas Gas Exploration Corp	Mount Simon /SD/	Vertical	New Field Wildcat-Dry (Including Temporarily Abandoned Well)	Dry And Abandoned
34117200330000	33	J W Henry	40.4366882	-82.9245091	995	981	4048	Dry & Abandoned	1961-12-17	1961-12-07	1962-01-08		Wehmeyer Karl	Precambrian	Vertical	Development Well-Dry (Including Temporarily Abandoned Well)	Dry And Abandoned
34107201410000		M & M Yewey	40.6316630	-84.5161187		830	3200	Suspended Well					Harner Union Oil	Unknown	Vertical	Suspended Well	Suspended Undesignated
34065200790000	0079	Wolf G W	40.6412534	-83.4841021	971	961	3002	Dry & Abandoned	1963-12-27	1963-12-17	1964-01-07	1964-01-07	McMahon-Bullington Drilling Co	Precambrian	Vertical	New Field Wildcat-Dry (Including Temporarily Abandoned Well)	Dry And Abandoned
34139204310000	431	Scott C D & K	40.6880856	-82.4805076	1448	1430	5503	Dry & Abandoned	1966-08-19	1966-08-09	1966-09-05		Tri-State Production	Precambrian	Vertical	Development Well-Dry (Including Temporarily Abandoned Well)	Dry And Abandoned
34041201260000	126	D Rouse	40.3802606	-82.9920322	974	965	3750	Dry & Abandoned	1964-07-28	1964-07-18	1964-11-14		Atha Howard D	Mount Simon /SD/	Vertical	New Field Wildcat-Dry (Including Temporarily Abandoned Well)	Dry And Abandoned
34175203360000	0336	Hensel	40.7397603	-83.4612210		912	2855	Oil Producer	2001-02-08	2001-02-05	2001-03-04		Mar Oil Co	Mount Simon	Vertical	Development Well-Oil	Oil
34161200440000		A A & M J Miller	40.7573706	-84.3995901	820	807	3242	Dry & Abandoned	1972-04-17	1972-04-07	1972-10-17		West Ohio Gas Co	Basement	Vertical	Development Well-Dry (Including Temporarily Abandoned Well)	Dry And Abandoned
34083240640000	4064	Ernest E	40.2971710	-82.4752453	1010	997	5234	Oil Producer	1994-11-02	1994-10-23	1995-02-15		Knox Energy Inc	Precambrian	Vertical	Development Well-Oil	Oil
34175202580000	258	Brocklesby C	40.8269305	-83.1862896	890	879	3169	Dry & Abandoned	1981-05-21	1981-05-11	1982-01-21		Berea Oil & Gas Corp	Granite	Vertical	New Field Wildcat-Dry (Including Temporarily Abandoned Well)	Dry And Abandoned
34101202070000	207	Forry Evelyn Etal	40.6919879	-83.1998594	913	896	3142	Dry & Abandoned	1997-12-31	1997-12-21	1998-01-06		Equitable Resources Exploration Inc	Mount Simon /SD/	Vertical	New Field Wildcat-Dry (Including Temporarily Abandoned Well)	Dry And Abandoned
34143202250000	225	Ohio Liquid Disposal Inc	41.3684006	-82.9805287	618	610	2960	Salt Water Disposal Oil & Gas Operator	1976-07-01	1976-01-26	1976-11-22		Ohio Liquid Disposal	Basement	Vertical	Injection	Disposal
34083239440000	3944	White Donald	40.2925587	-82.6692599	1212	1201	5024	Temporarily Abandoned - Gas	1991-06-24	1991-06-14	1991-06-30		Petro Evaluation Services	Granite	Vertical	New Field Wildcat-Discovery	Suspended Gas
34101600200000	0020	Strickler & Hanson	40.5981994	-83.1335671		961	1790	Dry & Abandoned	1899-12-17	1899-12-07	1900-01-01		Unknown	Trenton /LM/	Vertical	Development Well-Dry (Including Temporarily Abandoned Well)	Dry And Abandoned
34069200360000		K A Hall	41.3580850	-84.0229270	683	679	3480	Dry & Abandoned	1973-08-22	1973-08-12	1973-10-10		Callander & Kimbrel Inc	Cambrian	Vertical	Deeper Pool Wildcat-Dry	Dry And Abandoned
34083239150000	3915	Donaldson J	40.3101095	-82.5360991	1086	1079	5366	Dry & Abandoned	1990-12-02	1990-11-22	1990-12-18		Edco Drilling & Production	Precambrian	Vertical	New Field Wildcat-Dry (Including Temporarily Abandoned Well)	Dry And Abandoned
34003636910000	3691	Bp Chemical	40.7121144	-84.1304140	871	863	3409	Water Injection					Bp Amoco	Middle Run	Vertical	Injection	Water Injector
34033200440000	44	Spitler-Brown Unit	40.9179629	-83.0632980	977	968	3415	Dry & Abandoned	1965-05-15	1965-05-05	1965-05-30		Piggott G M Jr	Precambrian	Vertical	New Field Wildcat-Dry (Including Temporarily Abandoned Well)	Dry And Abandoned
34159200740000	74	Low	40.2248449	-83.2759002	975	965	3438	Dry & Abandoned	1984-12-27	1984-12-17	1985-01-05		Funk Exploration Inc	Trempealeau	Vertical	New Field Wildcat-Dry (Including Temporarily Abandoned Well)	Dry And Abandoned
34065200740000	74	D & D Jones	40.7505549	-83.5281295	941	929	2834	Dry & Abandoned-Gas Shows	1962-04-02	1962-03-23	1962-04-10		Edmund Norman W	Precambrian	Vertical	Development Well-Dry (Including Temporarily Abandoned Well)	Dry And Abandoned
34101200140000	0014	Key Harry D	40.6323274	-83.0026923		997	2882	Dry & Abandoned	1962-10-23	1962-10-13	1963-11-21		Adams John W	Maynardville	Vertical	Development Well-Dry (Including Temporarily Abandoned Well)	Dry And Abandoned
34159200700000	70	Kindig G M	40.3008828	-83.2757085	962	951	3353	Dry & Abandoned	1984-08-17	1984-08-07	1984-08-26		Funk Exploration Inc	Mount Simon /SD/	Vertical	New Field Wildcat-Dry (Including Temporarily Abandoned Well)	Dry And Abandoned
34175201740000	174	M E Bowen	40.7875872	-83.3343943		837	2902	Dry & Abandoned	1964-02-21	1964-02-11	1964-04-30		Texaco Inc	Precambrian	Vertical	Development Well-Dry (Including Temporarily Abandoned Well)	Dry And Abandoned
34117200120000	12	O & E Myers	40.5702510	-82.9119183		1007	4100	Abandoned Oil Producer	1961-07-06	1961-06-26	1961-07-28	1967-09-05	Ashland Oil Inc	Unknown	Vertical	Development Well-Oil	Abandoned Oil
34083239550000	3955	Parkinson	40.2499999	-82.4736965	1060	1050	4933	Oil Producer	1991-09-26	1991-09-16	1991-12-17		Maram Energy	Rome	Vertical	Development Well-Oil	Oil
34101201750000	175	Wenig George D et Ux	40.6383270	-83.3418085	909	899	2935	Dry & Abandoned	1985-01-14	1985-01-04	1986-08-15		Delray Oil Inc	Mount Simon /SD/	Vertical	New Field Wildcat-Dry (Including Temporarily Abandoned Well)	Dry And Abandoned
34175202110000	211	George Eyestone	40.8955690	-83.1209850		935	3260	Dry & Abandoned	1965-10-04	1965-09-24	1965-10-11		Minnesota Ohio Oil	Precambrian	Vertical	New Field Wildcat-Dry (Including Temporarily Abandoned Well)	Dry And Abandoned
34143202100000	210	Ohio Liquid Disposal	41.3712186	-82.9812707	620	614	2933	Dry & Abandoned	1972-03-02	1972-02-21	1972-03-17		Ohio Liquid Disposal	Precambrian	Vertical	Stratigraphic/Structure Test Hole	Dry And Abandoned
34101600220000	0022	Coulter Chas	40.6696536	-82.9782447		997		Dry & Abandoned					Unknown	Trenton /LM/	Vertical	Development Well-Dry (Including Temporarily Abandoned Well)	Dry And Abandoned
34091200180000		Virgil Johns Etal	40.4561775	-83.7716569		1161	3361	Dry & Abandoned	1947-05-21	1947-05-11	1947-07-09		Marathon Oil Co	Unknown	Vertical	Development Well-Dry (Including Temporarily Abandoned Well)	Dry And Abandoned
34117225500000	2550	J&J Irey	40.5882462	-82.9506825	1004	991	3876	Dry & Abandoned	1965-05-29	1965-05-19	1965-06-11		Otter Creek Exploration	Unknown	Vertical	Deeper Pool Wildcat-Dry	Dry And Abandoned
34173202360000	236	Smith V Ruth	41.4286015	-83.6612141	677	673	2786	Dry & Abandoned-Oil Shows	1964-12-23	1964-12-13	1965-02-10	1965-02-10	Kin-Ark Oil Co	Granite	Vertical	New Field Wildcat-Dry (Including Temporarily Abandoned Well)	Dry And Abandoned
34101200850000	0085	Parish L B & M D	40.6148829	-83.4189583		971	2985	Dry & Abandoned	1964-10-08	1964-09-28	1964-12-04	1964-12-12	Unknown	Precambrian	Vertical	New Field Wildcat-Dry (Including Temporarily Abandoned Well)	Dry And Abandoned
34147202110000	211	Shults Howard R	41.1900365	-83.1864420	723	709	2847	Temporarily Abandoned - Oil	1979-01-23	1979-01-13	1979-01-31		A & S Energy LLC	Basement	Vertical	Development Well-Oil	Suspended Undesignated
34041200980000	98	Russell Cryder	40.2867676	-83.1170370		942	3507	Dry & Abandoned	1964-06-22	1964-06-12	1964-07-06		Eastern Drilling	Cambrian Lower /Series/	Vertical	New Field Wildcat-Dry (Including Temporarily Abandoned Well)	Dry And Abandoned
34011200710000		Hoelscher 1 Comm	40.5038322	-84.3944028		883	3067	Suspended Well					West Ohio Gas Co	Unknown	Vertical	Suspended Well	Suspended Undesignated
34147201280000	128	Wella R Stigamire	41.1817740	-83.0566553		787	3175	Dry & Abandoned	1965-01-04	1964-12-25	1965-01-26		Ashland Oil Inc	Precambrian	Vertical	New Field Wildcat-Dry (Including Temporarily Abandoned Well)	Dry And Abandoned

UWI	Permit License Number	Wel Name	Bottomhole Latitude	Bottomhole Longitude	Kelly Bushing Elevation (feet above sea level)	Ground Surface Elevation (feet above sea level)	Max TD	Current Status	Spud Date	Permit License Date	Completion Date	Abandonment Date	Current Operator	Formation at TD	Hole Direction	Current Class	Plot Symbol Description
34101201730000	173	Oehler	40.5993014	-83.3742447	976	965	2989	Dry & Abandoned	1984-11-18	1984-11-08	1984-11-26		Texas Gas Exploration Corp	Rome	Vertical	New Field Wildcat-Dry (Including Temporarily Abandoned Well)	Dry And Abandoned
34063201390000	0139	Frazier C & M	40.9369635	-83.7685919		827	3017	Dry & Abandoned	1964-04-27	1964-04-24	1964-06-02	1964-06-04	Dever Frank M	Middle Run	Vertical	New Field Wildcat-Dry (Including Temporarily Abandoned Well)	Dry And Abandoned
34117240120000	4012	Morris L & R	40.5685695	-82.6971418	1331	1316	3936	Oil Producer	1991-02-27	1991-02-17	1991-04-12		Maram Energy	Trempealeau	Vertical	Development Well-Oil	Oil
34091200870000	87	Earnest Hemleben	40.3858632	-83.6739143	1364	1365	3276	Suspended Well	1976-05-16	1976-05-06			Worthington Oil	Mount Simon /SD/	Vertical	Suspended Well	Suspended Undesignated
34143202370000	0237	Ohio Liquid Disposal Inc	41.3715824	-82.9908852	618	610	2943	Water Injection	1980-11-01	1980-06-11	1980-11-16		Ohio Liquid Disposal	Precambrian	Vertical	Injection	Water Injector
34159200690000	69	Yoder	40.2276614	-83.2653682	971	958	3505	Dry & Abandoned	1984-08-09	1984-07-30	1984-08-17		Funk Exploration Inc	Granite	Vertical	New Field Wildcat-Dry (Including Temporarily Abandoned Well)	Dry And Abandoned
34063203600000	20360	Knox High	41.1676796	-83.8051319	729	715	2992	Dry & Abandoned	2018-03-30	2018-02-02	2019-11-06		Hilcorp Energy Co	Black River /LM/	Vertical	Development Well-Dry (Including Temporarily Abandoned Well)	Dry And Abandoned
34117241900000	4190	Lee Family Trust	40.5652210	-82.8983607	1028	1020	4200	Dry & Abandoned	2007-02-03	2007-01-30	2007-02-18		Knox Energy Inc	Precambrian	Vertical	Development Well-Dry (Including Temporarily Abandoned Well)	Dry And Abandoned
34159200670000	67	Graver J & B	40.2494120	-83.2760066	966	955	3446	Dry & Abandoned	1984-07-29	1984-07-19	1984-08-08		Funk Exploration Inc	Granite	Vertical	New Field Wildcat-Dry (Including Temporarily Abandoned Well)	Dry And Abandoned
34101201650000	165	McNamara John & Sarah	40.5138357	-83.0498038	965	958	3657	Dry & Abandoned	1984-08-07	1984-07-28	1987-12-22		Double D Well Service	Mount Simon /SD/	Vertical	New Field Wildcat-Dry (Including Temporarily Abandoned Well)	Dry And Abandoned
34139206780000	678	Copperweld Shelby Division	40.8742519	-82.6728873	1100	1099	4113	Abandoned Gas Producer	1993-09-21	1993-09-11	1993-10-01	1995-05-08	Copperweld Energy	Kerbel	Vertical	New Field Wildcat-Discovery	Abandoned Gas
34093207940000	794	Born A & A	41.2894675	-82.3204912		847	4590	Dry & Abandoned-Oil Shows	1960-07-15	1960-07-05	1960-11-14		East Ohio Gas Co, The	Precambrian	Vertical	Development Well-Dry (Including Temporarily Abandoned Well)	Dry And Abandoned
34117200470000	47	A C Windbigler	40.6905103	-82.6813541	1398	1388	4891	Abandoned Gas Producer	1962-10-01	1962-09-21	1962-11-02	1970-12-04	Pan American	Granite	Vertical	Development Well-Gas	Abandoned Gas
34159200130000	13	Ralph & Alta Lane	40.4654762	-83.4032390	1003	994	2989	Dry & Abandoned	1964-07-11	1964-07-01	1964-07-28		T & W Oil Co	Precambrian	Vertical	New Field Wildcat-Dry (Including Temporarily Abandoned Well)	Dry And Abandoned
34083240000000	4000	McCoy	40.2714749	-82.4602501	987	978	5216	Oil Producer	2007-05-21	1992-09-10	2007-07-18		Knox Energy Inc	Precambrian	Vertical	New Field Wildcat-Discovery	Oil
34101201670000	167	Herr John F	40.6446413	-83.3417084	905	892	2934	Dry & Abandoned	1984-04-25	1984-04-15	1984-05-05		Delray Oil Inc	Granite	Vertical	New Field Wildcat-Dry (Including Temporarily Abandoned Well)	Dry And Abandoned
34175201730000	173	Isodore Frey	40.8184779	-83.4131473		863	2875	Dry & Abandoned	1964-01-02	1963-12-23	1964-02-01		Comanche Oil Co	Trempealeau Sd	Vertical	New Field Wildcat-Dry (Including Temporarily Abandoned Well)	Dry And Abandoned
34063201520000		Jesse Drummelsmith	40.9855418	-83.6392618	809	801	2807	Dry & Abandoned-Oil & Gas Shows	1966-07-03	1966-06-23	1966-07-13		Kin-Ark Oil Co	Granite	Vertical	Deeper Pool Wildcat-Dry	Dry And Abandoned
34147202120000	212	Watson John W	41.1581965	-83.1841853	741	732	2859	Dry & Abandoned	1979-02-11	1979-02-01	1979-02-24		A & S Energy LLC	Precambrian	Vertical	Deeper Pool Wildcat-Dry	Dry And Abandoned
34083214680000	1468	Gerald D Larimore	40.3256659	-82.5644442		1194	5376	Dry & Abandoned-Gas Shows	1962-12-01	1962-11-21	1963-01-09		Ohio Fuel Gas	Basal/SD/	Vertical	Development Well-Dry (Including Temporarily Abandoned Well)	Dry And Abandoned
34117238500000	3850	Hershner	40.5881176	-82.8270012	1166	1158	4300	Dry & Abandoned	1988-06-21	1988-06-11	1988-06-29		United Operating Co	Mount Simon /SD/	Vertical	Deeper Pool Wildcat-Dry	Dry And Abandoned
34147202160000	216	Watson John W	41.1521605	-83.1837594	760	742	2796	Oil Producer	1979-09-15	1979-09-05	1979-10-17		A & S Energy LLC	Precambrian	Vertical	Development Well-Oil	Oil
34117219350000	1935	E-V Bush	40.5173965	-82.9575862	999	988	3867	Dry & Abandoned-Oil Shows	1964-08-06	1964-07-27	1964-08-22		Comanche Oil Co	Granite	Vertical	New Field Wildcat-Dry (Including Temporarily Abandoned Well)	Dry And Abandoned
34089220570000	2057	H-M Roberts	40.2332768	-82.7155645	1178	1168	4952	Dry & Abandoned	1964-01-29	1964-01-19	1964-02-29		Atha Howard D	Precambrian	Vertical	New Field Wildcat-Dry (Including Temporarily Abandoned Well)	Dry And Abandoned
34117242540000	24254	Bush	40.5731586	-82.9038007	1030	1014	2952	Oil Producer	2012-12-14	2012-12-04	2013-02-04		Salamanca Energy LLC	Trempealeau	Vertical	Development Well-Oil	Oil
34143203120000	312	Weickert B T Unit	41.4213676	-83.1039396	591	584	2773	Gas Producer	2009-06-25	2009-06-15	2009-09-01		Fo Energy LLC	Mount Simon	Vertical	Development Well-Gas	Gas
34077201030000	103	Wolf Unit	41.2736652	-82.3436367	856	847	4574	Dry & Abandoned	1981-09-26	1981-09-16	1982-10-22		Appalachian Exploration LLC	Precambrian	Vertical	New Field Wildcat-Dry (Including Temporarily Abandoned Well)	Dry And Abandoned
34143202380000	238	Oil Liquid Disposal Inc	41.3733236	-82.9853559		604	2955	Salt Water Disposal Oil & Gas Operator	1980-11-18	1980-05-02	1980-11-26		Ohio Liquid Disposal	Basement	Vertical	Injection	Disposal
34033200040000	0004	White G	40.7040808	-83.1062714		951	2532	Dry & Abandoned	1961-10-12	1961-10-02	1961-11-07	1961-11-13	Reliance Oil Corp	Trempealeau	Vertical	New Field Wildcat-Dry (Including Temporarily Abandoned Well)	Dry And Abandoned
34101200030000	0003	Baker Stanley W	40.6274717	-83.0294239		988	2711	Dry & Abandoned	1954-04-28	1954-04-18	1954-06-02	1954-06-05	White	Unknown	Vertical	Development Well-Dry (Including Temporarily Abandoned Well)	Dry And Abandoned
34143202260000	226	Ohio Liquid Disposal Inc	41.3687776	-82.9769386	618	607	2910	Salt Water Disposal Oil & Gas Operator	1976-07-15	1976-01-26	1976-11-25		Ohio Liquid Disposal	Basement	Vertical	Injection	Disposal
34083239310000	3931	Carter James D	40.2904339	-82.4853310	1032	1020	5111	Dry & Abandoned-Gas Shows	1991-04-17	1991-04-07	1991-04-26		B & J Drilling Co	Mount Simon /SD/	Vertical	Deeper Pool Wildcat-Dry	Dry And Abandoned
34117213880000	1388	J-B McBee	40.3561830	-82.8228123	1140	1135	4450	Dry & Abandoned	1964-03-19	1964-03-09	1964-04-20		Wray Robert	Precambrian	Vertical	New Field Wildcat-Dry (Including Temporarily Abandoned Well)	Dry And Abandoned
34101200490000	49	F L Gruber	40.5664459	-83.0508906	981	974	3459	Dry & Abandoned	1964-05-02	1964-04-22	1964-06-16		Midland Drilling	Precambrian	Vertical	New Field Wildcat-Dry (Including Temporarily Abandoned Well)	Dry And Abandoned
34101201740000	174	Gracely Farms	40.5870922	-83.2277396	916	909	3198	Dry & Abandoned	1984-11-02	1984-10-23	1984-11-08		Texas Gas Exploration Corp	Granite	Vertical	New Field Wildcat-Dry (Including Temporarily Abandoned Well)	Dry And Abandoned
34139204480000	448	Empre Reves Stl Div	40.7789409	-82.5192094	1176	1168	5085	Dry & Abandoned	1967-07-27	1967-07-17	1967-08-18		Empire Reeves Steel Div	Precambrian	Vertical	Development Well-Dry (Including Temporarily Abandoned Well)	Dry And Abandoned
34083239770000	3977	Miller	40.4406071	-82.6124067	1128	1116	4506	Abandoned Gas Producer	1992-05-27	1992-05-17	1992-06-06	1993-04-29	Dalton & Hanna Co	Rome	Vertical	New Field Wildcat-Discovery	Abandoned Gas

UWI	Permit License Number	Wel Name	Bottomhole Latitude	Bottomhole Longitude	Kelly Bushing Elevation (feet above sea level)	Ground Surface Elevation (feet above sea level)	Max TD	Current Status	Spud Date	Permit License Date	Completion Date	Abandonment Date	Current Operator	Formation at TD	Hole Direction	Current Class	Plot Symbol Description
34143201470000	147	Paul L Kerbel	41.4377145	-83.3162147	647	637	2785	Dry & Abandoned	1965-11-24	1965-11-14	1965-11-30		Maguire Russell	Granite	Vertical	New Field Wildcat-Dry (Including Temporarily Abandoned Well)	Dry And Abandoned
34091200960000	96	Prinkey R Unit	40.4135902	-83.6164695	1125	1122	3260	Dry & Abandoned-Oil & Gas Shows	1991-10-29	1991-10-19	1991-11-06		Ashtola Exploration Co Inc	Granite	Vertical	New Field Wildcat-Dry (Including Temporarily Abandoned Well)	Dry And Abandoned
34041203220000	322	Jolliff	40.3513067	-83.2260640	933	922	3382	Dry & Abandoned	1985-01-09	1984-12-30	1985-01-19		Funk Exploration Inc	Granite	Vertical	New Field Wildcat-Dry (Including Temporarily Abandoned Well)	Dry And Abandoned
34063202320000	232	Holman W & S	41.0998422	-83.4772431		810	2525	Dry & Abandoned	1981-09-03	1981-08-24	1982-11-19		Belden & Blake & Co	Mount Simon	Vertical	New Field Wildcat-Dry (Including Temporarily Abandoned Well)	Dry And Abandoned
34143202240000	224	Ohio Liquid Disposal Inc	41.3711966	-82.9833068	618	607	2961	Salt Water Disposal Oil & Gas Operator	1976-06-17	1976-01-26	1976-11-24		Ohio Liquid Disposal	Basement	Vertical	Injection	Disposal
34091200860000	86	Comer Lena	40.3439842	-83.6347888	1439	1437	3402	Dry & Abandoned	1976-04-28	1976-04-18	1976-05-12		Worthington Oil	Mount Simon /SD/	Vertical	New Field Wildcat-Dry (Including Temporarily Abandoned Well)	Dry And Abandoned
34101201680000	168	Gracely Farms	40.5863717	-83.2541960	924	915	3074	Dry & Abandoned	1984-06-12	1984-06-02	1984-06-20		Anschutz Corp	Granite	Vertical	New Field Wildcat-Dry (Including Temporarily Abandoned Well)	Dry And Abandoned
34173202390000	0239	Asmusclarence Etal	41.4610772	-83.7111862	670	659	2825	Dry & Abandoned	1965-05-10	1965-04-30	1965-05-25	1965-05-26	J R S Co	Precambrian	Vertical	New Field Wildcat-Dry (Including Temporarily Abandoned Well)	Dry And Abandoned
34065201330000	133	Fewell	40.7517413	-83.5415305	934	925	2928	Dry & Abandoned-Oil Shows	1997-03-14	1997-03-04	1997-03-21	1999-11-17	Knox Energy Inc	Precambrian	Vertical	Deeper Pool Wildcat-Dry	Dry And Abandoned
34083214130000	1413	E E Cunningham	40.5199086	-82.3873072	1253	1253	5747	Dry & Abandoned-Oil & Gas Shows	1961-07-10	1961-06-30	1961-08-07		Cantway David L	Granite	Vertical	New Field Wildcat-Dry (Including Temporarily Abandoned Well)	Dry And Abandoned
34159200250000	25	George A Beeson	40.2901574	-83.3848298	1027	1017	3187	Dry & Abandoned	1964-07-30	1964-07-20	1964-08-16		Branoco Of Ohio	Mount Simon /SD/	Vertical	New Field Wildcat-Dry (Including Temporarily Abandoned Well)	Dry And Abandoned
34043201540000	154	Baum Elton	41.3626514	-82.7610645	735	722	3394	Dry & Abandoned	1991-07-05	1991-06-25	1991-07-14		Peninsula Group	Mount Simon /SD/	Vertical	New Field Wildcat-Dry (Including Temporarily Abandoned Well)	Dry And Abandoned
34091200910000	91	Robson Kerman et Ux	40.3819275	-83.5864357		1096	3013	Dry & Abandoned-Gas Shows	1980-01-05	1979-12-26	1980-03-10		Allerton Resources	Mount Simon /SD/	Vertical	New Field Wildcat-Dry (Including Temporarily Abandoned Well)	Dry And Abandoned
34147202130000	213	Sendelbach Nancy M	41.1595775	-83.2553844	769	755	2610	Temporarily Abandoned - Oil	1979-08-30	1979-08-20	1979-10-10		A & S Energy LLC	Basement	Vertical	Development Well-Oil	Suspended Undesignated
34117240430000	4043	Hickok E & F	40.6052484	-82.7231822	1398	1394	4707	Dry & Abandoned-Oil & Gas Shows	1991-08-28	1991-08-18	1991-10-23		Eei Inc	Granite	Vertical	Deeper Pool Wildcat-Dry	Dry And Abandoned
34041200220000	22	F Jones	40.3699741	-83.1556842	945	932	3426	Dry & Abandoned	1963-12-30	1963-12-20	1964-01-16		Southern Triangle Oil Co	Precambrian	Vertical	New Field Wildcat-Dry (Including Temporarily Abandoned Well)	Dry And Abandoned
34063202330000	233	Rader M & P	41.0928775	-83.4333104		824	2410	Dry & Abandoned	1981-08-21	1981-08-11	1982-11-08		Belden & Blake & Co	Mount Simon	Vertical	New Field Wildcat-Dry (Including Temporarily Abandoned Well)	Dry And Abandoned
34137200310000	0031	Barlage Louis	41.0954422	-84.0894263		738	3377	Dry & Abandoned	1943-12-17	1943-12-07	1944-03-21		Ohio Oil Co	Precambrian	Vertical	Development Well-Dry (Including Temporarily Abandoned Well)	Dry And Abandoned
34043200110000	11	Krysik-Wakefield	41.3036450	-82.3506625	828	824	4463	Oil Producer	1966-05-11	1966-05-01	1966-06-24		Franklin Gas & Oil Co LLC	Precambrian	Vertical	New Field Wildcat-Discovery	Oil
34033200500000	50	Leonhardt V E	40.9099887	-82.8834086	1008	997	3775	Dry & Abandoned	1965-09-30	1965-09-20	1965-10-12		Fishburn Producing	Trempealeau	Vertical	New Field Wildcat-Dry (Including Temporarily Abandoned Well)	Dry And Abandoned
34043200070000	7	M P Sayler	41.3024566	-82.3985275		814	4424	Dry & Abandoned-Gas Shows	1960-01-01	1959-12-22	1960-10-15		East Ohio Gas Co, The	Granite Wash	Vertical	New Field Wildcat-Dry (Including Temporarily Abandoned Well)	Dry And Abandoned
34089258170000	5817	Dager J	40.2319482	-82.4590194	958	948	4972	Gas Producer	2006-05-24	2006-05-18	2006-06-20		Knox Energy Inc	Precambrian	Vertical	Development Well-Gas	Gas
34083240170000	4017	Ernest Unit	40.2958391	-82.4721019	1003	994	5238	Oil Producer	1993-04-12	1993-04-02	1993-06-14		Knox Energy Inc	Mount Simon /SD/	Vertical	Development Well-Oil	Oil

18. Appendix 1C-Seismic Events

Earthquakes recorded by USGS within 100 miles of the Stonewell Project (USGS, 2025). (mw=moment magnitude scale, mwr=regional moment magnitude, mb=body wave magnitude, md=duration magnitude, lg=surface wave magnitude, mfa=mantle faulting assessment magnitude, mb_lg=combines both body wave magnitude and surface wave magnitude.)

Date	Latitude	Longitude	Depth (km)	Magnitude	Magnitude Type	Place
12/29/2024	41.28030	-84.75650	9.48	2.90	mb_lg	1 km SSE of Hicksville, Ohio
4/22/2024	41.54950	-83.47510	9.47	2.30	mb_lg	4 km SSE of Walbridge, Ohio
3/18/2024	41.54910	-83.46890	5.61	2.50	mb_lg	4 km WSW of Millbury, Ohio
12/9/2023	40.43220	-84.10840	6.79	2.90	mwr	5 km W of Jackson Center, Ohio
5/20/2023	41.55290	-83.48340	6.10	2.60	mb_lg	3 km SSE of Walbridge, Ohio
1/2/2023	40.24450	-84.51333	8.62	2.43	md	3 km NW of Versailles, Ohio
12/22/2022	41.10900	-83.45300	9.91	2.40	mb_lg	5 km E of Arcadia, Ohio
7/11/2022	41.81580	-83.51230	5.00	2.40	ml	5 km W of Luna Pier, Michigan
3/20/2022	39.27117	-83.48683	8.46	2.35	md	8 km N of Highland Holiday, Ohio
1/22/2021	40.72250	-84.14270	5.61	2.40	mb_lg	3 km SW of Lima, Ohio
8/21/2020	41.91250	-83.31790	9.20	3.20	mwr	2 km SSE of Detroit Beach, Michigan
7/14/2020	40.41650	-84.08760	9.78	2.30	mb_lg	Ohio
7/14/2020	40.44030	-84.08650	9.64	1.80	ml	3 km W of Jackson Center, Ohio
3/6/2019	41.45920	-81.65290	5.00	2.00	ml	1 km NE of Newburgh Heights, Ohio
2/7/2016	41.65030	-82.89690	5.00	2.50	ml	6 km W of Put-in-Bay, Ohio
6/12/2015	40.95500	-84.76200	5.00	2.60	mb_lg	6 km NW of Convoy, Ohio
1/20/2014	41.40830	-81.90560	13.00	2.10	md	1 km ESE of North Olmsted, Ohio
11/20/2013	39.44500	-82.20500	8.00	3.50	mb_lg	2 km SW of Buchtel, Ohio
9/7/2012	41.86400	-83.07600	5.10	2.50	mblg	17 km ESE of Stony Point, Michigan
6/5/2011	41.03000	-82.08000	5.00	3.00	mblg	5 km W of Lodi, Ohio
4/26/2011	40.86000	-83.54000	5.00	2.40	mblg	4 km SSE of Mount Blanchard, Ohio
5/17/2010	41.24000	-81.51000	5.00	2.70	mblg	2 km S of Boston Heights, Ohio
5/14/2010	41.39000	-83.30000	5.00	2.70	mblg	1 km ENE of Gibsonburg, Ohio
2/25/2010	41.22000	-83.29000	5.00	2.40	mblg	2 km S of Kansas, Ohio
9/30/2008	40.41000	-84.31000	5.00	2.80	mblg	5 km SW of Kettlersville, Ohio
4/12/2007	41.72200	-82.92400	5.00	2.80	mblg	11 km NW of Put-in-Bay, Ohio
8/15/2006	40.71000	-84.11000	5.00	2.50	mblg	3 km NE of Fort Shawnee, Ohio

Date	Latitude	Longitude	Depth (km)	Magnitude	Magnitude Type	Place
5/12/2006	40.74000	-84.08000	5.00	2.80	mblg	2 km E of Lima, Ohio
3/13/2005	40.67000	-84.62000	5.00	2.20	mblg	2 km SE of Rockford, Ohio
1/30/2004	40.67000	-84.65000	5.00	2.50	mblg	2 km S of Rockford, Ohio
11/25/1998	41.07100	-82.40500	5.00	2.70	mblg	1 km SSW of New London, Ohio
4/4/1994	40.40000	-84.40000	5.00	2.90	mblg	2 km WNW of Minster, Ohio
6/4/1990	41.09800	-83.63800	5.00	2.50	mblg	4 km SSE of Van Buren, Ohio
4/17/1990	40.46000	-84.85200	5.00	3.00	mblg	8 km NW of Fort Recovery, Ohio
7/12/1986	40.53700	-84.37100	10.00	4.50	mb	1 km ESE of Saint Marys, Ohio
1/14/1984	41.64500	-83.42700	5.00	2.50	md	4 km E of Oregon, Ohio
8/20/1980	41.94100	-83.01000	5.00	3.20		19 km SSE of Amherstburg, Canada
6/17/1977	40.70700	-84.58200	5.00	3.20		5 km ENE of Rockford, Ohio
2/2/1976	41.96000	-82.67000	10.00	3.40	lg	11 km SSW of Leamington, Canada
9/29/1974	41.23800	-83.36100	1.00	3.00	lg	6 km ESE of Risingsun, Ohio
6/20/1952	39.64000	-82.02300	9.00	4.00	fa	6 km ENE of Rendville, Ohio
3/9/1937	40.47000	-84.28000	3.00	5.40	fa	3 km NNW of Kettlersville, Ohio
3/2/1937	40.48800	-84.27300	2.00	5.00	fa	3 km E of New Knoxville, Ohio
9/20/1931	40.42900	-84.27000	5.00	4.70	fa	1 km SSW of Kettlersville, Ohio
9/30/1930	40.30000	-84.30000	0.00	4.20	fa	5 km E of Newport, Ohio
9/19/1884	40.70000	-84.10000	0.00	4.80	mfa	Near Lima, Ohio
2/9/1882	40.40000	-84.20000	0.00	3.10	mfa	Near Anna, Ohio
6/18/1875	40.20000	-84.00000	0.00	4.70	mfa	Western Ohio
2/8/1812	39.40000	-84.10000	0.00	4.40	mw	Northeast of Cincinnati, Ohio

Earthquakes recorded by OH Seismic Network within 100 miles of the Stonewell Project (OhioSeis, 2025)

Latitude	Longitude	Year	Month	Day	Depth (km)	Magnitude	County
39.60000	-84.30000	1834	Nov	20	0	3.5	Montgomery
41.50000	-81.70000	1836	Jul	9	0	3.1	Cuyahoga
40.10000	-83.80000	1843	Jun	19	0	3.5	Champaign
39.65000	-82.53000	1848	Apr	6	0	3.7	Fairfield
39.40000	-83.70000	1854	Jan	11	0	3.5	Clinton
39.71000	-82.60000	1870	Jan	16	0	2.9	Fairfield
40.20000	-83.00000	1873	Jan	4	0	3.8	Delaware
39.70000	-84.20000	1873	Apr	23	0	3	Montgomery
40.20000	-84.00000	1875	Jun	18	0	4.7	Champaign
40.40000	-84.20000	1876	Jun	0	0	3.4	Shelby
40.40000	-84.20000	1882	Feb	9	0	3.1	Shelby
41.35000	-82.10000	1883	Jan	5	0	3	Lorain
40.40000	-84.20000	1884	Dec	23	0	2.9	Shelby
41.15000	-81.55000	1885	Jan	18	0	3.8	Summit
40.97000	-81.70000	1886	Sep	11	0	3.1	Wayne
41.49000	-81.69000	1888	Feb	9	0	3.3	Cuyahoga
41.00000	-81.50000	1888	Feb	11	0	3.4	Summit
40.40000	-84.20000	1889	Sep	0	0	2.9	Shelby
40.55000	-84.57000	1892	Apr	15	0	3.8	Mercer
40.30000	-84.20000	1896	Mar	15	0	3.1	Shelby
41.49000	-81.69000	1898	Oct	29	0	2.9	Cuyahoga
41.17000	-82.12000	1899	Sep	14	0	3.3	Lorain
39.30000	-83.00000	1899	Nov	12	0	3.1	Ross
41.50000	-81.70000	1906	Apr	20	0	2.9	Cuyahoga
39.80000	-83.90000	1925	Mar	27	0	3.4	Greene
40.40000	-84.20000	1925	Oct	0	0	2.9	Shelby
41.70000	-83.60000	1926	Oct	28	0	3.4	Lucas
41.70000	-83.60000	1926	Oct	28	0	3.1	Lucas
40.70000	-82.50000	1927	Feb	17	0	3.1	Richland
40.70000	-82.50000	1927	Feb	17	0	2.5	Richland
40.40000	-84.10000	1928	Oct	27	0	3	Shelby
40.40000	-84.20000	1929	Mar	8	0	3.7	Shelby
41.50000	-81.70000	1929	Jun	10	0	2.9	Cuyahoga
40.50000	-84.00000	1930	Jun	26	0	3.2	Auglaize
40.50000	-84.00000	1930	Jun	27	0	3.1	Auglaize
40.60000	-83.20000	1930	Jul	11	0	3.1	Marion
40.30000	-84.20000	1930	Sep	29	0	2.9	Shelby
40.30000	-84.30000	1930	Sep	30	0	4.2	Shelby

Latitude	Longitude	Year	Month	Day	Depth (km)	Magnitude	County
40.40000	-84.20000	1931	Mar	21	0	3	Shelby
40.40000	-84.00000	1931	Apr	1	0	2.9	Logan
40.43000	-84.27000	1931	Sep	20	0	4.7	Shelby
40.40000	-84.20000	1931	Oct	9	0	2.9	Shelby
40.40000	-84.20000	1933	Feb	23	0	3.3	Shelby
41.20000	-83.20000	1936	Jan	31	0	3.1	Seneca
41.20000	-83.20000	1936	Jan	31	0	2.5	Seneca
40.49000	-84.27000	1937	Mar	2	0	4.9	Auglaize
40.70000	-84.00000	1937	Mar	3	0	3.2	Allen
40.70000	-84.00000	1937	Mar	3	0	2.9	Allen
40.47000	-84.28000	1937	Mar	9	0	5.4	Shelby
40.70000	-84.00000	1937	Apr	23	0	3.1	Allen
40.70000	-84.00000	1937	Apr	27	0	3.1	Allen
40.70000	-84.00000	1937	May	2	0	3.1	Allen
40.40000	-84.00000	1939	Mar	18	0	2.5	Shelby
40.40000	-84.00000	1939	Mar	18	0	3.3	Shelby
40.30000	-84.00000	1939	Jun	18	0	3.1	Logan
40.30000	-84.00000	1939	Jul	9	0	2.5	Logan
40.90000	-82.30000	1940	Jun	16	0	3.1	Ashland
40.90000	-82.30000	1940	Jul	28	0	2.9	Ashland
40.90000	-82.30000	1940	Aug	15	0	2.9	Ashland
40.90000	-82.30000	1940	Aug	20	0	2.9	Ashland
40.40000	-84.40000	1944	Nov	13	0	4.1	Auglaize
41.70000	-83.60000	1948	Jan	18	0	2.9	Lucas
39.80000	-84.20000	1950	Apr	20	0	3.1	Montgomery
39.64000	-82.02000	1952	Jun	20	0	3.9	Morgan
39.70000	-82.10000	1953	May	7	0	2.7	Perry
41.70000	-83.60000	1953	Jun	12	0	3.5	Lucas
41.29000	-81.57000	1955	May	26	0	3.3	Cuyahoga
40.50000	-84.00000	1956	Jan	27	0	3.7	Logan
40.40000	-84.20000	1956	Jan	27	0	3.7	Shelby
41.20000	-83.30000	1961	Feb	22	0	3.7	Seneca
39.65000	-82.53000	1967	Apr	8	0	3.7	Fairfield
41.30000	-83.20000	1975	Feb	3	0	3.3	Sandusky
41.40000	-83.50000	1992	Oct	4	0	2.5	Wood
40.70000	-84.10000	1884	Sep	19	0	4.8	Allen
40.20000	-81.90000	1776	0	0	0	4.5	Coshocton
40.20000	-81.90000	1779	Feb	3	0	2.9	Coshocton
40.42000	-84.11000	1980	Jul	10	0	0.9	Shelby
40.43000	-84.09000	1980	Sep	26	0	0.5	Shelby

Latitude	Longitude	Year	Month	Day	Depth (km)	Magnitude	County
40.43000	-84.11000	1980	Dec	10	0	1.2	Shelby
40.42000	-84.10000	1981	Jan	4	0	1.8	Shelby
40.44000	-84.11000	1981	Feb	7	0	1.8	Shelby
41.05000	-84.32000	1981	Mar	15	0	1.2	Putnam
40.88000	-84.34000	1981	May	15	0	0.8	Putnam
40.42000	-84.10000	1981	May	19	0	1.2	Shelby
40.43000	-84.10000	1983	Jul	12	0	1.2	Shelby
41.59000	-84.39000	1983	Sep	30	0	1.2	Williams
40.43000	-84.10000	1983	Nov	4	0	0.3	Shelby
40.43000	-84.10000	1983	Nov	4	0	0.7	Shelby
41.70000	-83.50000	1983	Dec	7	0	2	Lucas
40.52000	-84.39000	1985	Mar	10	0	1.4	Auglaize
40.52000	-84.40000	1985	Mar	10	0	1.7	Auglaize
39.65000	-83.46000	1985	Mar	17	0	1.9	Fayette
40.97000	-84.22000	1985	Aug	25	0	1.5	Putnam
40.43000	-84.18000	1968	Jul	26	0	3	Shelby
41.21000	-83.49000	1974	Sep	29	0	3	Wood
40.57000	-84.67000	1977	Jun	17	0	3.3	Mercer
39.80000	-83.75000	1980	Oct	4	0	2	Clark
40.43000	-84.10000	1983	Jul	5	0	2.1	Shelby
41.67000	-83.45000	1984	Jan	14	0	2.6	Lucas
40.55000	-84.39000	1986	Jul	12	10	4.5	Auglaize
40.45000	-84.11000	1988	Oct	22	0	2.2	Shelby
41.08000	-83.51000	1990	Jun	4	0	2.3	Hancock
41.18000	-83.68000	1992	Jul	4	0	2	Wood
41.18000	-83.68000	1992	Jul	14	0	2	Wood
41.65000	-83.50000	1993	Oct	10	0	2	Lucas
41.40000	-83.50000	1993	Nov	9	0	2	Wood
40.40000	-84.00000	1994	Apr	4	0	2.9	Logan
40.80000	-82.68000	1995	Jan	12	0	3.3	Richland
41.02000	-82.54000	1998	Nov	25	5	3.2	Huron
41.01000	-82.55000	2001	Jul	26	5	2.7	Huron
41.15000	-81.46000	1998	Dec	25	18	2.8	Summit
40.67000	-84.62000	2004	Jan	30	5	2.4	Mercer
40.68000	-84.60000	2005	Mar	13	5	2.2	Mercer
40.74000	-84.08000	2006	May	12	5	2.8	Allen
40.71000	-84.11000	2006	Aug	15	5	2.5	Allen
41.71000	-82.93000	2007	Apr	12	5	2.5	Ottawa
41.75000	-82.90000	2007	Apr	24	5	2.3	Ottawa
41.73000	-82.22000	2007	Oct	18	5	2.7	Lorain

Latitude	Longitude	Year	Month	Day	Depth (km)	Magnitude	County
41.16000	-83.41000	2010	Feb	25	5	2.9	Seneca
40.41000	-84.31000	2008	Sep	30	5	2.8	Shelby
41.24000	-81.51000	2010	May	17	5	2.5	Summit
41.39000	-83.30000	2010	May	14	5	2.6	Sandusky
40.86000	-83.54000	2011	Apr	26	5	2.4	Hancock
41.03000	-82.08000	2011	Jun	5	5	2	Medina
39.67000	-83.07000	2013	Oct	21	20	2	Pickaway
39.45000	-82.21000	2013	Nov	20	8	3.5	Athens
41.41000	-81.91000	2014	Jan	20	13	2.1	Cuyahoga
41.86000	-83.08000	2012	Sep	7	5.1	2.5	Ottawa
40.76000	-81.41000	2006	Mar	27	5	2.2	Lake
40.95000	-84.75000	2015	Jun	12	20	2.6	Van Wert
41.65000	-82.90000	2016	Feb	7	5	2.5	Ottawa
39.72000	-82.55000	2016	Nov	24	2	1.5	Fairfield
40.98000	-82.09000	2014	Oct	21	5	2.2	Wayne
40.73000	-84.15000	2015	Jan	10	2	2	Allen
39.79000	-82.08000	2017	Jun	2	13	2	Perry
39.65000	-82.40000	2018	Apr	29	5	2	Hocking
41.47000	-81.66000	2019	Mar	6	15	2	Cuyahoga
40.72000	-84.15000	2019	Oct	20	15	1	Allen
40.65000	-83.85000	2020	Jun	30	5	2	Hardin
40.49000	-84.29000	2020	Mar	14	5	0	Auglaize
40.42000	-84.11000	2020	Jul	14	2	3	Shelby
40.43000	-84.11000	2020	Jul	14	3	2	Shelby
40.44000	-84.10000	2020	Aug	3	3	1	Shelby
40.43000	-84.11000	2021	Jan	15	7	2	Shelby
40.73000	-84.14000	2021	Jan	22	5	3	Allen
40.72000	-84.15000	2021	Feb	11	3	2	Allen
40.44000	-84.10000	2021	Apr	15	5	2	Shelby
40.43000	-84.10000	2021	Jul	16	3	2	Shelby
40.43000	-84.10000	2021	Aug	18	3	2	Shelby
39.58000	-82.78000	2021	Nov	7	4	2	Fairfield
39.57000	-82.78000	2021	Nov	7	7	1	Fairfield
39.24000	-83.47000	2022	Mar	20	5	2	Highland
41.27000	-81.89000	2022	Jun	4	10	2	Medina
39.28000	-83.42000	2022	Sep	4	8	1	Highland
40.71000	-83.02000	2022	Sep	24	5	2	Crawford
41.11000	-83.44000	2022	Dec	22	1	3	Hancock
40.24000	-84.54000	2023	Jan	2	2	2	Darke
41.57000	-83.48000	2023	May	20	2	3	Wood

Latitude	Longitude	Year	Month	Day	Depth (km)	Magnitude	County
39.29000	-82.95000	2023	Jul	10	5	1	Ross
39.45000	-82.31000	2023	Aug	1	7	2	Hocking
41.07000	-84.34000	2023	Oct	1	5	2	Paulding
40.44000	-84.10000	2023	Dec	9	7	3	Shelby
41.57000	-83.48000	2024	Mar	18	3	2	Wood
41.56000	-83.47000	2024	Apr	22	2	3	Wood
40.43000	-84.10000	2024	Aug	29	3	1	Shelby
41.37000	-83.90000	2024	Sep	27	2	2	Henry
39.29000	-82.72000	2024	Nov	2	6	1	Vinton
41.54000	-83.48000	2024	Dec	18	2	1	Wood
41.31000	-84.79000	2024	Dec	29	5	3	Defiance
39.34000	-82.58000	2025	Feb	19	10	1	Hocking
41.74000	-82.00000	2025	May	7	5	1	Lake
40.61000	-84.57000	2025	Jun	9	5	2	Mercer

19. Appendix 1D-Suitability of Selected Materials

The accompanying Zip File titled “Appendix 1D” includes information verifying the suitability of the selected materials. The files are too large to insert into this document.

This page intentionally left blank.